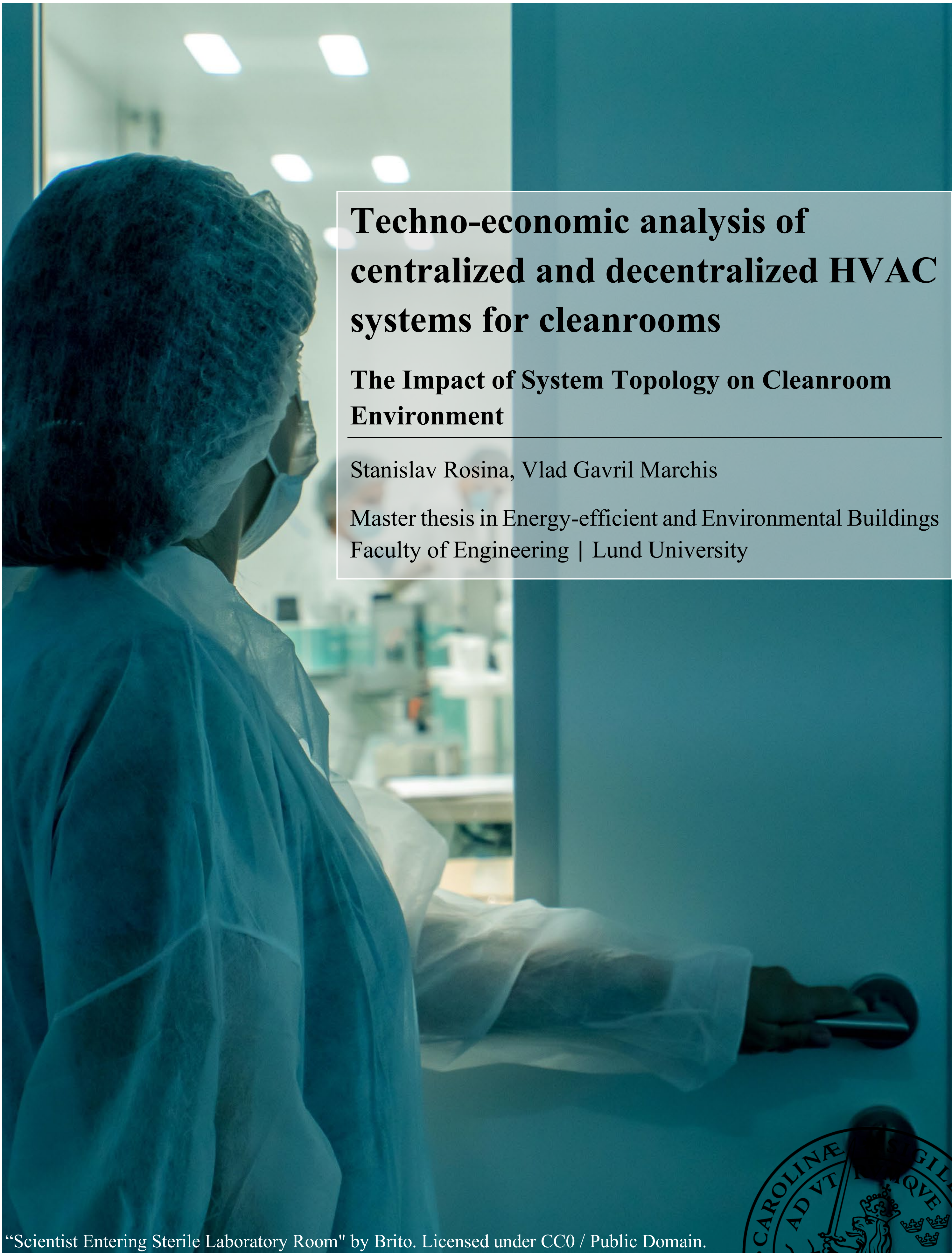

Techno-economic analysis of centralized and decentralized HVAC systems for cleanrooms

The Impact of System Topology on Cleanroom Environment

Stanislav Rosina, Vlad Gavril Marchis

Master thesis in Energy-efficient and Environmental Buildings
Faculty of Engineering | Lund University

Lund University

Lund University, with eight faculties and numerous research centers and specialized institutes, is the largest research and higher education institution in Scandinavia. The main part of the University is situated in the small city of Lund, which has about 112 000 inhabitants. Several research and education departments are, however, located in Malmö. Lund University was founded in 1666 and has today a total staff of 6000 employees and 47 000 students attending 280 degree programmes and 2 300 subject courses offered by 63 departments.

Master Programme in Energy-efficient and Environmental Building Design

This international programme provides knowledge, skills and competencies in the field of Energy-efficient and Environmental Building Design in cold climates. The goal is to train highly skilled professionals who will significantly contribute to and influence the design, construction, or renovation of energy-efficient buildings, considering architecture and the environment, inhabitants' behavior and needs, their health and comfort, and overall economy.

The degree project is the final part of the master's programme leading to a Master of Science (120 credits) in Energy-efficient and Environmental Buildings.

Examiner: Dennis Johansson (Division of Building Services)

Supervisors: Ilia Iarkov (Division of Building Services), Birgitta Nordquist (Division of Building Services), Martin Petříček (CAREOFAIR s.r.o.)

Keywords: Age of air, Cleanroom, CFD, Centralized ventilation, Decentralized ventilation, HVAC ventilation, LCC.

Publication year: 2026

Abstract

Cleanrooms in the pharmaceutical industry are energy-intensive environments where HVAC systems account for roughly 50-75% of energy use due to high air changes per hour and strict conditioning requirements for indoor humidity and temperature. This thesis presents a techno-economic analysis comparing two of the most common HVAC system types. These systems are centralized, using one large AHU to provide airflow and conditioning, while the other, decentralized system with filter fan units, provides per-room airflow and air conditioning. This thesis uses a quantitative approach to study fluid dynamics in cleanrooms, validating pressure cascades, temperatures, and variables such as age of air, and includes a detailed technical design for a centralized system. The findings reveal a significant difference in energy performance: the decentralized system uses 218 MWh annually, whereas the centralized system requires 1 607 MWh annually. This discrepancy is primarily driven by the decentralized system's ability to provide per-room conditioning and its significantly lower ductwork resistance, leading to a superior Specific Fan Power. CFD simulations further highlighted that while both systems maintained the required pressure levels, internal heat gains from packaging machinery in cleanroom 1 raised the temperature to 21.3 °C, near the design limit of 19 °C ±3 °C. This suggests that high Air Change Rates alone cannot compensate for insufficient localized cooling capacity. This study concludes that while a centralized system requires a lower initial investment, it quickly catches up to the decentralized system due to significantly higher operating costs.

Acknowledgments

We sincerely thank our supervisor, Ilia Iarkov, co-supervisor Birgitta Norquist, and co-supervisor Martin Petríček for their invaluable support, guidance, and stimulating discussions throughout this research.

Completing this thesis marks an important milestone in our education.

Existing project credits

Presented drawings related to the existing project are either material received directly from the partner company or reproduced by the authors based on the project materials received. Therefore, they are credited to the partner company.

HVAC decisions, strategies, applicable standards, and parameter values for the existing project are attributed to the partner company.

The description of the existing project presented here reflects the authors' interpretation of the project based on the project materials received. Analysis described in the methods and subsequent chapters is credited to the authors.

Parameter values assumed for the following analysis related to the existing project are presumed to be a qualified assumption made with the help of the partner company, based on their design, engineering experience, technical and market data, unless otherwise clearly stated. For transparency and to facilitate the validation of this study, all parameters needed for the presented analysis are clearly stated.

Table of contents

Nomenclature

CFD	Computational Fluid Dynamics
ISO	International Organization for Standardization
ACH	Air Changes per Hour
AHU	Air Handling Unit
SFP	Specific Fan Power
EPW	EnergyPlus Weather
UDAF	Unidirectional Airflow
HVAC	Heating, Ventilation, and Air Conditioning
FFU	Filter Fan Unit
2D	Two-Dimensional
3D	Three-Dimensional
IFC	Industry Foundation Classes
LCC	Life Cycle Cost
HEPA	High-Efficiency Particulate Air
RH	Relative Humidity
ASHRAE	American Society of Heating, Refrigerating and Air-Conditioning Engineers

1 Introduction

1.1 Global context

Studies have identified global warming as a fundamental threat to humanity, calling for immediate measures to stop and mitigate the negative environmental impacts on Earth. The consequences of global warming are seen across multiple sectors, including healthcare, agriculture, the economy, the environment, and individuals (Christoph Nikendei et al., 2020).

In a rare global effort, countries came together to establish a common approach to climate change, as the negative impacts of global warming became more visible, leading to the Paris Agreement, which sets a common climate framework and goals for participants (United Nations, 2015). Recent studies claim that the most favorable scenario outlined in the Paris Agreement is already out of reach, but the worst climate outcome is still avoidable; therefore, they renew the call for immediate action to mitigate this threat, which is changing life on Earth as we know it (International Energy Agency, 2025).

Mitigating climate change requires both scientific and social solutions; this complexity cannot be addressed with a single universal solution; rather, it requires a multitude of solutions applied across multiple sectors (Berry Pam M. et al., 2015; Qian Ye, 2011). Studies have identified multiple major polluters that are arguably part of every individual's life, such as the transportation sector (Skeie Ragnhild Bieltvedt et al., 2009), energy sector (Beising Rüdiger, 2007), agricultural sector (Thamarai P. et al., 2024), construction sector (Kumaresan B. and Vijayaraghavan N., 2015).

While certain global regions or sectors experience a harsher impact from negative climate change, effects are interconnected and must be addressed as a whole (Berry Pam M. et al., 2015; Martinich Jeremy and Crimmins Allison, 2019).

1.2 Construction Industry

The construction industry is one of the sectors where improvements that lead to a reduction in the carbon footprint might be most fruitful, as it accounts for roughly 40% of global greenhouse emissions and energy usage (Vijayan Dhanasingh Sivalinga et al., 2025).

Depending on the building function, operational energy over the facilities' life span can account for up to 80%-90% of the energy demand, while embodied energy accounts for roughly 10-20% (Devender Dahiya and Boeing Laishram, 2024). Therefore, the most significant improvements could be achieved by reducing operational energy demand.

HVAC operational energy accounts for approximately 25% to 70%, depending on multiple factors, such as building topology, system efficiency, building function, or most notably the surrounding climate determined by the geographical position (Pinar Mert Cuce and Erdem Cuce, 2026).

1.3 Cleanrooms

Cleanrooms are highly controlled environments where airborne particles are kept within strict limits. These limits depend on the processes taking place. Cleanroom ventilation technology aims to reduce contamination from people, processes, or equipment. Initially used in hospitals and high-precision manufacturing, cleanrooms now serve a range of essential industries, including pharmaceutical/biotechnology, semiconductor, aerospace, and defense (ASHRAE, 2019).

Driven by growth in key industries, such as pharmaceutical (Matej Mikulic, 2025) and semiconductor (Semiconductor Industry Association, 2025), forecasts show the cleanroom industry will almost double by decade's end. Growth is driven by higher production demands and stricter requirements for product quality and contamination control ("Cleanroom Technology Market (2025 - 2030)," n.d.).

In ventilation, ASHRAE distinguishes between unidirectional, laminar airflow, characterized by smooth, parallel movement, and mixed, turbulent airflow (ASHRAE, 2025) based on *Reynolds number*

("Reynolds number," n.d.). In an ideal ventilation scenario, unidirectional airflow should travel from the supply, maintaining directionality without blending with the adjacent air. As more adjacent air blends with the supplied air, the airflow becomes more turbulent, as measured by the *Reynolds number*. Ideal unidirectional airflow is unachievable in practice, while nearly unidirectional airflow can be achieved only in miniature, thoroughly controlled environments (KHANKARI KISHOR, 2019). Laminar airflow is preferable for a thorough prevention and control of air contamination compared to turbulent airflow, which often fails to meet strict requirements (R. J. Knudsen and S. M. N. Knudsen, 2021).

The claim that turbulent airflow fails to meet strict requirements is further reinforced by best-practice standards that recommend (International Organization for Standardization, 2022), or regulatory standards that mandate the use of unidirectional airflow for sterile manufacturing inside the European Union, depending on the cleanroom grade (EUROPEAN COMMISSION, 2022). In ISO's best-practice standard, purity class 1 to purity class 5 is achieved through unidirectional, laminar airflow (International Organization for Standardization, 2022).

Quantitative data is not available for how often decentralized HVAC FFU systems are used to establish laminar airflow, but arguably, based on identified and analyzed papers, in general, cleanroom practices, laminar airflow is achieved through decentralized, FFU-dominated systems (Arup Bhattacharya et al., n.d.; Indra Permana et al., 2025; Permana Indra et al., 2024; Zonghua Huang et al., n.d.).

1.4 Cleanroom energy usage

Compared to average rooms, cleanroom energy usage can be several orders of magnitude higher per square meter (Fedotov A., 2014). HVAC systems generally account for 50%-75% of a cleanroom's total energy use. This is mainly due to the high number of air changes per hour required to meet and maintain the cleanliness criteria, as well as the continuous control of temperature, humidity, and pressure. Many facilities operate under a 24/7 regime, further increasing overall energy usage (Marcel G.L.C. Loomans et al., 2019).

Several arguments are drawn up for improving the energy efficiency of cleanrooms. From an environmental perspective, their energy usage results in greenhouse gas emissions, with 1 m^2 of cleanroom floor area equivalent to up to 25 m^2 of general floor area from an operational perspective. From an economic perspective, HVAC system operational costs account for a large share of a facility's running costs over its lifetime (Xinran Zeng and Chunhui Li, 2025). Additionally, geopolitical instability and energy price fluctuations have increased the focus on reducing energy usage and improving overall efficiency (Niraj P. Koirala, 2025).

Over recent years, there has been a trend toward reducing energy use in all sectors, from small consumer-oriented electronic devices to entire buildings or industrial sectors (S&P Global, 2026). Cleanrooms should not be excluded from this development, given the high potential of even a small improvement to generate large savings. Previous studies have established the urgency of reducing cleanroom energy use while maintaining cleanliness standards and operational requirements (Justin Z. Lian, 2024).

Increasing the energy efficiency of cleanrooms is of interest to researchers worldwide. Sun et al found that airflow determined air changes per hour are generally much higher than ought to be, due to old rule of thumbs set by standards that do not account for several relevant parameters that are project specific, such as particle generation rate, filter efficiency etc. due to "*design and operating engineers still choose to obey the existing rule to avoid being challenged*" resulting in a higher energy usage than actually needed to achieve requirements and calling for improvements (Sun Wei et al., 2010).

Chen et al identified, analyzed and ranked 10 relevant parameters that are energy usage driving factors for semiconductor cleanrooms, through multiple computer simulations with different parameter values, concluding that the amount of air changes per hour is a more influential parameter than, among others, supply temperature or air efficiency, effectively establishing a list of parameters where improvements are most useful in reducing the energy usage of a cleanroom (Chen Yiling et al., n.d.).

In a study focusing on optimizing the energy usage of ventilation fans by combining coils to reduce pressure drops, Ma et al have identified a possibility to reduce the pressure drop inside the AHU by up to 10.7% to 17.2% if coils are combined where possible, and possible energy savings of up to 29% for the FFUs, by reducing the return airflow (Zhiyao Ma et al., 2021).

Yang et al determined that it is possible to decrease the energy use of laminar flows in cleanrooms by up to 17.3% through a protective, curtain-like airflow layer with low turbulence, even claiming to improve air cleanliness compared to the classic laminar flow setup (Yang Bi et al., 2025).

Ma et al conducted a performance and improvement analysis of air filtration in semiconductor cleanrooms to reduce overall energy use, driven primarily by high air changes per hour and high airflow friction. A new air filtration system was proposed, where outdoor air and recirculation air were filtered separately before mixing, resulting in a drop in total energy usage of 25% to 45% due to lower airflow friction (Zhiyao Ma et al., 2020).

1.5 Centralized, Decentralized cleanroom ventilation solutions

Studies such as Merzkirch et al have delved into comparing centralized and decentralized ventilation solutions in residential applications and determined that, among other things, decentralized ventilation solutions are more energy-efficient compared to centralized ventilation solutions, due to the lower specific fan power based on the lower friction losses determined by a smaller amount of ducts (Merzkirch Alexander et al., 2016). While this strays from the application of cleanrooms, since the reasoning is based on lower friction losses resulting from less ducting in decentralized ventilation solutions, it could be argued that the result is generally applicable, as the laws of physics and mathematical quantification principles are constant.

A study by Tsao et al analyzed five different ventilation solutions for a case study, with different degrees of decentralization, where a partially decentralized solution with an AHU and FFUs, a completely decentralized system with recirculation units and supply diffusers, or a centralized system with an AHU and supply diffusers are compared, among others. Findings suggest that the partially decentralized ventilation system is the most efficient, only by a slight margin when compared to the centralized system. Tsao et al.'s study focused on a singular semiconductor production facility located in Taiwan. Tsao et al have not investigated the economics of the different solutions involved in their analysis (Jhy-Ming Tsao and Shih-Cheng Hu, 2007). Tsao et al's results cannot be generalized automatically, as they focus on a single case study for a specific application.

1.6 Study perspectives

While researching cleanrooms, energy usage seems to be a topic of interest for the academic community based on the amount of research available. However, literature that undertakes a clear techno-economic comparison between centralized and decentralized HVAC systems in cleanrooms, based on a case study or multiple case studies, is scarce, to say the least. Therefore, an opportunity for a techno-economic comparison between the two solutions presents itself.

1.7 Aim

This study aims to provide a techno-economic evaluation of an existing decentralized ventilation filter fan unit's (FFU) design, provided by a partner company as a case study, against a hypothetical centralized AHU system design. Both systems are assessed for technical performance and economic viability across a pharmaceutical packaging production facility operating under ISO 7/ISO 8 standards.

2 Existing project basis

A partner company provides an existing project that includes two cleanrooms within a multipurpose manufacturing facility. The stated purpose of these cleanrooms is to produce high-quality, hygienic, plastic packaging for pharmaceutical products.

According to client requirements, hygienic packaging must be produced under conditions defined by purity classes in accordance with ISO 14644-1:2015 (International Organization for Standardization, 2015). These conditions are already set by the partner company and followed for the purpose of this study.

Hygienic packaging is produced using a thermoforming machine located in Cleanroom 1, measuring roughly 4x12x3 m (WxLxH), weighing approximately 12 t, with an average electrical usage of 32 kW and an average heat output of 10 kW.

2.1 Project climate

The project is located in a medium-sized urban region of Slovakia. Due to client confidentiality, the exact location of the project is not disclosed. Further information is provided in Table 1.

Table 2 presents comparable values for the capital of Slovakia, Bratislava.

Table 1. Winter and summer HVAC design conditions, data retrieved from the partner company

Winter conditions

City	Altitude/ m	Outdoor temperature/ °C	Enthalpy/ (kJ/kg)	RH/ %
Undisclosed	320	-15	-13.20	74.7

Summer conditions

City	Altitude/ m	Outdoor temperature/ °C	Enthalpy/ (kJ/kg)	RH/ %
Undisclosed	320	+32	+58.20	34.3

Table 2. Winter and summer conditions in Bratislava, data retrieved from ASHRAE(ASHRAE, n.d.)

Winter conditions

City	Altitude/ m	Outdoor temperature/ °C	Enthalpy/ (kJ/kg)	RH/ %
Bratislava	140	-11	-9.0	90

Summer conditions

City	Altitude/ m	Outdoor temperature/ °C	Enthalpy/ (kJ/kg)	RH/ %
Bratislava	140	+33	+60.5	38

2.2 Existing project composition

The project comprises two cleanrooms where the production processes described in the chapter 2 take place, three airlocks, and a personnel dressing room. In cleanroom environments, airlocks are anterooms that serve as transition spaces between environments with different purity classes. Their primary purpose is to ensure and maintain a controlled pressure gradient and to prevent the entrance of contaminants during the movement of personnel or materials (Zhonglin Xu, 2013).
ISO purity classes, defined by ISO 14644-1:2015, categorize cleanrooms and their controlled environments by airborne particle concentration. Stricter limits on particle size and quantity are imposed as the ISO purity class decreases. As the purity class number increases, the count of airborne particles increases by a factor of 10, or, rather, the air becomes 10 times dirtier in terms of particle count and size (International Organization for Standardization, 2015).

ISO purity class standards are the ventilation industry's best practice standards for production industries such as semiconductor, pharmaceutical, or aerospace manufacturing, where microscopic contamination can cause product failure or safety hazards (International Organization for Standardization, 2015).

The predefined parameters for the analyzed spaces by the partner company are presented in Table 3. The air exchange rate data is based on measurements taken by the partner company after the project's completion and represents actual values that differ slightly from the design values. For this study, on-site-measured validation data are used when available. A continuous flow is assumed for the whole year, as no usage profile is defined.

Table 3. Project zones

Space	ISO class	Area/ m^2	Volume/ m^3	Temperature/ °C	RH/ %	ACH/ (1/h)
Cleanroom 1	ISO 7	75.26	263.41	19±3	40-60	51.46
Personnel airlock 1	ISO 7	3.74	9.72	22±3	40-60	84.03
Personnel airlock 2	ISO 8	10.10	26.26	22±3	40-60	41.65
Dressing room	ISO 8	10.10	26.26	22±3	40-60	42.24
Cleanroom 2	ISO 8	29.98	104.93	19±3	40-60	37.84
Material airlock	ISO 8	6.71	23.48	22±3	40-60	46.18

2.3 HVAC Strategy

Cleanroom premises are ventilated, heated, and air-conditioned using a decentralized HVAC system. The system consists of one AHU, FFU devices, and direct evaporative supply units.

Fresh air, which accounts for 10% of the total ventilation needs of the given spaces, as determined by measured air changes, is supplied to the spaces by the AHU from the exterior environment. This air is then mixed with recirculated air extracted from the given spaces through recirculation towers, accounting for 90% of the need, and taken through one of the direct evaporative supply units and afterward delivered to the given premises through the FFUs.

Recirculation towers are custom-made components, in this case composed of rectangular ducts, H14 HEPA filters, and ventilation grills acting as an air exhaust unit.

An overpressure cascade is established in Cleanroom 1 and Cleanroom 2 to ensure air exfiltration. Ducting is realized using circular, rectangular, and flex ducts. Ducting accessories such as rain shields, dampers, silencers, temperature/pressure sensors, etc., are installed to augment the system.

A schematic of the HVAC system, as well as HVAC plans are available in Appendix G.

Although the up-named schematic represents an HVAC system with signatures in accordance with the Slovak Technical Standard set by the Slovak Office of Standards (Slovak Office of Standards, Metrology and Testing, n.d.), it is augmented with a legend describing the components. Heavy machinery, such as the AHU, is marked with numbers. Therefore, technical units are described in Table 4. Specific manufacturers are removed from the product description for confidentiality reasons.

Table 4. Existing air conditioning units

Unit number	Description
1.1	Air handling unit inlet: 3000 m^3/h
1.12	Outdoor air conditioner unit. Q cooling:28 kW
1.13	Outdoor air conditioner unit. Q cooling:28 kW
1.14	Outdoor air conditioner unit. Q heating:74.92 kW Q cooling:47.39 kW
1.15	Internal cooling unit. Q: 1200 m^3/h
1.2	Condensing unit. Q: 3.4 kW
1.3	Internal cooling unit. Q: 4200 m^3/h
1.31	Humidification unit. Capacity: 16 kg/h
1.7	Outdoor conditioner unit. Q heating:17.15 kW Q cooling:11.43 kW

2.4 Software used throughout the study

Table 5. Collection of used software

Software	Description of use
Autodesk Revit(“Autodesk Revit,” n.d.)	General 3D model of the received project
MagiCAD for Revit(“MagiCAD for Revit,” n.d.)	System Families creator, calculations
Ansys Workbench suite(“Ansys Workbench,” n.d.)	Complete CFD process
SystemAirCAD(“SystemAirCAD,” n.d.)	AHU design and energy calculations
LadyBug tools(“Ladybug tools,” n.d.)	Energy use calculations
ClimateStudio (Solemma LLC, 2024)	Energy use calculations
Grasshopper(“Grasshopper,” n.d.)	Energy use calculations
IDA ICE(“IDA ICE,” n.d.)	Cooling load calculations
Mollier sketcher(“Mollier sketcher,” n.d.)	Initial Mollier sketches

3 Methods

3.1 Computational Fluid Dynamics – Existing project

Computational Fluid Dynamics (CFD) analysis of the existing project was conducted to assess the system's overall performance after conditioned air is released into the room. Cleanroom conditions are measured using several technical standards. This included checking that air pressure keeps contaminants out, ensuring the air flows smoothly without excessive swirling (turbulence), and verifying that temperatures remain steady. The age of the air was also analyzed to ensure that fresh air circulates effectively throughout the space.

To conduct the CFD, various software was used. Revit was used to recreate the two-dimensional drawings received from the collaboration company into a three-dimensional model, which can then be imported into the CFD software. Furthermore, the Ansys Workbench suite of apps was used for the actual analysis. Specifically, Ansys-Space Claim to further simplify the model, Ansys Meshing to create a detailed mesh of objects and spaces, Ansys CFX-pre to set the model's actual boundaries and conditions, and Ansys CFX-post to visualize the results. What's more, in Ansys-Workbench, the Fluid flow CFX system node was selected to run the simulation that includes all the mentioned Ansys applications (Ansys, Inc., 2026).

It is important to note that CFD was performed only on relevant spaces in the project, such as cleanroom 1 and cleanroom 2, as other spaces do not serve any special purpose for manufacturing or have strict cleanliness requirements and airflow management. Analyzed spaces can be seen highlighted using red lines, below, in Fig. 1.

Moreover, all unmentioned settings were left at their default; only the mentioned changes were made if the corresponding setting in the other software was changed.

Furthermore, a comprehensive flowchart divided into 6 subheading sections for easier understanding of the CFD methods section can be seen below in Fig. 2. This flowchart outlines the workflow for conducting CFD analysis, detailing all major steps and software used at each step.

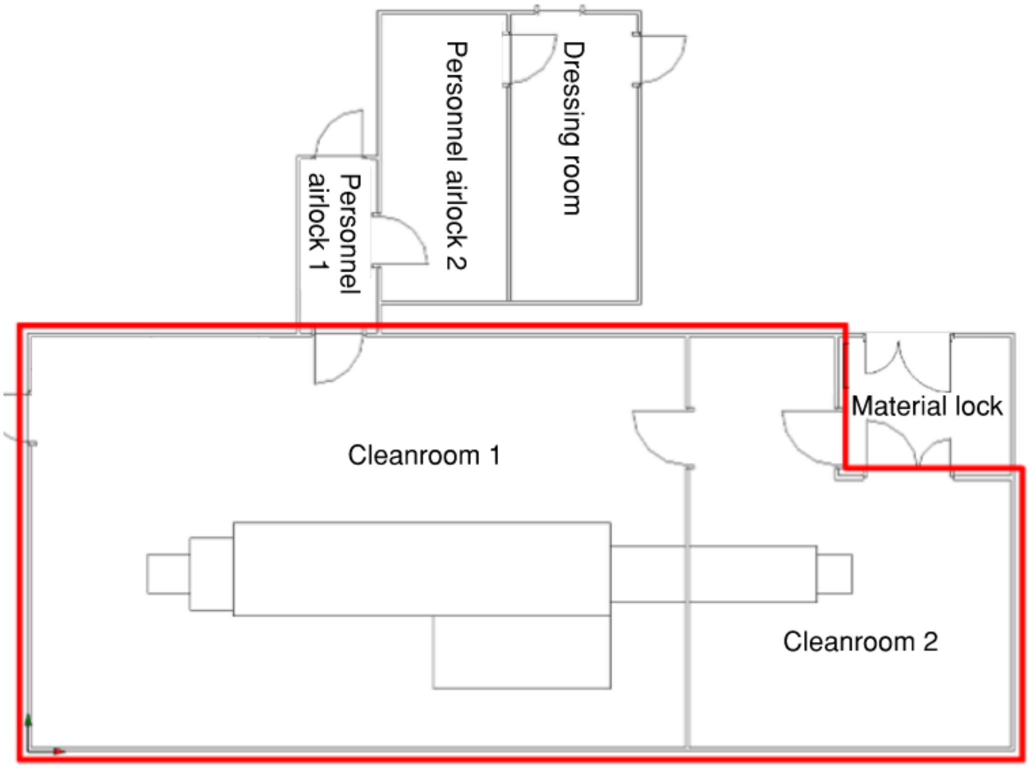

Fig. 1. CFD study boundary

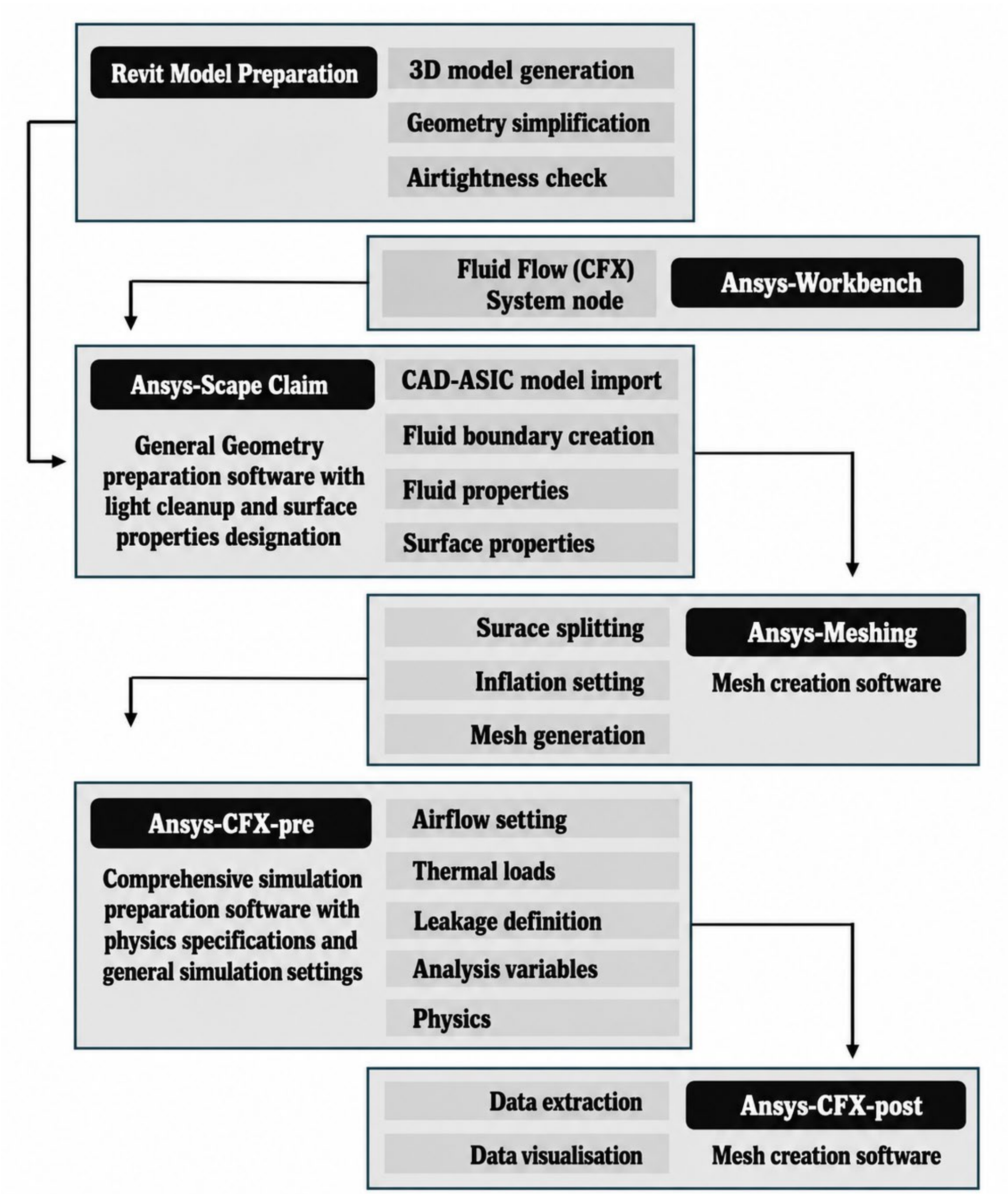

Fig. 2. CFD method section flowchart

3.1.1 Revit Model Preparation

A 3D model was generated in Revit from the existing project materials to represent the given spaces. To reduce the computational power required to run the CFD, the Revit model was heavily simplified, retaining only the essential surfaces and objects. These objects mainly include furniture and machinery that influence the air velocity.

The illustrative floor plan can be seen in Fig. 3, as well as basic information about individual rooms that can be seen in Table 6.

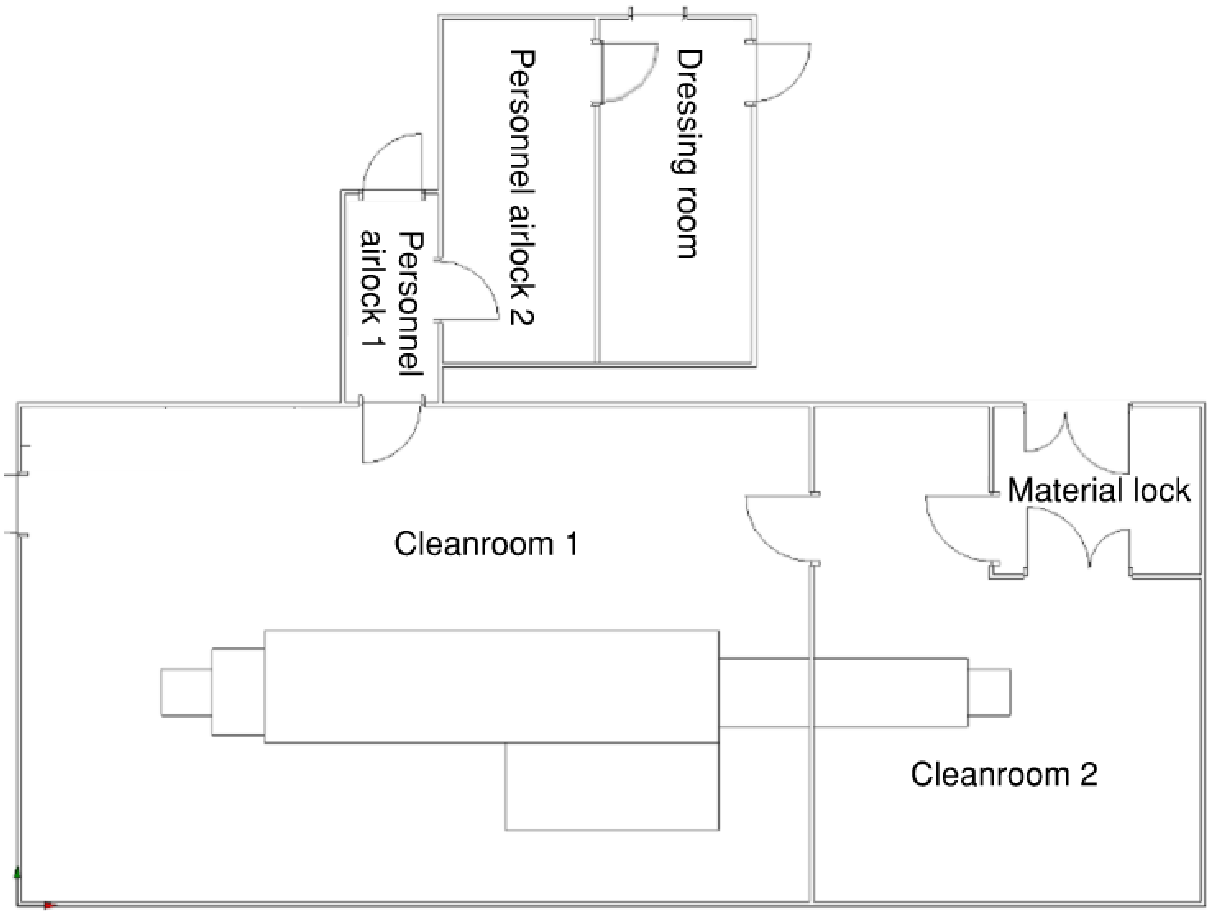

Fig. 3. Illustrative floor plan with location and names of individual rooms

Table 6. Information about individual rooms

Room name	**Area/ m²**	**Volume/ m³**	**Ceiling height/ m**
Cleanroom 1	75.26	263.41	3.50
Cleanroom 2	29.98	104.93	3.50
Material Lock	6.71	23.48	3.50
Personnel Airlock 1	3.74	9.72	2.60
Personnel Airlock 2	10.10	26.26	2.60
Dressing Room	10.10	26.26	2.60

3.1.2 Ansys-Workbench (Setting up the workflow)

As stated in the section 3.1 the Fluid Flow (CFX) system node was selected for the analysis. This was because it offers a variety of functions to properly scrutinize cleanrooms while remaining beginner-friendly. In this section, the analysis is divided into two parts, each representing a cleanroom (CR1 and CR2). The other rooms in the project are completely left out of the simulation due to their lack of importance and the spaces' use cases.

3.1.3 Ansys-Space Claim (Geometry preparation)

SpaceClaim is native 3D modeling software for Ansys Workbench, used to further simplify models imported from Revit.

First, the Revit model was exported to CAD-ASIC, a file format supported by Space Claim. To verify that the model was complete, an airtightness check is performed. This was done by selecting an enclosure function in the “prepare” tab and drawing a large box that encompasses the cleanrooms from all sides. The enclosure function, then, if the model is properly airtight, creates a negative imprint of the model. This was then reduced to only internal surfaces representing the fluid boundary (air). However, to make the fluid boundary act like air, a density of 1.225 Kg/m^3 was specified in the properties bar, which is the density of air (“Density of air,” 2026).

Based on the project plans received from the supervising company, the enclosure's exterior surfaces were divided into exhaust and supply diffusers at their appropriate locations to preserve the integrity of the CFD analysis and keep it grounded in reality.

These surfaces were then grouped into named selections. Named selections were grouped based on the properties or rules that they obey. As an example, a named selection for all exhaust diffusers was created so that, later in Ansys-Meshing, the named selection is highlighted and properties can be applied to those surfaces all at once rather than one by one. This reduces the time spent actually applying all the properties, as the project has over 30 diffusers of both kinds.

3.1.4 Ansys-Meshing (Analysis mesh preparation)

This step was integral to CFD detailing as it governs the level of detail for the movement of air. The mesh in the model, split into two sectors, has one mesh governing the structure in the actual space and the other governing the air at the inlets, outlets, and leakage ports.

Furthermore, Table 7 represents the values for meshing and inflation settings. In Meshing, the value sets the maximum node size; the lower the value, the more nodes and greater detail in the mesh. On the other hand, while the level of detail is greater, computational time increases as well, making the analysis take longer (Ansys, Inc., 2024, 2020).

Moreover, the table specifies the inflation option, set to the first-layer thickness, and the height to 0.15mm. This indicates that Ansys will create a boundary layer of a specified thickness to better capture airflow around boundary surfaces. To further improve the quality of the boundary-layer air, an additional 12 layers were added on top of the surface, each increasing in size by a factor of 1.2 (Ansys, Inc., 2023).

The fully generated mesh for both cleanrooms can be seen in Fig. 4 below.

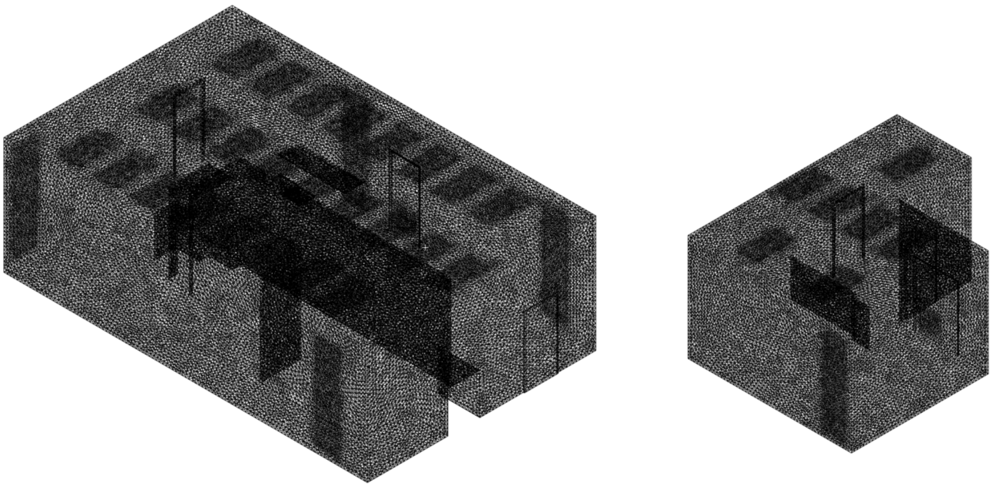

Fig. 4. Generated mesh of Cleanroom 1 (left) and Cleanroom 2 (right)

Table 7. Ansys-Meshing setting parameters

Meshing Settings	
Setting Name	**Value**
Inlets	0.05 mm
Outlets	0.05 mm
Leakage Ports	0.05 mm
General Space (Rest of surfaces)	0.10 mm
Inflation Settings	
Setting Name	**Value**
Inflation Option	First layer thickness
First Layer Height	0.15 mm
Maximum Layers	12
Growth Rate	1.20

3.1.5 Ansys-CFX-pre (Simulation properties preparation)

In this stage of the CFD analysis, all remaining information received from the supervising company was incorporated into the model.

Supply diffusers' airflow values were set based on validation measurements from the supervising company in 2024. However, Ansys uses mass flow rather than volumetric flow, which means values were converted using equation (1). This conversion was performed automatically by the software's expression function. This expression was set individually for all supply surfaces based on Table 8, which provides volumetric flow of each supply diffuser based on validation documentation from 2024.

On the other hand, exhaust diffusers did not include any validation numbers from the supervising company, so initial numbers based on the project were used. The exhaust air value is 10% of the supply air to create a pressure cascade. For cleanroom 1, the total exhaust volumetric flow is 12 170 m^3/h, while cleanroom 2 has only 3530 m^3/h. These were then equally distributed among the exhaust panels throughout the walls. Again, equation (1) was used to convert the received volumetric flow rates into mass flow rates that Ansys can understand.

Based on the exhaust and supply values, the total air changes per hour (*ACH*) in cleanroom 1 is 51.46 and in cleanroom 2 is 37.84, both well above the initially projected values of 30 and 8, respectively, as per the validation report and technical documentation.

The location of supply and exhaust diffusers in the cleanrooms is provided in Fig. 5 and Fig. 6 below.

Turbulence for both supply and exhaust ports was set to 5%. This number was derived from a meeting with the company supervisor.

The temperature of the incoming air was set to 19°C, as specified by the cleanroom's original design criterion.

Furthermore, after entering all values for supply and exhaust, there is a 10% excess of supply airflow compared to exhaust airflow. With these settings, the pressure would continue to rise indefinitely. That's why leakage ports were specified in the model. This was done by assigning predefined leakage ports, mostly located on the doors between the rooms, with leakage properties. These ports were modeled as exhaust boundary surfaces; rather than using the mass flow option, as is the case for supply and exhaust surfaces, the static pressure option was used. According to the validation documents, the pressure in cleanroom 1 is 44.4Pa, and in cleanroom 2 is 35.4Pa. These values were inputs to the static pressure option, making the boundary surface act as a valve: if the pressure in the cleanrooms reaches the desired levels, the valves open to release excess air mass flow. The positions of the leakage ports are highlighted in Fig. 7.

Moreover, a large packaging machine is located only in cleanroom 1. Based on technical documentation, this machine inputs around 10kW of heat into the space. Thus, surfaces representing the machine were assigned a heat-flux wall boundary of 132 W/m^2. This was because the machine's total heat output is 10kW and its surface area is 74 m^2. If these values are divided, the final heat-flux value is obtained. To reiterate the beginning of this paragraph, this machine outputs heat only to cleanroom 1; cleanroom 2 is unaffected.

After that, basic analysis variables needed to be created in CFX-pre before running the simulation. These were the unidirectional air flow (*UDAF*), which studies the unidirectionality of airflow within the cleanroom, and the age of air, which studies how long the air remains concentrated in the cleanroom. These should, among other things, show whether the cleanroom HVAC system operates as intended, with particles filtered out by the ducting system's filters.

UDAF shows the directionality of air and whether the air is or isn't turbulent. If the air is turbulent inside the cleanroom, particles remain longer, flying from place to place rather than being directed into exhaust diffusers and filtered out (Cleanroom.net, 2024). The variable was expressed in CFX-pre as shown in equation (2). Results from the equation will range from 1 (laminar flow, unidirectional flow) to -1 (totally turbulent, non-unidirectional flow).

In the age of air setup, the age of air variable was created, and subsequently, all supply boundary surfaces were assigned a source value of 0, making the air at the supply boundary zero seconds old before it entered the room. At the moment the air enters the cleanroom, the timer starts counting how long it takes for the air particles to leave the room, either through exhaust diffusers or through leakage ports.

Lastly, buoyancy was turned on in the Y-direction (the model's vertical direction) with a value of -9.806m/s^2("Gravitational acceleration," 2026). This value represents the gravitational acceleration, which further improves the reliability of the results.

$$m_a\left[\frac{\mathrm{kg}}{\mathrm{h}}\right] = V\left[\frac{m^3}{\mathrm{h}}\right] \times \rho\left[\frac{\mathrm{kg}}{m^3}\right] \tag{1}$$

In this Equation, m_a represents the Mass flow of dry air, V is the Volumetric Airflow, and ρ corresponds to the Density of air at a specific temperature.

$$UDAF = (V_y\left[\frac{\mathrm{m}}{\mathrm{s}}\right] \times (-1))/(V_{tot}\left[\frac{\mathrm{m}}{\mathrm{s}}\right] + 1e - 10) \tag{2}$$

In this Equation, *UDAF* represents unidirectionality (1 or -1), V_y represents the Vertical direction of air, and V_{tot} corresponds to the Total velocity of all air.

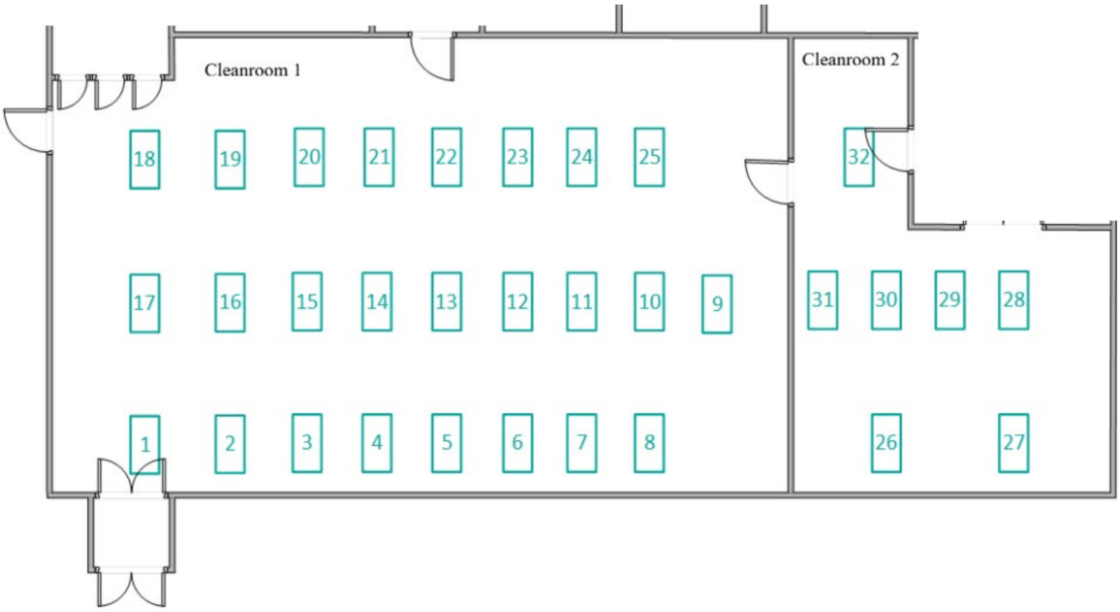

Fig. 5. Cleanrooms 1 and 2 supply and exhaust diffuser placement and numbering

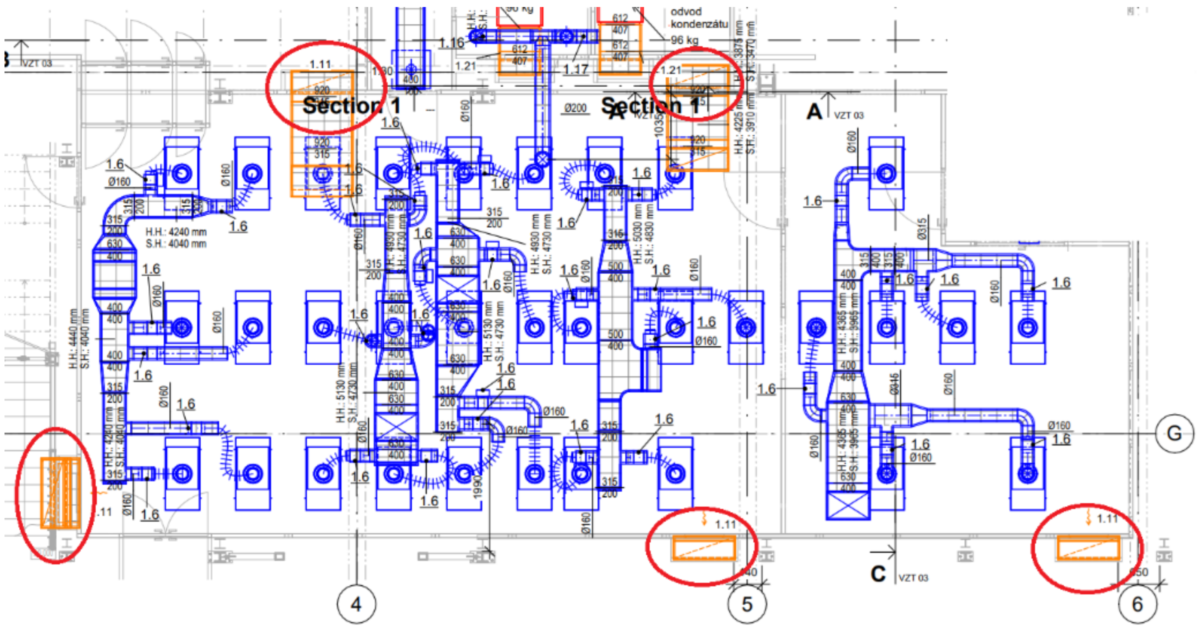

Fig. 6. Exhaust panels location in cleanrooms

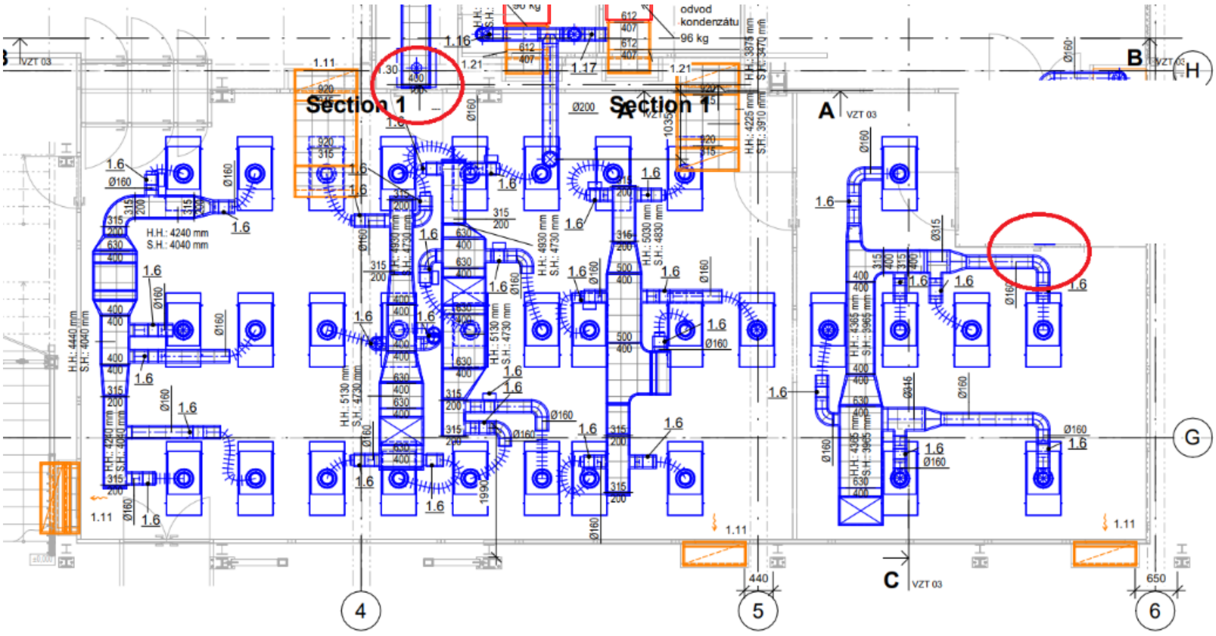

Fig. 7. Location of leakage valves in cleanrooms

Table 8. Volumetric flow of supply diffusers based on their corresponding number

Diffuser Number	**Measured Flow/ (m^3/h)**	**Diffuser Number**	**Measured Flow/ (m^3/h)**
1	524	**17**	584
2	603	**18**	483
3	562	**19**	508
4	543	**20**	587
5	474	**21**	474
6	621	**22**	439
7	550	**23**	625
8	587	**24**	552
9	541	**25**	557
10	510	**26**	581
11	580	**27**	561
12	616	**28**	530
13	463	**29**	508
14	490	**30**	553
15	537	**31**	642
16	510	**32**	546
Cleanroom 1 total:	13 520	**Cleanroom 2 total:**	3 921

3.1.6 Ansys-CFX-post

CFX-post was used to visualize and extract results based on the inputs provided in all previous steps. Also, in this section of the study, results such as temperature and pressure in cleanrooms are checked to determine whether they fall within the allowed deviations specified in the project's technical documentation.

Volume averages, or averages over the air state, were analyzed. This includes pressures, age of air, *UDAF*, temperatures, and velocities. This provides an overall system functionality and ensures proper simulation and HVAC setup.

The age of air is determined by how long the air remains in the cleanroom before being filtered and recirculated. Results were shown in seconds, based on the air's actual age. This means that the more seconds a result had, the longer it stayed.

Moreover, for *UDAF*, results are shown as unitless numbers ranging from 1 (laminar or unidirectional flow) to -1 (completely turbulent or non-unidirectional flow).

The temperature of the outgoing air from cleanrooms was also recorded in the CFD analysis and subsequently used as the initial interior temperature for the Mollier Diagram.

Lastly, the visual representation of average result values for age of air, *UDAF*, and air velocity on isosurfaces was rendered and studied.

3.2 Air behavior study

This study was conducted to improve the air behaviors observed in Cleanroom 1. This part of the study was conducted only for cleanroom 1, as this is where the machine is located and where all the raw materials are handled.

3.2.1 Scenario one

This scenario examines changes in the age of air and unidirectionality values resulting from changes in the layout of the exhaust and supply diffusers.

Almost all settings remained the same as in the previous methodology section 3.1. The settings that changed concern the actual volumetric flow inlets and outlets inside the room. On top of the already existing wall exhaust devices seen in Fig. 6 the middle part of the ceiling supply diffusers was converted into exhaust diffusers, as shown in Fig. 8. The reasoning is that those diffusers are located directly above the machine and disrupt airflow by pushing it sideways rather than downward, worsening the air's unidirectionality. To see the clearance between the ceiling and the packaging machine, see Fig. 9. So, the idea was to get rid of sideways flowing air, improving the unidirectionality of the diffusers 1-8, and 18-25, seen in Fig. 8.

In Ansys-CFX-pre, the middle row was converted into exhaust diffusers, on top of the already existing wall diffusers, among which 12 170 m^3/h of airflow was divided equally after being converted from volumetric flow to mass flow, as understood by Ansys. Moreover, the supply airflow of 13 520 m^3/h was evenly distributed among the remaining 16 supply diffusers, each supplying 845 m^3/h.

Furthermore, the number of iterations was set to 200, and the simulation was conducted. After it finishes, only numerical results were considered and compared to the original design results, i.e., age of air and UDAF.

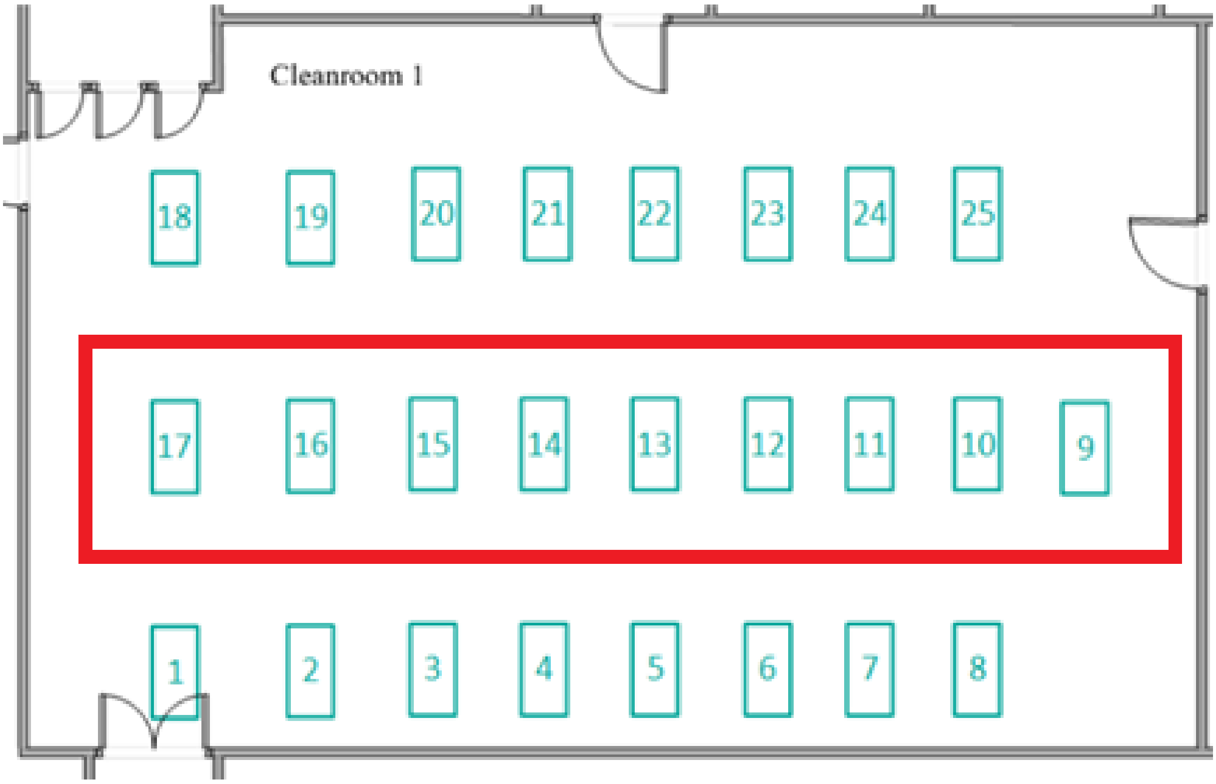

Fig. 8. Supply diffusers that are swapped for exhaust diffusers

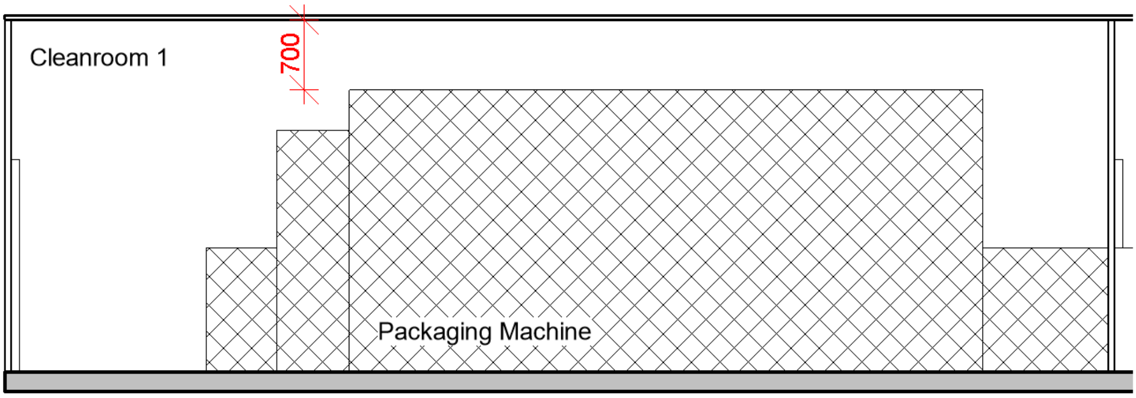

Fig. 9. Height clearance between the ceiling and the packaging machine

3.3 Cooling load – Existing project

The purpose of analyzing the cooling load for the given rooms was to verify that the existing HVAC design can maintain the required temperature as specified in the project's technical specifications.

This measure was necessary, particularly for Cleanroom 1, where production machinery with significant heat output is present. Cooling loads were determined using IDA ICE 5.1.

A maximum temperature difference of 3 °C was assumed. The density of air was assumed to be 1.225 kg/m^3, and the specific heat capacity of air was assumed to be 1006 J/kg·°C. Equation (3) served as the basis for this analysis.

$$Q[\mathrm{W}] = \dot{V}\left[\frac{m^3}{\mathrm{s}}\right] \times \rho\left[\frac{\mathrm{kg}}{m^3}\right] \times c_\mathrm{p}\left[\frac{\mathrm{J}}{\mathrm{kg}} / {}^\circ\mathrm{C}\right] \times \Delta T[^\circ\mathrm{C}] \tag{3}$$

In this Equation, Q represents the Cooling load, V is the Air volume flow rate, ρ corresponds to the Density of air, c_p is the Specific heat capacity of air, and ΔT is the Temperature difference.

3.3.1 Model setup

The Revit model described in section 3.1.1 was simplified to represent only the physical boundaries needed to determine the future thermal zones. The model was exported using IFC2x3 Coordination View 2.0 settings, and the generated IFC file was imported into IDA ICE. IFC spaces were converted to thermal zones using IDA ICE's native function.

Thermal zones were defined as indicated by the architectural plans; no simplifications or changes were made, so each room was its own thermal zone.

Thermal zones were located at least 12.2m away from the exterior façade line of the production facility, and at least 4.9m below the roof eave level. Therefore, it resulted in adiabatic walls and ceilings. The flooring was directly on the ground. The defined thermal zone parameters are shown in Table 9.

Ventilation was set to VAV with pressure control. Although IDA ICE allows AHU customization, given the project's limited time frame and the system's complexity, a predefined library version was used.

Based on the ASHRAE library available in IDA ICE, the actual project location inside Slovakia was used.

Table 9. Thermal zones parameters

Thermal zone	Area/ m^2	Ceiling height/ m	Cooling setpoint/ °C
Cleanroom 1	75.26	3.50	21
Personnel airlock 1	3.74	2.60	24
Personnel airlock 2	10.10	2.60	24
Changing room	10.10	2.60	24
Cleanroom 2	29.98	3.50	21
Material airlock	6.71	3.50	24

3.3.2 Schedules

Per the partner company's guidance, no fixed usage profile was defined for the thermal zones in question. The real usage profile depended on the number of orders received and the subsequent number of shifts for the respective period and was considered unpredictable.

Therefore, schedules assumed the zones were used at maximum capacity in three working shifts per day. Cleanroom 1 and Cleanroom 2 were set to always be on during weekdays. The rest of the rooms were set to a schedule of two 1-hour sessions during weekdays.

A custom holiday schedule was defined based on the Slovakian public holidays for 2026 (Ministry of Foreign Affairs and European Affairs of the Slovak Republic, n.d.), as shown in Table 10.

Table 10. Public holidays in Slovakia in 2026

Slovakian public holidays	
Holiday	**Date**
Day of the Establishment of the Slovak Republic	01.01.2026
Epiphany	06.01.2026
Good Friday	03.04.2026
Easter Monday	06.04.2026
Labour Day	01.05.2026
St. Cyril and Methodius Day	05.07.2026
Slovak National Uprising Anniversary	29.08.2026
All Saints' Day	01.11.2026
Christmas Eve	24.12.2026
Christmas Day	25.12.2026
Second Day of Christmas	26.12.2026

3.3.3 Internal loads

Occupant loads were determined assuming a maximum of 2 people per zone at any given time.

Equipment loads outside the cleanrooms were assumed to be 0 W/m^2 or negligible. Cleanroom 2 was equipped with a conveyor belt that delivered the items produced in Cleanroom 1 for packaging. An average equipment load of 10 W/m^2 was assumed.

Cleanroom 1 was equipped with the thermoforming machine mentioned in chapter 2. Based on the partner company's estimates, an average equipment load of 10kW was assumed.

Lighting loads were estimated at an average of 4.2 W/m^2 based on visual observations of the number of lighting fixtures, assuming T8 LED tubes with a Power of 18 W were used (CoreGain LTD, n.d.).

Table 11 summarizes these values for each thermal zone.

Considering the reduced loads outside Cleanroom 1, only the cooling load for Cleanroom 1 was validated.

Table 11. Defined internal loads

Thermal zone	**Occupant load/ (W/m^2)**	**Equipment load/ (W/ m^2)**	**Lighting load/ (W/m^2)**
Cleanroom 1	0.02	133	4.20
Personnel airlock 1	0.53	0	4.20
Personnel airlock 2	0.19	0	4.20
Changing room	0.19	0	4.20
Cleanroom 2	0.06	10	4.20
Material airlock	0.29	0	4.20

3.3.4 Building envelope

Considering that the cleanroom spaces were enclosed within a larger facility where the surrounding spaces were conditioned to the same temperature, no heat transfer was expected through the walls and ceilings bounding the analyzed thermal zones. Due to their adiabatic setup, no changes were made to the default components.

The floor component was modeled using the actual construction materials of the existing project, given that it was located directly above ground and heat transfer was expected due to ground temperature fluctuations throughout the year.

Since no insulation was present within the floor deck construction, no cold bridge was defined for the building component, as the whole component effectively acted as a cold bridge. Table 12 presents the floor deck that was defined in the energy model.

Table 12. Floor deck component

Component	Material	Thickness/ m	Density/ (kg/m^3)	Conductivity/ (W/m · °C)	Specific heat capacity/ (J/kg · °C)
Floor deck	Cast-in-situ concrete	0.13	2 400	2	1 000

3.4 Centralized HVAC system design

The overall goal for this section of the analysis was to modify the current system, which uses decentralized components such as FFUs and cooling towers, into a centralized system that combines air-conditioning and airflow management into a single large air-handling unit (AHU).

Moreover, the original airflows, along with the positions of the exhaust and supply diffusers, were kept unchanged. Also, the same type of exhaust diffuser was kept unchanged; however, since the current system uses FFUs, new supply diffusers were selected.

Furthermore, the current decentralized system uses vast numbers of rectangular ducts, which are more space-efficient but incur higher friction losses and are harder to clean (ASHRAE, 2025; HoodFilters.com, 2019). Thus, this centralized system was redesigned from the ground up using circular ducts.

It's important to note that this section of the analysis was not intended to strictly improve the design and make it ultra-efficient. This section describes the creation of a comparable design, which was then compared with the original design in terms of economy and energy use.

3.4.1 New supply diffusers

To find the right diffusers for the centralized system, design rules were established. As the centralized system was mostly composed of circular ducts, either a top-c or a side-c circular connection was preferred. To ensure the air entering the cleanrooms was properly conditioned, the diffuser housing was configured with a HEPA filter adapter. Moreover, the diffuser's face plate was configured as a perforated grid, providing downward-pointing airflow to promote unidirectional flow (Camfil, n.d.). Furthermore, to keep the supply diffusers consistent across all rooms, the same design was used to handle airflow from 439 m^3/h to 795 m^3/h while remaining relatively quiet and maintaining acceptable pressure drops.

With these characteristics in mind, the Sound Level and ΔP – Graph Finder (Camfil, n.d.), was used to select the appropriate diffuser. The supply diffuser was chosen to be Clean Seal Side-C (Camfil, 2024a), for the side connection, and Clean Seal Top-C (Camfil, 2024b) for the top connection. More specifically, exact product names for both can be found in Table 13, and graphs based on which the diffusers were chosen can be seen in Fig. 10 and Fig. 11.

These diffusers are a standardized size of 11P5 (Camfil, 2024c), which stands for a housing footprint of 1195mm x 595mm and a filter size of 1108mm x 508 mm. Moreover, they feature leakproof, welded housing for superior airtightness and a toolless filter change at the bottom of the diffuser.

Table 13. Product names and codes of chosen diffusers

Name	Product Code (Camfil, 2024a, 2024b)	Connection Type	Connection Size/ mm
Clean Seal Side-C	CL-SW-11P5-P-xx-S-C-315-N-xx-AAA0	Circular	315
Clean Seal Top-C	CL-SW-11P5-P-xx-S-C-315-N-xx-AAA0	Circular	315

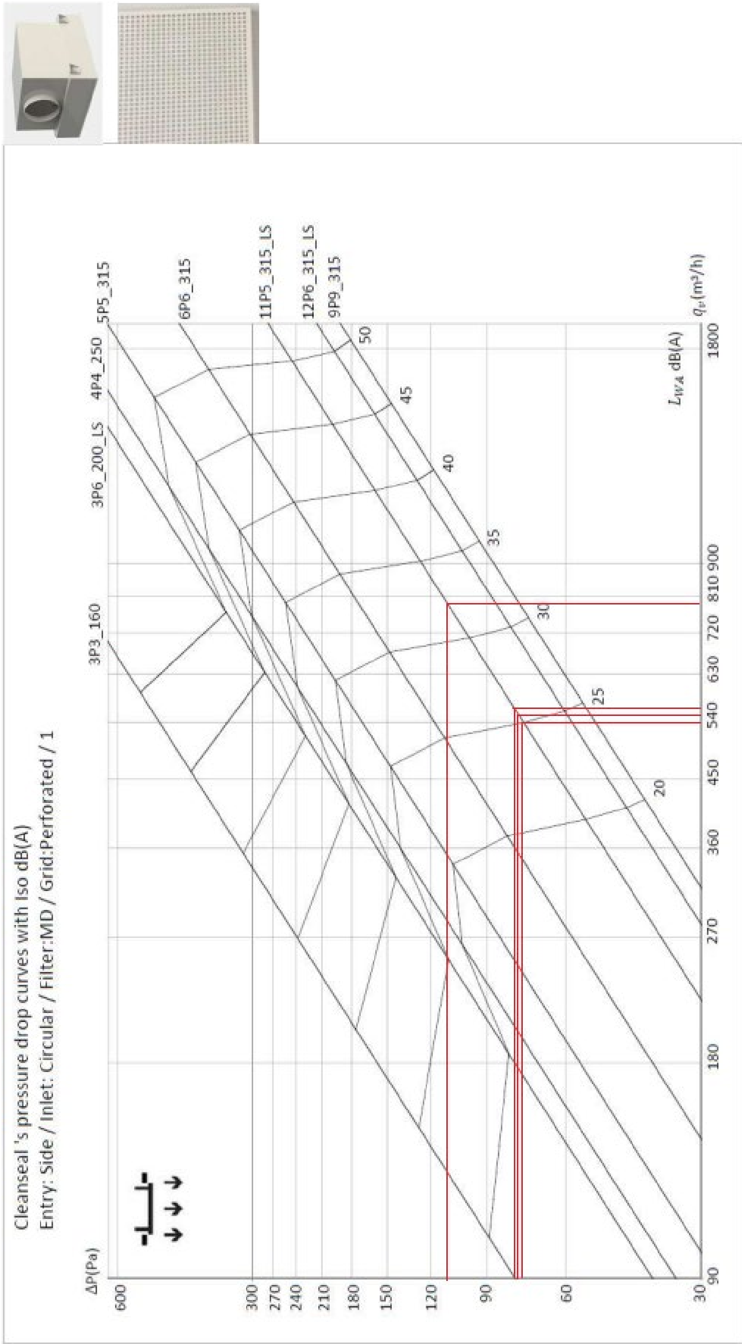

Fig. 10. Side entry supply diffuser choice. Figure adapted from (Camfil, n.d.)

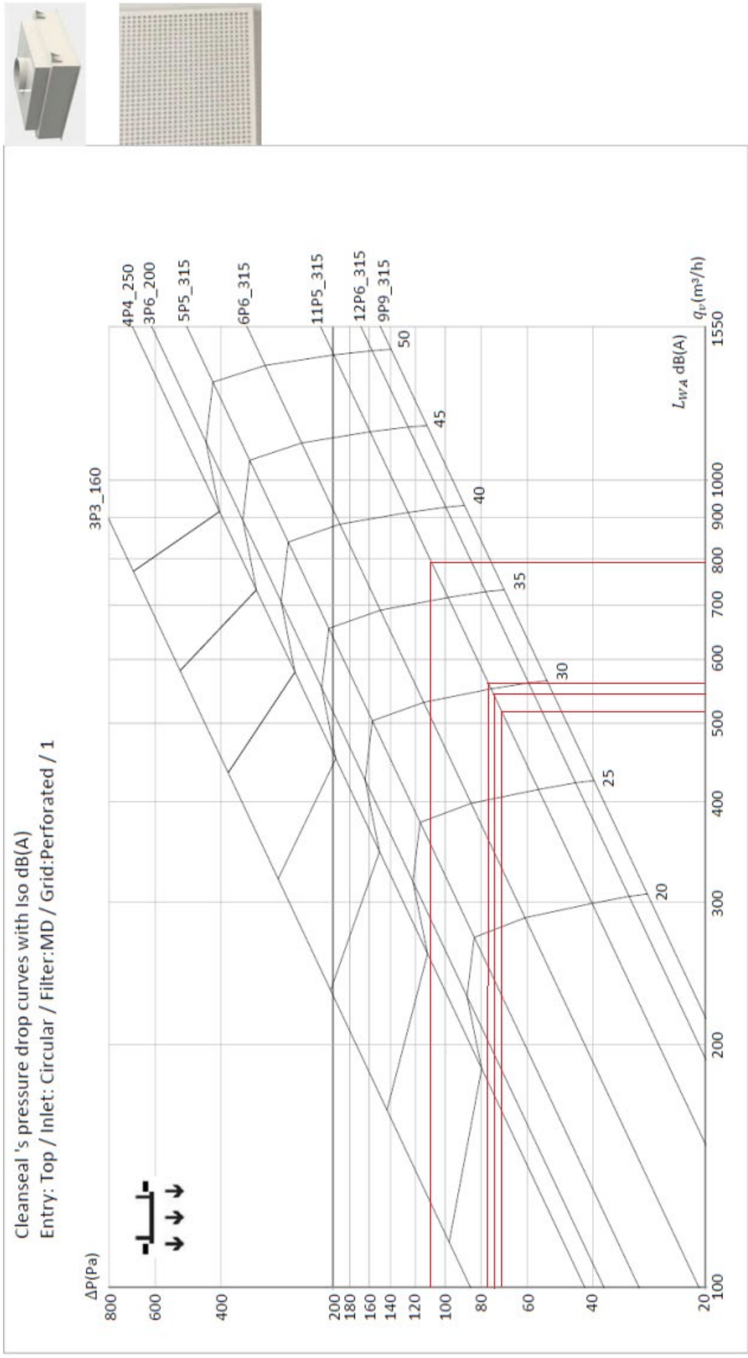

Fig. 11. Top entry supply diffuser choice. Figure adapted from (Camfil, n.d.)

3.4.2 Duct design

As stated in the section 3.4, the locations of the supply and exhaust diffusers remained largely unchanged from the original project. The new duct design mainly incorporates changes to the duct runs and shapes, mostly shifting from rectangular to circular to reduce friction losses (ASHRAE, 2025). Furthermore, when designing the ducts, a specific duct-sizing rule was applied. To avoid having many sizes in a single project, a minimum jump of two sizes was required. To keep the system relatively efficient, the maximum pressure drop was usually maintained within 1-5 Pa/m whenever possible.

Most pressure loss calculations for the runs were performed automatically in Revit, the primary modeling software, and in MagiCAD, which imports mechanical equipment from manufacturers, such as diffusers, AHUs, and others.

According to ASHRAE Fundamentals, the roughness of rectangular and circular ducts for friction-loss calculations in Revit was set to 0.09 mm and 0.05 mm, respectively (ASHRAE, 2025).

As Revit, in terms of airflow values, uses liters per second [l/s] and all the values in the following tables and in the received project technical specifications were in cubic meters per hour [m^3/h], a conversion must have been calculated with a use of equation (4) below.

Firstly, an initial sketch was created of the supply runs leading from the main T-junction to the diffusers. Starting with the supply side was necessary because the number of supply diffusers was relatively high compared to the number of exhaust diffusers. Across the entire project, there are exactly 39 supply diffusers and only seven exhaust diffusers. A sketch of the supply run is shown in Fig. 12.

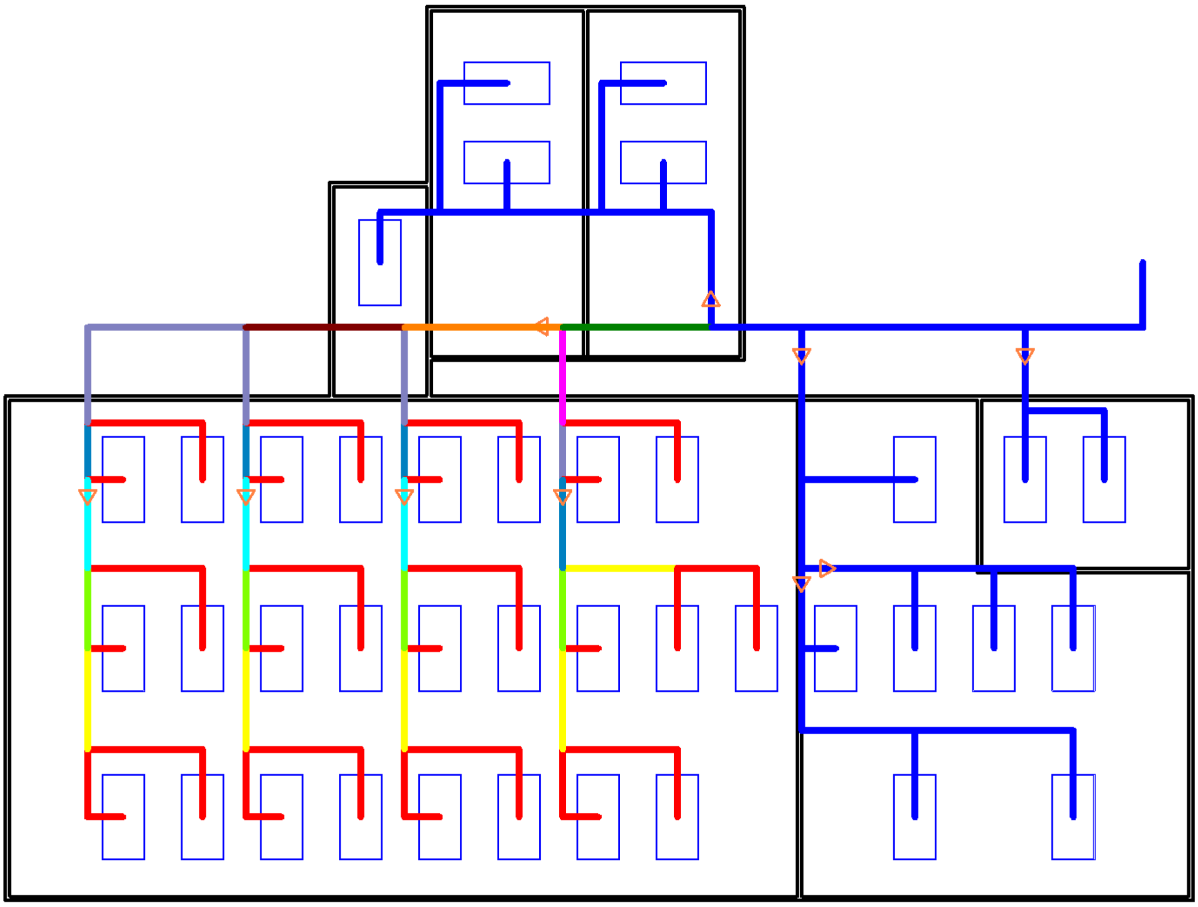

Fig. 12. Initial supply ducts principal schematic

Furthermore, after the initial principal schematic was completed, a 3D model of the supply runs and the duct design was being prepared. These, as stated before, were done at the same time because Revit automatically calculated pressure losses during modeling, allowing the ducts to be dimensioned along the way and thus bypassing the need to use the ASHRAE friction-loss graph, or the original form of Darcy-Weisbach equation (ASHRAE, 2025), (Darcy, 1856). After the supply side was finished, exhaust ducting was fitted into the 3D model in the same manner as the supply side. The finished ducting system in 3D view is shown in Fig. 13.

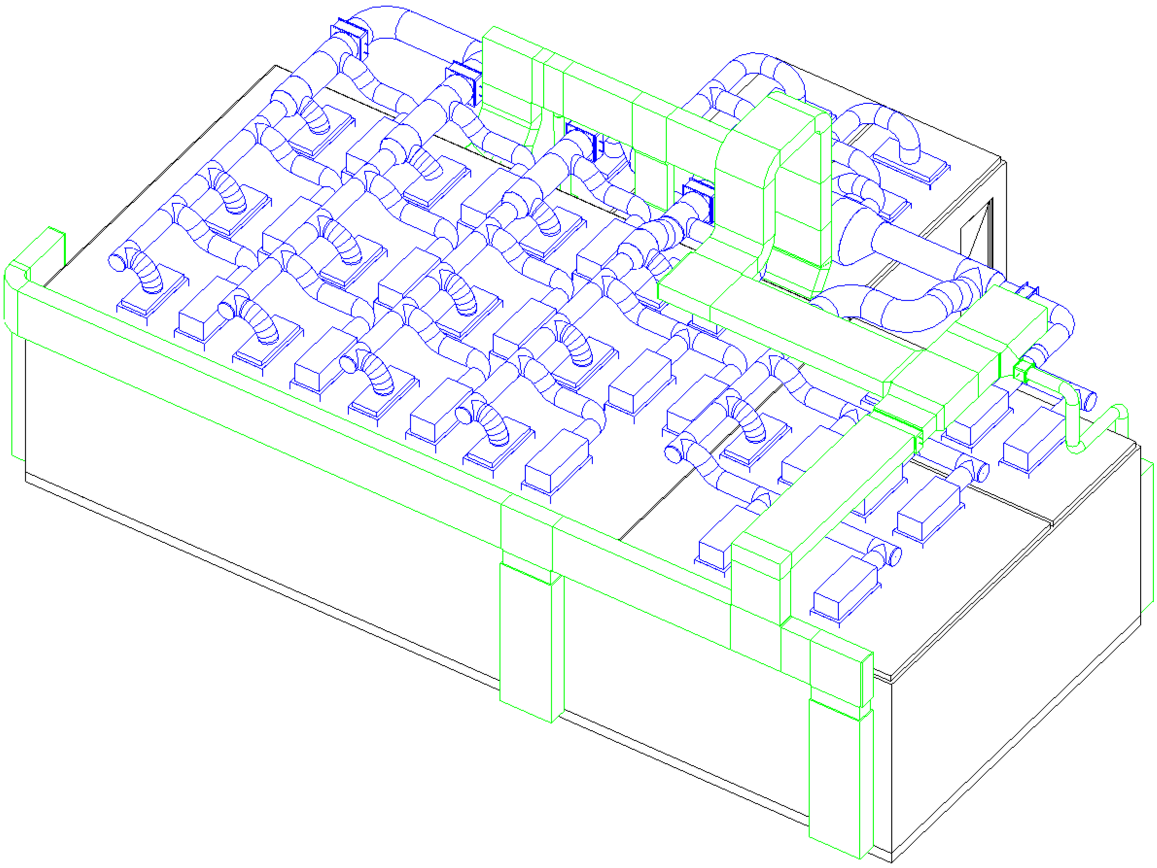

Fig. 13. 3D view of finished ducting

More detailed information that was used while designing the ducting system can be seen in Table 14 and Table 15. The tables specify which diffuser types were used in different rooms, their corresponding pressure drops, the airflow each diffuser provides, and the operational noise for supply diffusers. It is important to note that for exhaust diffusers, the pressure drop was assumed to result solely from the presence of HEPA filters. This was because the exhaust diffusers were products specifically made for this project and did not include a technical specification list. Meaning that if the diffuser type is a 4-way diffuser, it has four face plates sticking into the room and features 4 HEPA filters. Each HEPA filter was designed to have a 65 Pa pressure drop. If the pressure drop of a filter is multiplied by the number of face plates, the final designed pressure drop is 260 Pa. This conclusion was based on information received from a company supervisor and applied to both centralized and decentralized system design evaluation.

Lastly, due to an unresolved issue with the default duct family setup in Revit, none of the fitting pressure drops were calculated automatically. The solution was to set an assumed pressure drop for each fitting, which was then used to calculate the pressure drop across all analyzed project variants for consistency. Assumed pressure drops of fittings can be seen in Table 16.

The final pressure drop of a fitting was assumed to be the product of the pressure drop of the leading duct with the highest airflow and the assumed multiplication factor.

$$V\left[\frac{l}{s}\right] = \frac{V\left[\frac{m^3}{h}\right] \times 1000}{3600} \tag{4}$$

In this Equation, *V* corresponds to the volumetric flow.

Table 14. Supply diffusers with a side and top connection

Room	Airflow/diffuser/ (m^3/h)	Number of diffusers	ΔPa diffuser/ Pa	Operational noise dB(A)
Side- C				
Cleanroom 1	541	13	82	29
Cleanroom 2	560	5	85	31
Material Lock	521	2	80	27
Top- C				
Room	**Airflow/diffuser/ (m^3/h)**	**Number of diffusers**	**ΔPa diffuser/ Pa**	**Operational noise/ dB(A)**
Cleanroom 1	541	12	75	29
Cleanroom 2	560	2	78	31
Personnel Lock 1	795	1	110	34
Personnel Lock 2	561	2	78	31
Dressing Room	548	2	76	30

Table 15. Exhaust diffusers

Room	Type	Number of diffusers	Airflow/diffuser/ (m^3/h)	ΔPa diffuser/ Pa
Cleanroom 1	4-way diffuser	4	3 040	260
Cleanroom 2	4-way diffuser	1	3 530	260
Material Lock	2-way diffuser	1	940	130
Personnel Lock 2	2-way diffuser	1	1 010	130
Personnel Lock 1	2-way diffuser	1	720	130
Dressing Room	2-way diffuser	1	990	130

Table 16. Assumed pressure drop multiplication for fittings

Fitting name	Assumed pressure drop multiplication
Tee	**15**
Elbow	**10**
Reduction	**2**
Y-junction	**8**

3.4.3 Centralized AHU design configuration

Compared to a decentralized system, in which the air is conditioned outside the AHU and most of the airflow is supplied by FFUs, a centralized system combines both functions into a single, larger AHU. This AHU was designed to handle and air-condition the whole 21 493 m^3/h of air.

In this stage, two systems were used to dimension the AHU. One way to get a general idea of how the air behaves was to draw the conditioning process on a Mollier diagram; the other was to create a complete, functional design in SystemAirCAD.

SystemAirCAD automatically calculated the fan power and specific fan power (*SFP*); there was no need to hand-calculate these two, and thus their equations and calculation methodology are not mentioned in this section.

Moreover, LadyBug tools were used to assess worst-case scenarios for seasonal weather.

Firstly, to properly dimension the AHU for extreme weather conditions, weather data were analyzed using Ladybug Tools. The EPW file was downloaded from the Climate One Building website repository, from an undisclosed location near the project site. The seasonal weather conditions can be seen in Table 17 (OneBuilding.org, 2024).

Based on the technical documentation received for the project, both cleanrooms must be conditioned to 19°C ±3°C and 40-60% RH.

As stated previously, 90% of the air (19 360 m^3/h) is recirculated back into the various spaces, which means a mixing station, either inside or outside the AHU, must be installed. This means the AHU does not need any additional heat recovery device installed, as 10% of the remaining air (2133 m^3/h) supplied from the exterior is mixed directly with the air from the spaces.

Moreover, while the AHU was designed to handle a maximum RH of 34.3% during summer peak, conditions such as rain during warm seasons can drive the humidity even higher. To solve this issue, the AHU was configured with two intakes: one from the exterior for normal operation and a second for the extreme-case scenario, in which the air is drawn from inside the production building, where the cleanrooms are located. This, in turn, protects the delicate air conditions required for the manufacture of medical packaging against plausible extremes. This feature was implemented based on the company's supervisor's consultancy advice, who also said that the same system is implemented in the current configuration of the decentralized system.

For proper Mollier diagram construction, both exterior and interior (exhaust-air) conditions were required. This indoor exhaust temperature is 294.5 K (21.3°C), based on the CFD analysis results for the decentralized system. This value remains relevant for the centralized system, as the airflow and heat loads in the cleanrooms were the same for both systems.

To convert volumetric flow to mass flow for calculating the enthalpy of the mixed air, the mass flow of dry air was calculated using equation (5). With this value, the mass of water vapor was calculated separately in equation (6), where specific humidity [Kg/Kg] was obtained from the Mollier Diagram, and the two values were then multiplied to obtain the mass flow of water vapor. Lastly, the mass flow of dry air was added to that of water vapor to obtain the overall mass flow of air.

Since the exterior and interior air are mixed, equation (7) was used to determine the air state at the AHU mixing station.

After the enthalpies of the conditioned air were determined from the Mollier Diagram, equation (8) was used to determine the power requirements for the heating and cooling coils.

A complete Mollier Diagram air-conditioning scheme can be seen in Appendix B and Appendix C.

Furthermore, the second stage of the AHU design involved entering all air-conditioning information into SystemAirCAD. The workflow in this software was divided into two steps: the first is called "Default values", where target supply temperatures for both seasons are primarily set up, and the second is called “Drawing”, where information such as pressure drop of ducting, airflows, type of unit, and unit-specific air conditioning was specified.

In the “Default values” section, the target supply temperature was set to 19°C for both seasons. This was in line with the cleanroom's design requirements as outlined in its technical documentation. Due to the centralized nature of the system, other spaces in the project, such as dressing rooms, material locks, and personnel locks, will be air-conditioned to the same standard as the cleanrooms; in the decentralized system, external cooling towers are provided on a room-by-room basis. In that system, all rooms except cleanrooms were maintained at 22°C and 40-60% RH.

In the “Drawing” section, the larger unit, called “Geniox-2” size 27, was selected for its ability to achieve the desired volumetric flow. The graph of sizes can be seen in Fig. 14. Moreover, as SystemAirCAD uses volumetric flow in m^3/s, the conversion from m^3/h was performed using equation (9). The actual values used to dimension the AHU can be seen in Table 18.

Furthermore, the final design of the AHU was based on the Mollier diagram. To ensure the AHU can handle extreme weather conditions beyond its design specifications, components such as fans, heating coils, and cooling coils were assigned a sizing factor of 1.15, resulting in a 15% oversize system capacity.

Final component sizes, AHU schematics, and energy-specific results are presented in the results section.

$$m_a\left[\frac{\mathrm{kg}}{\mathrm{h}}\right] = V\left[\frac{m^3}{\mathrm{h}}\right] \times \rho\left[\frac{\mathrm{kg}}{m^3}\right] \tag{5}$$

In this Equation, m_a represents the Mass flow of dry air, V is the Volumetric Airflow, and ρ corresponds to the Density of air at a specific temperature.

$$m_\omega\left[\frac{\mathrm{kg}}{\mathrm{h}}\right] = m_a\left[\frac{\mathrm{kg}}{\mathrm{h}}\right] \times x\left[\frac{\mathrm{kg}}{\mathrm{kg}}\right] \tag{6}$$

In this Equation, m_w represents the Mass of water vapor, m_a is the Mass flow of dry air, and x corresponds to the Specific Humidity.

$$h_B\left[\frac{\mathrm{kJ}}{\mathrm{kg}}\right] = \frac{(m_A\left[\frac{\mathrm{kg}}{\mathrm{h}}\right] \times h_A\left[\frac{\mathrm{kJ}}{\mathrm{kg}}\right]) + (m_C\left[\frac{\mathrm{kg}}{\mathrm{h}}\right] \times h_C\left[\frac{\mathrm{kJ}}{\mathrm{kg}}\right])}{m_A\left[\frac{\mathrm{kg}}{\mathrm{h}}\right] + m_C\left[\frac{\mathrm{kg}}{\mathrm{h}}\right]} \tag{7}$$

In this Equation, h_B corresponds to the Enthalpy of mixed air, h_A is the Enthalpy of exterior air, h_C represents the Enthalpy of interior air, m_A is the Mass flow of exterior air, and m_C is the Mass flow of recirculated air.

$$P\ [\mathrm{kW}] = V\left[\frac{m^3}{\mathrm{s}}\right] \times \rho\left[\frac{\mathrm{kg}}{m^3}\right] \times \Delta h\left[\frac{\mathrm{kJ}}{\mathrm{kg}}\right] \tag{8}$$

In this Equation, P represents the Power, V is the Volumetric flow, ρ is the Density of air (typically 1.225), and Δh corresponds to the Enthalpy difference.

$$V\left[\frac{m^3}{s}\right] = V\left[\frac{m^3}{h}\right]/3600 \tag{9}$$

In this Equation, V corresponds to the volumetric flow.

Table 17. Seasonal weather from the EPW file (OneBuilding.org, 2024)

Season	Temperature/ °C	Relative Humidity (RH)/ %
Warm season	32	34.3
Cold season	-15	74.7

Table 18. SystemAirCAD "Drawing" input values

Airflow

Position	Volumetric flow/ (m^3/s)
Supply	5.97
Extract	5.38

Pressure Drops

Position	Pressure Drop/ Pa
Before the supply fan	45
After the supply fan	350
Before the extract fan	450
After the extract fan	40

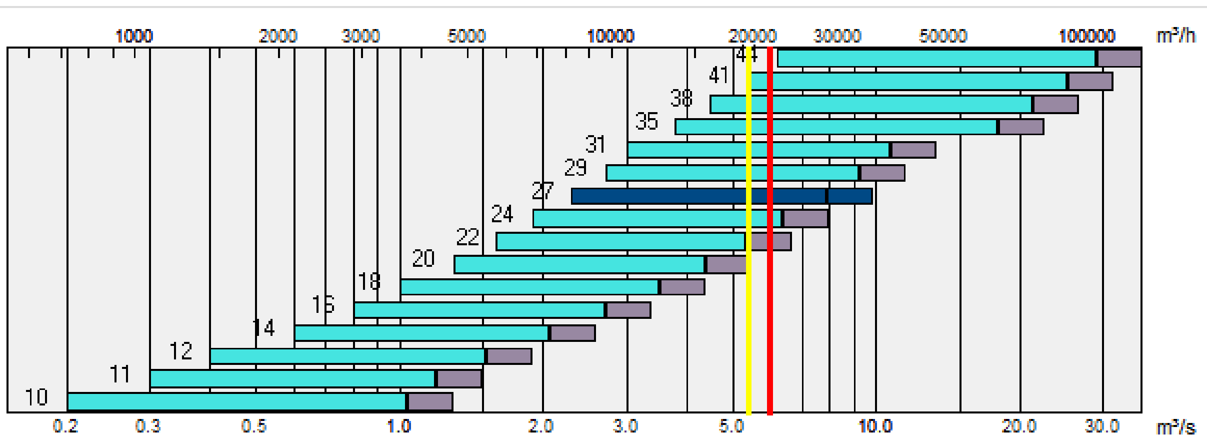

Fig. 14. Chosen Geniox-2 size, based on airflow

3.5 Decentralized HVAC – Energy Analysis

For an economic comparison between the existing decentralized system and the new, hypothetical centralized system within the same boundaries, two energy metrics were examined: annual fan electric power and annual AHU conditioning power. The sum of these two metrics was referred to as annual energy usage.

3.5.1 Specific Fan Power

To determine the annual fan electrical power, the system's specific fan power was calculated. Annual fan electric power was defined by equation (10).

Specific fan power was calculated using equation (11). To determine the *SFP* of the existing decentralized system, pressure losses for ducting, filters, fans, technical units, ducting accessories, fittings, supply units, and recirculation towers were accounted for. The decentralized ventilation system in question comprised 40 fans: 1 in the AHU and 39 in the FFUs. Therefore, not only was the pressure loss along the system's critical path identified and calculated, but it was also calculated for all branches of the system.

In accordance with guidance from the partner company, a fan efficiency of 0.7 was assumed for the AHU fan, while a fan efficiency of 0.6 was assumed for the FFU fan. These values were incorporated into equation (12), which serves for fan power calculations.

As mentioned in the initial description of the HVAC strategy for the existing system in chapter 2.3, the AHU is responsible for fresh air delivery up to the mixing station located before the internal cooling unit, identified as 1.3 on the HVAC plans available in Appendix G. Subsequently, the critical path of the AHU was determined to be a branch leading to one of the mixing stations.

The pressure differential required to move air through the recirculation towers and deliver mixed air to the FFUs was provided by the 39 FFU fans. As a result, each FFU branch became its own critical path. As all FFUs within a room delivered the same airflow rate, it was assumed that, within the shared branches, the pressure losses were divided equally among the FFUs connected to those branches.

This strategy led to 40 individual *SFPs*. A simplified comparison to the centralized design was enabled through a new parameter, SFP_{system}. $SFPs_{ystem}$ was defined as the equivalent specific fan power required by the entire decentralized HVAC system to deliver the specified airflow and was calculated using equation (13).

(10)

$$E[kWh] = SFP\left[\frac{\mathrm{kW}}{\frac{\mathrm{m^3}}{\mathrm{s}}}\right] \times \dot{V}\left[\frac{\mathrm{m^3}}{\mathrm{s}}\right] \times t[\mathrm{h}]$$

In this Equation, *E* represents the energy use, *SFP* is the Specific fan power, *V* corresponds to the Air volume flow rate, and *t* is the annual number of hours.

(11)

$$SFP\left[\frac{\mathrm{kW}}{\frac{\mathrm{m^3}}{\mathrm{s}}}\right] = \frac{P[\mathrm{kW}]}{V\left[\frac{\mathrm{m^3}}{\mathrm{s}}\right]}$$

In this Equation, *SFP* represents the Specific fan power, *P* is the Fan power, and *V* corresponds to the Air volume flow rate.

(12)

$$P[\mathrm{kW}] = (\Delta p[\mathrm{Pa}] \times \dot{V}\left[\frac{\mathrm{m^3}}{\mathrm{s}}\right]) / \eta$$

In this Equation, Prepresents the Fan power, $\Delta p$is the Pressure rise across the fan, Vcorresponds to the Air volume flow rate, and η is the Fan efficiency.

(13)

$$\mathrm{SFP}_{\mathrm{System}} = \frac{\sum P[\mathrm{kW}]}{\sum \dot{V}\left[\frac{\mathrm{m}^3}{\mathrm{s}}\right]}$$

In this Equation, SFP_{System} represents the Specific fan power of the system, $\sum P$ is the sum of the fan power of all fans, and $\sum V$ is the sum of the Air volume flow rates of all fans.

3.5.2 Pressure loss calculations

Duct pressure losses for the existing decentralized system were determined using the ASHRAE friction loss chart(ASHRAE, 2025) for round ducts, based on duct diameter and air volume flow rate. Once the value was determined in Pa/m through the chart, it was multiplied by the length calculated extracted from the received plans in running meters; the resulting value was the total pressure loss of the respective branches in Pa.

Air volume flow rates were determined based on the measured air changes per hour for each room. The resulting value for each room was then split equally among the existing FFUs.

Rectangular duct sizes from the project were converted to equivalent diameter for pressure losses using equation (14).

Studies show that pressure losses in flex ducts depend on many factors, such as the fabrication material, the number and angle of bends, diameter, etc. A standard flex duct diameter of 0.16m was encountered in the decentralized design; a pressure loss value of 20 Pa/m is assumed, in line with recent studies (Yu-Ra Son and Jeong-Hoon Yang, 2020).

Table 19 lists assumptions that were made for ducting accessories, air terminal units, filters, and ducting junctions. Technical units, noted 1.1, 1.15, 1.3 and described in chapter 2.3 were incorporated as well.

Given the custom-made nature of the recirculation towers, they were calculated as a sum of all components composing them, namely ducts, filters, and air extraction terminals. No on-site or manufacturer measurements of pressure losses were available.

(14)

$$D_{\mathrm{e}}[\mathrm{m}] = \sqrt{\frac{4 \times W[\mathrm{m}] \times \mathrm{H}[\mathrm{m}]}{\pi}}$$

In this Equation, D_e represents the Equivalent diameter, W is the Duct width, and H corresponds to the Duct height.

Table 19. Pressure loss assumptions – decentralized design

Component	Pressure loss value/Pa
1.1	350
1.15	140
1.3	140
Tee	15
Elbow	10
Diameter reducer	2
Flexible duct	20
H14 Filter	65

Component	Pressure loss value/Pa
FFU	80
Damper FFU	20 Pa
Air extraction terminal	30 Pa

3.5.3 Air conditioning power

Mollier charts for the decentralized design were not available within the existing project material. Therefore, they were roughly reverse-engineered from available project information and schematics to facilitate the calculation of the annual AHU conditioning power. Mollier charts for the decentralized system are shown in Appendix D and Appendix E.

The power needed to condition the air according to the Mollier chart of the system was obtained using equations (15) and (16).

The air density was assumed to be 1.225 kg/m^3. The air volume flow rate was calculated based on the HVAC strategy, which set the fresh air amount to 10% of the total, resulting in 0.597 m^3/s.

A script was built in Grasshopper, using Ladybug and Climate Studio components to determine the outside enthalpy for every hour of the year. Dry-bulb temperature and relative humidity were extracted from the Weather component and plugged into LB Humidity Metrics.

Enthalpy values generated by the LB Humidity Metrics components were plugged into a component that represented equation (15) as the equivalent of h_y. The value for h_x value was the first enthalpy value at which the AHU conditioned the air, as shown on the Mollier chart. After either the positive or negative values were excluded, depending on whether the calculation represented the cooling or heating season, the results were plugged into the Mass Addition component, and a total value was achieved.

As the two Mollier charts for the decentralized system, one for each of the cooling and the heating season, the calculation was split into heating and cooling hours. The number of both cooling and heating hours was determined by subtracting h_y from h_x. Based on the order of parameter connections, values above 0 were considered heating hours, while values below 0 were considered cooling hours. A representation of the script is available in Appendix F.

The power needed for the remaining steps was calculated in a similar manner, with the outside enthalpy replaced by another value from the Mollier chart corresponding to the number of cooling or heating hours defined in the first step.

Although defined on the Mollier chart, given the system's decentralized nature, air conditioning beyond the mixing stage was provided by the internal cooling unit, identified as 1.3 on the HVAC drawings. The physics principles were the same; regardless, the calculation was performed as described. However, the air volume flow rate changes to 5.97 m^3/s, as the recirculated air was included in the enthalpy step.

$$P[\mathrm{kW}] = \dot{m}\left[\frac{\mathrm{kg}}{\mathrm{s}}\right] \times \left(h_{\mathrm{x}}\left[\frac{\mathrm{J}}{\mathrm{kg}}\right] - h_{\mathrm{y}}\left[\frac{\mathrm{J}}{\mathrm{kg}}\right]\right) \tag{15}$$

In this Equation, P represents the Power, $\dot{m}$ is the Mass flow rate of air, h_x corresponds to the Specific enthalpy of the air at the X state, and h_y is the Specific enthalpy of the air at the Y state.

$$\dot{m}\left[\frac{\mathrm{kg}}{\mathrm{s}}\right] = \rho\left[\frac{\mathrm{kg}}{\mathrm{m}^3}\right] \times \mathrm{V}\left[\frac{\mathrm{m}^3}{\mathrm{s}}\right] \tag{16}$$

In this Equation, $\dot{m}$ represents the Mass flow rate of air, ρ is the Density of air, and V corresponds to the Air volume flow rate.

3.6 Centralized HVAC energy scrutiny

The energy required by the centralized HVAC system was determined using a methodology similar to that described for the decentralized HVAC system. The same two metrics were scrutinized, namely annual fan electric power and annual AHU conditioning power.

The total annual energy usage for the centralized system was defined as the sum of the annual fan electric power and the power required by the AHU to condition the fresh air, as determined from the Mollier charts for the centralized HVAC system.

The same equations (10), (11), (12) were used to determine the Annual fan electric power, representing the ventilation fans' annual electricity usage.

Regarding the power needed for the AHU to condition the fresh air, the process presented a key difference. The calculation was still governed by equation (15). Nonetheless, as described already in chapter 3.4, the fresh air was mixed with the recirculated air before conditioning. Therefore, the number of heating and cooling hours was no longer defined by the number of positive or negative values resulting from the difference between the internal and external enthalpies.

The only difference between the heating and cooling seasons in the Mollier charts for the centralized HVAC system was the enthalpy due to mixing fresh and recirculated air. The provided values represented the extremes when recirculated air was mixed with fresh air, namely the lowest and highest temperatures for which the system was designed. These values were obtained using equation (7) for mixed air. Subsequently, the average enthalpy between the two extremes was used to calculate the power required to condition the air for each step on the Mollier chart over the entire year.

The remaining air conditioning steps were accounted for in the same manner as in the decentralized chapter.

3.7 Life cycle cost (LCC)

3.7.1 LCC Strategy

Life-cycle costs were analyzed for both HVAC systems to enable comparison between the two from an economic perspective. This assessment was performed in Slovakia's local currency, the Euro.

The life-cycle cost was defined as the sum of the initial investment and the annual operating energy cost. This calculation was performed over a 20-year period.

Four different scenarios were analyzed from a discount interest rate perspective. Scenario 1 represented a world in which real energy prices remained unchanged. In Scenario 2 and Scenario 3, energy became more expensive over time, and their values were arbitrarily chosen based on inflation fluctuations in Slovakia over the past 30 years (Statista Research Department, n.d.). Scenario 4 represented a world in which energy became increasingly cheap over time and was purely speculative.

3.7.2 HVAC systems running cost

Regarding annual energy usage, the energy price was determined based on the local market. According to data from June 2025, the price for one kWh of electricity for a business user was 0.16 EUR ("Slovakia electricity prices," 2025).

Since the annual fan electric power obtained from equation (12) already accounts for fan efficiency, the resulting values represent the gross energy. On the other hand, the AHU conditioning power results obtained using equation (15), did not account for coil efficiency and represented net energy values. To obtain gross values for an LCC analysis, coil efficiency was introduced, as shown in equation (17).

To determine the 20-year running cost based on the annual energy usage results of the two HVAC systems, equations (18), (19), (20), and (21) were used. A summary of all rates for the four scenarios is available in Table 20.

$$P[\text{kW}] = \frac{\dot{m}\left[\frac{\text{kg}}{\text{s}}\right] \times \left(h_{\text{x}}\left[\frac{\text{J}}{\text{kg}}\right] - h_{\text{y}}\left[\frac{\text{J}}{\text{kg}}\right]\right)}{\eta_{coil}} \tag{17}$$

In this Equation, P represents the Power, $\dot{m}$ is the Mass flow rate of air, h_x corresponds to the Specific enthalpy of the air at the X state, h_y is the Specific enthalpy of the air at the Y state, and η_{coil} corresponds to coil efficiency.

$$PV_i[\text{EUR}] = \frac{c_i[\text{EUR}]}{(1 + r_{di})^n} \tag{18}$$

In this Equation, PV_i represents the Present value of an expenditure occurring after n years, C_i is the Expenditure in today's value, r_{di} corresponds to the Discount interest rate, and n is the Number of years.

The discount interest rate is defined as:

$$r_{di} = r_r - r_{pi} \tag{19}$$

In this Equation, r_{di} represents the discount interest rate, r_r is the Real interest rate, and r_{pi} corresponds to the Real price increase of a certain thing.

$$r_r = r_n - r_f \tag{20}$$

In this Equation, r_r represents the Real interest rate, r_n is the Nominal interest rate, and r_f corresponds to the Inflation.

$$r_{pi} = r_{ci} - r_f \tag{21}$$

In this Equation, r_{pi} represents the Real price increase of a certain thing, r_{ci} is the Nominal price increase of a certain thing, and r_f corresponds to the Inflation.

Table 20. Life cycle cost rates

Scenario	**1**	**2**	**3**	**4**
Nominal Interest rate	0.03	0.04	0.01	0.01
Inflation	0.04	0.08	0.02	0.02
Nominal price increase of energy	0.03	0.06	0.02	-0.02
Real price increase of energy	-0.01	-0.02	0.00	-0.04
Real interest rate	-0.01	-0.04	-0.01	-0.01
Real discount rate	0.00	-0.02	-0.01	0.03

3.7.3 HVAC systems initial investment

The initial investment cost was calculated as the sum of the following components and their quantities in the HVAC design: ducting, ducting junctions, air terminal units, air conditioning units, and filters. Recirculation towers were included in the calculation based on the individual components.

The following components were excluded from the initial cost calculation: mounting, connecting, and sealing materials; hanging and anchoring materials; pipe insulation, sensors, and additional secondary items in general. They were presumed to be similar for both systems.

Craftsmanship for installation was presumed similar and excluded from the initial cost calculation. Therefore, only the stated equipment was considered, not its subsequent installation.

According to the partner company, maintenance for the client was provided by a third party on a monthly fee basis. This fee was paid regardless of whether maintenance was needed, and when it was, no additional cost was incurred. The value of this fee and the maintenance fee for the centralized HVAC system were unknown. Therefore, it was assumed that the maintenance fee for both systems was the same. Subsequently, maintenance is excluded from the analysis.

Prices for the existing decentralized system were based on the actual construction cost obtained from the partner company. While prices for the new centralized system were based on data from the partner company, where applicable, or assumptions from the partner company based on their market data and experience, where not applicable. VAT was excluded.

In terms of quantities, for the decentralized project, the same amounts were used as in the pressure loss calculation, while for the centralized project, quantities were extracted directly from the 3D Revit model.

Table 21 lists the type, quantity and price of components encountered in the decentralized HVAC design, while Table 22 presents the same data for the centralized HVAC design.

Table 21. Component price assumptions - decentralized design

Type	Item	Quantity	Price per unit/ EUR
Ducts	160 mm	28.2 m	17
	160 mm (flex)	43.4 m	16
	200 mm	14.3 m	21
	315 mm	1.5 m	41
	400x100 mm	2.6 m	45
	315x200 mm	10.7 m	47
	400x250 mm	8.6 m	59
	630x250 mm	3 m	79
	400x400 mm	2.8 m	72
	500x400 mm	1.1 m	81
	612x407 mm	7.8 m	92
	630x400 mm	8 m	93
	920x315 mm	28 m	100
	626x726 mm	23.6 m	122

Type	Item	Quantity	Price per unit/ EUR
Elbows	160 mm	23 pcs.	29
	200 mm	12 pcs.	38
	400x100 mm	1 pcs.	40
	315x200 mm	3 pcs.	42
	400x250 mm	2 pcs.	55
	630x250 mm	2 pcs.	78
	612x407 mm	2 pcs.	90
	630x400 mm	14 pcs.	95
	920x315 mm	12 pcs.	115
	626x726 mm	7 pcs.	130
Diameter reducer (transition)	160 mm	30 pcs.	26
	200 mm	4 pcs.	53
	400x100 mm	1 pcs.	33
	315x200 mm	6 pcs.	35
	400x250 mm	1 pcs.	45
	630x250 mm	1 pcs.	69
	400x400 mm	3 pcs.	63
	612x407 mm	1 pcs.	81
	630x400 mm	5 pcs.	84
Tee	160 mm	1 pcs.	74
	200 mm	1 pcs.	78
	400x250 mm	1 pcs.	75
	400x400 mm	1 pcs.	95
	630x400 mm	1 pcs.	130
Air terminal units	FFU	39 pcs.	1 750
	Diffuser	1 pcs.	500
	Exhaust unit	29 pcs.	200
Air conditioning unit	1.1	1 pcs.	21 800
	1.12	1 pcs.	7 450
	1.13	2 pcs.	7 450

Type	Item	Quantity	Price per unit/ EUR
	1.14	3 pcs.	7 850
	1.15	2 pcs.	220
	1.2	2 pcs.	4 250
	1.3	5 pcs.	3 350
	1.31	1 pcs.	6 100
	1.7	1 pcs.	7 500
Accessories	Silencer	4 pcs.	850
	H14 Filter	67 pcs.	550
	Damper	43 pcs.	100

Table 22. Component price assumptions – centralized design

Type	Item	Quantity	Price per unit/ EUR
Ducts	160 mm	1.5 pcs.	17
	160 mm (flex)	0.3 pcs.	16
	200 mm	3.3 pcs.	21
	315 mm	47.9 pcs.	41
	315 mm (flex)	7 pcs.	31
	500 mm	9.9 pcs.	78
	1000 mm	3.9 pcs.	205
	612x200 mm	3.4 pcs.	65
	612x407 mm	3.4 pcs.	100
	920x315 mm	48.9 pcs.	100
	1000x500 mm	1.7 pcs.	120
	2700x1200 mm	3.1 pcs.	400
Elbow	160 mm	2 pcs.	29
	200 mm	3 pcs.	38
	315 mm	51 pcs.	60
	500 mm	7 pcs.	130
	612x200 mm	3 pcs.	70
	920x315 mm	11 pcs.	115

Type	Item	Quantity	Price per unit/ EUR
Diameter reducer	315 mm	2 pcs.	55
	500 mm	7 pcs.	140
	1000 mm	2 pcs.	340
	612x200 mm	1 pcs.	65
	920x315 mm	1 pcs.	100
	1000x500 mm	1 pcs.	175
	2700x1200 mm	1 pcs.	510
Tee	315 mm	31 pcs.	180
	500 mm	12 pcs.	300
	1000 mm	3 pcs.	670
	612x200 mm	1 pcs.	95
	920x315 mm	7 pcs.	160
	1000x500 mm	2 pcs.	600
Air terminal units	Cleanseal T-C PF	20 pcs.	1 150
	Cleanseal S-C PF	20 pcs.	1 150
	Exhaust unit	24 pcs.	200
Air conditioning unit	Geniox-2, size 27	1 pcs.	75 000
Accessories	Damper	8 pcs.	100
	Endcap	3 pcs.	65
	H14 Filter	63 pcs.	550

4 Limitations

Despite the methods employed in this thesis, several limitations must be noted given the project's specific origins.

Firstly, most of the prices used to calculate the LCC of the centralized systems are based on the partner company's assumptions. As it is not possible to determine accurate, comparable installation and maintenance costs for the centralized system, these costs were excluded from the initial investment for both designs. These factors may influence life-cycle cost results.

The fact that the initial cost calculation for the decentralized design may be more accurate than the initial cost calculation of the centralized design, as it represents a project that actually exists and probably incorporates more analyses for parameters that are not included in this study, while the centralized design is theoretical and may suffer changes once more parameters are taken into account.

"Anything that can go wrong will go wrong." ("Murphy's law," n.d.). The life-cycle cost analyses assume maintenance will be equally expensive in both scenarios due to a lack of data, whereas the decentralized system, with its more complex components distributed across different locations that must be easily accessible, might require more maintenance. More components, especially complex ones, increase the likelihood of component failure; therefore, maintenance is needed.

Secondly, the received decentralized project did not include any specific energy measures or a relevant Mollier diagram, necessitating reverse-engineering the Mollier diagram and calculating the energy based on enthalpy over the entire year. This may lead to discrepancies with the system's actual energy use.

Thirdly, the energy scrutiny of the centralized system assumes that the average enthalpy resulting from mixing outside air at the coldest or warmest moment of the year is a sufficient measure to determine the air-conditioning power for the respective step. This could be improved by calculating the mixed-air enthalpy for all 8 760 hours in a year, rather than only at the extreme points.

A potential energy-use reduction measure that this study does not investigate is changing the air supply temperature. Improvements could potentially paint a slightly different picture when comparing the two systems from an energy perspective.

Lastly, due to time constraints, only one CFD study on top of the existing system was completed, which is insufficient to draw any specific conclusions about whether the system can or cannot be improved with respect to the given parameter type.

5 Results

5.1 Computational Fluid Dynamics – Existing project

5.1.1 Cleanroom 1

The CFD analysis of Cleanroom 1 yielded results shown in Table 23.

All results are presented as volume averages, meaning the average state across the entire area is considered. All results are scrutinized based on the technical documentation received for the original project.

Pressure is maintained at 46.8 Pa, above the originally designed >30 Pa threshold, and validated at 44.4 Pa, highlighting the effectiveness of the cleanroom's pressure cascade system and confirming the validity of CFD analysis. Temperature, however, comes close to the design limit of 19°C ±3°C, hovering at 21.3°C, suggesting relatively high internal heat gains for the given ACH or cooling capacity. The mean interior velocity is 0.294 m/s^{-1}, representing the global air movement for the entire cleanroom 1 volume. Moreover, the Age of Air analysis suggests that air entering the cleanroom through the supply FFU units does not remain inside longer than 60.7 seconds on average. The maximum amount of time the air stays is 138.15 seconds. Lastly, the unidirectionality of air is average, falling roughly midway between unidirectional and non-unidirectional flow.

Moreover, Fig. 15, Fig. 16, and Fig. 17 show visualizations of average values and simulated results for the age of air, *UDAF*, and air velocity project. The supply diffusers are highlighted in white, while the exhaust panels are highlighted in green.

Table 23. Cleanroom 1 CFD analysis results

Analysis	**Volume average**
Pressure	46.8 Pa
Temperature	294.5 K = 21.3 °C
Interior air velocity	0.294 m/s
Age of air	60.7 s
UDAF	0.099

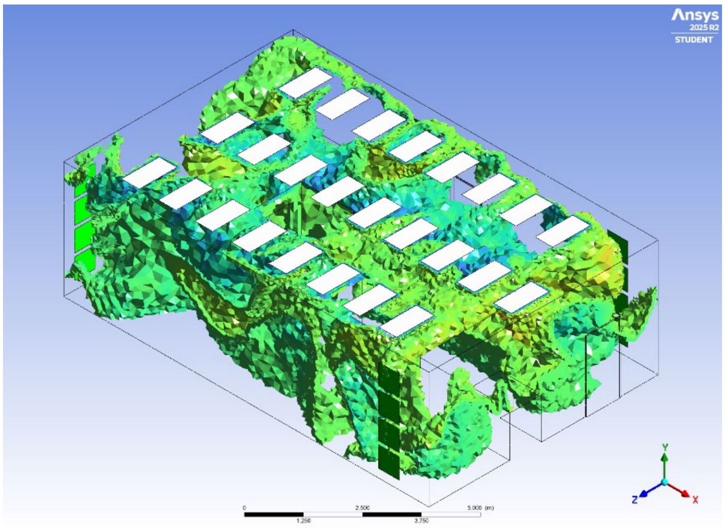

Fig. 15. Age of air, isosurface depicting average value

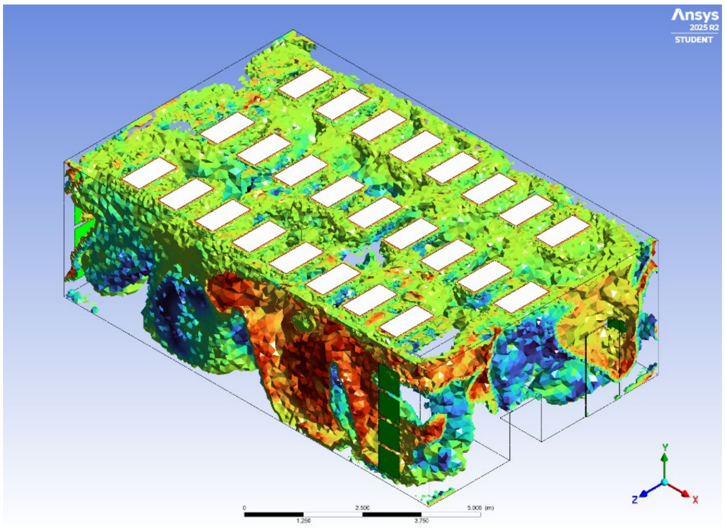

Fig. 16. UDAF, isosurface depicting average value

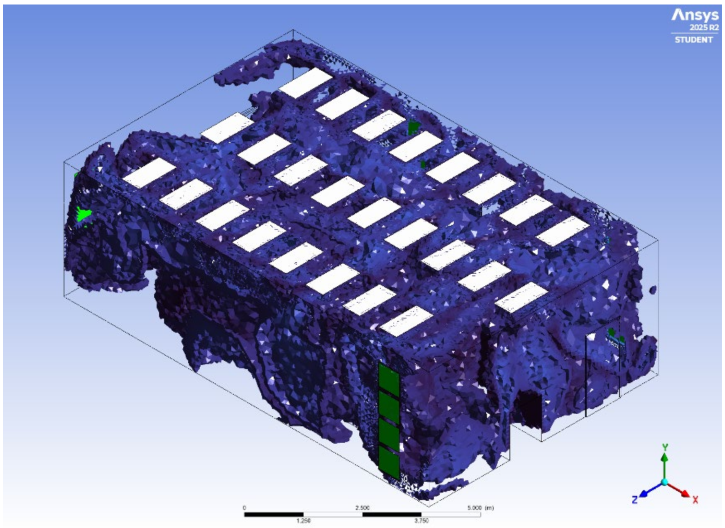

Fig. 17. Velocity, isosurface depicting average value

5.1.2 Cleanroom 2

The CFD analysis of Cleanroom 1 yielded results shown in Table 24.

All results are presented as volume averages, meaning the average state across the entire area is considered. All results are scrutinized based on the technical documentation received for the original project.

Pressure is maintained at 35.5 Pa, above the originally designed >20 Pa threshold, and validated at 35.4 Pa, highlighting the effectiveness of the cleanroom's pressure cascade system and confirming the validity of CFD analysis. Temperature, due to the lack of any meaningful heat load inside Cleanroom 2, stays planted at the designed 19°C. The mean interior velocity is 0.114 m/s^{-1}, representing the global air movement for the entire cleanroom 1 volume. Moreover, the age of air analysis suggests that air entering the cleanroom through the supply FFU units does not remain inside for more than 93.8 seconds on average. The maximum amount of time the air stays is 473.94 seconds. Lastly, the unidirectionality of air is average, staying roughly within the middle bounds between unidirectional and non-unidirectional flow.

Moreover, Fig. 18, Fig. 19, and Fig. 20 show visualizations of average values and simulated results for the age of air, *UDAF*, and air velocity project. The supply diffusers are highlighted in white, while the exhaust panels are highlighted in green.

Table 24. Cleanroom 2 CFD analysis results

Analysis	Volume average
Pressure	35.5 Pa
Temperature	292.2 K = 19.1 °C
Interior air velocity	0.114 m/s
Age of air	93.8 s
UDAF	0.075

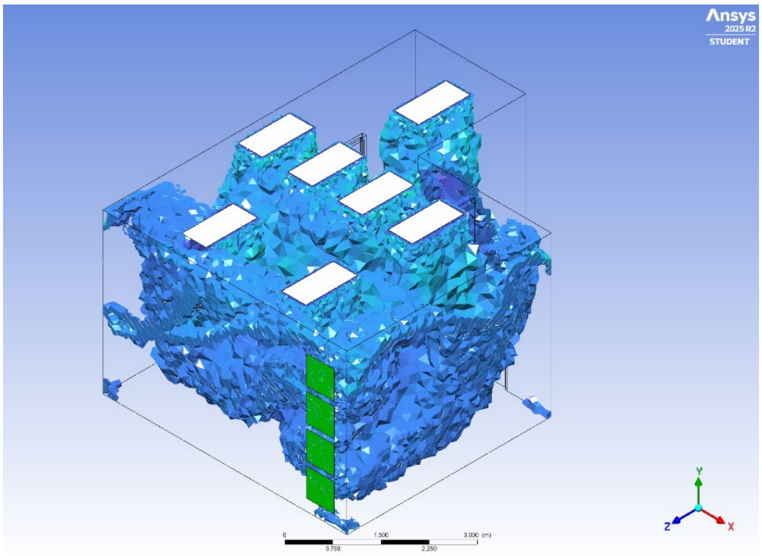

Fig. 18. Age of air, isosurface depicting average value

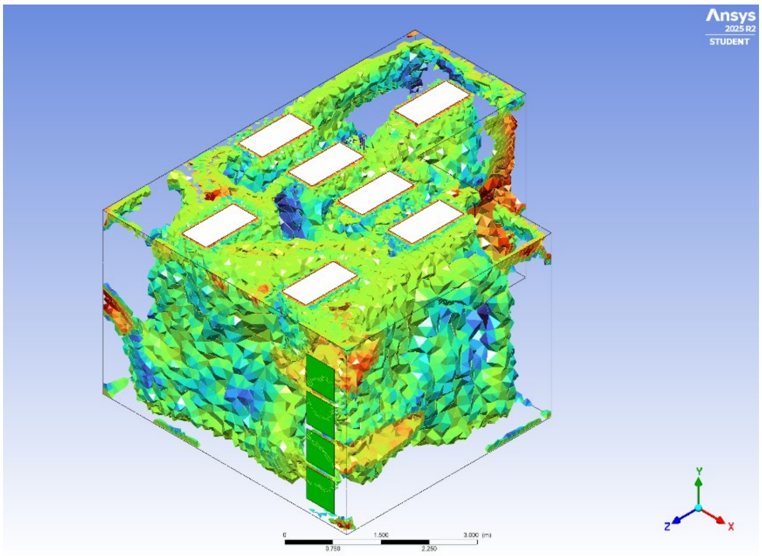

Fig. 19. UDAF, isosurface depicting average value

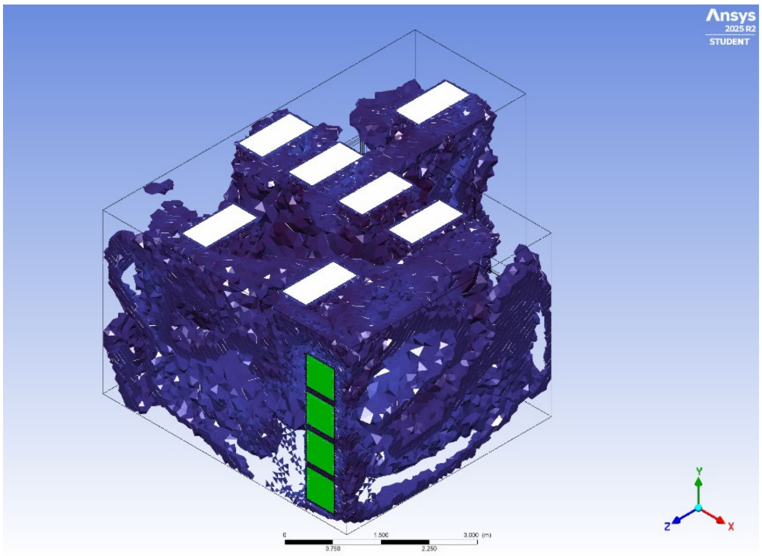

Fig. 20. Velocity, isosurface depicting average value

5.2 Air behavior study results

5.2.1 Scenario one results

As stated in the methodology section of this part of the report, only numerical results are considered in this study.

All of the results represent volume averages of the Cleanroom 1 environment and can be seen in Table 25.

Table 25. Scenario one results

Parameter	Value
Age of Air	53.44 s
UDAF	0.029

5.3 Centralized system design

5.3.1 Mollier diagram

Table 26 represent data gathered from the Mollier diagram during the conditioning process of air during summer exterior and winter exterior conditions, respectively. To calculate the required power for the cooling and heating coils, an atmospheric pressure of 1 013 mbar and an airflow of 5.97 m^3/s are used.

The air-conditioning process inside the AHU is the same in both the cold and warm seasons; only the required power to achieve the same enthalpy differs.

In both scenarios, exterior air is first mixed with exhaust air from cleanrooms. After that, the air travels through the cooling coil, which brings it down to the desired temperature's dew point, where it is heated again to one degree below the desired temperature, as the fan motor provides the remaining heating. The mixing process, along with all air conditioning, can be found in Appendix A.

In summer, or the cooling season, the power requirement for the cooling coil is 124.3 kW, and for the heating coil, 70.9 kW. On the other hand, during winter, or the heating season, the required cooling power drops to 71.4 kW, while the required heating power remains the same at 70.9 kW.

Meaning, the final power used in the AHU is 124.3 kW for the cooling coil and 70.9 kW for the heating coil.

Both Mollier diagrams visualizing the air-conditioning process are shown in Appendix B and Appendix C.

Table 26. Mollier diagram data for the summer conditioning process

Summer conditioning process				
Point	**Point explanation**	**Temperature/ °C**	**RH/ %**	**Enthalpy/ (kJ/kg)**
1	State of the air after being extracted from the Cleanroom	21.3	50	41.4
2	State of the air after the extract fan heat gain	22.3	47	42.5
3	State of the air supplied from outside	32	34.3	58.2
4	State of the air after mixing the extract with the outside air	22.7	46.1	42.91
5	State of the air after cooling coils	8.3	100	25.6
6	State of the air after heating coils	18	53.5	35.5
7	Final state of the air after the supply fan's heat gain	19	50	36.4
Winter conditioning process				
Point	**Point explanation**	**Temperature/ °C**	**RH/ %**	**Enthalpy/ (kJ/kg)**
1	State of the air after being extracted from CR	21.3	50	41.4
2	State of the air after the extract fan heat gain	22.3	47	42.5
3	State of the air supplied from outside	-15	74.4	-13.2
4	State of the air after mixing the extract with the outside air	18.9	53.5	37.38
5	State of the air after cooling coils	8.3	100	25.6
6	State of the air after heating coils	18	53.5	35.5
7	Final state of the air after the supply fan's heat gain	19	50	36.4

5.3.2 SystemAirCAD and AHU schematics

As stated in the section 3.4.3, all the calculations, such as fan power and specific fan power are automatically calculated using SystemAirCAD. All the results can be seen in Table 27.

Furthermore, a schematic visualizing the AHU is created after the AHU design is finalized in SystemAirCAD. The schematics are shown in Appendix A. In the schematics, the exterior intake is split into 2 sections. One intake draws air from outside during normal operation, and the other draws air from inside the hangar, where the cleanrooms are located. This solution, as stated in the methodology section 3.4.3, is implemented due to unexpected weather events in which RH exceeds the AHU's design values. During a summer warm thunderstorm, the temperature can remain roughly 32 °C, while the RH can climb to the dew point. Moreover, the schematics also depict the mixing stage being outside the AHU. This is a limitation of SystemAirCAD: it can recirculate only 80% of the air, whereas this design requires

100% recirculation. Furthermore, due to the limited capacity of the heating coils for the chosen AHU size, the heating coils had to be split into 2 smaller units to meet the airflow requirements, one with a 25.9 kW power rating and the other, a larger one, with 46.8 kW. What's more, the schematic shows the connections of the condensation lines to the mixing station and the cooling coil. This is because during the heating-season mixing process, as shown on the Mollier diagram for winter, the mixing line passes through a region above saturation, causing condensation. In reality, the mixing line would never go above the saturation line, as such an air state does not exist. In reality, the mixing process would have traveled at the saturation line, but this is just a limitation of the Mollier sketcher, which only allows straight lines. The same applies to both heating and cooling periods, where the air travels along the condensation line until it reaches the desired temperature.

The value of $SFP_{v,}$ extracted directly from SystemAirCAD, corresponds to the SFP_{system} parameter defined for the decentralized system. This value is used for later comparison between the decentralized and centralized systems.

Table 27. SystemAirCAD unit results

Parameter	**Supply**	**Extract**
Airflow	5.97 m^3/s	5.38 m^3/s
Unit size	27	
Face velocity (Unit)	1.8 m/s	1.62 m/s
Fan efficiency	71.2 %	71.5 %
Fan power	10.5 kW	10.5 kW
SFPv (Clean filters)	0.97 kW/(m^3/s)	0.77 kW/(m^3/s)
SFPv (Clean Filters),(Unit)	1.66 kW/(m^3/s)	

5.4 Cooling load – Existing Project

According to the Cleanroom 1 cooling load calculation, the decentralized HVAC system inside the room can handle a maximum cooling load of 13 382 W.

Throughout a year IDA ICE reports a maximum cooling load of 10 262 W. Therefore, the existing HVAC system is validated in terms of cooling capacity for Cleanroom 1.

5.5 Decentralized system design

5.5.1 Specific fan power

Table 28 presents the results achieved for the SPF of the decentralized design. Results are rounded up to 3 decimal places.

Full pressure loss calculations that are used to determine the total pressure rise of the fans are available in Appendix H.

Table 28. Specific fan power results - decentralized design

Unit	**Airflow/ (m³/s)**	**Fan total Power rise/ kPa**	**Power electric/ kW**	**SFP/ (kW/(m³/s))**
AHU	0.597	0.730	0.063	0.106
FFU 1	0.150	0.269	0.068	0.454
FFU 2	0.150	0.288	0.072	0.480

Unit	Airflow/ (m³/s)	Fan total Power rise/ kPa	Power electric/ kW	SFP/ (kW/(m³/s))
FFU 3	0.150	0.269	0.068	0.454
FFU 4	0.150	0.284	0.071	0.474
FFU 5	0.150	0.316	0.079	0.527
FFU 6	0.150	0.319	0.080	0.534
FFU 7	0.150	0.262	0.066	0.440
FFU 8	0.150	0.257	0.065	0.434
FFU 9	0.150	0.265	0.067	0.447
FFU 10	0.150	0.260	0.065	0.434
FFU 11	0.150	0.261	0.066	0.440
FFU 12	0.150	0.326	0.082	0.547
FFU 13	0.150	0.324	0.081	0.540
FFU 14	0.150	0.324	0.081	0.540
FFU 15	0.150	0.325	0.082	0.547
FFU 16	0.150	0.288	0.072	0.480
FFU 17	0.150	0.269	0.068	0.454
FFU 18	0.150	0.277	0.070	0.467
FFU 19	0.150	0.287	0.072	0.480
FFU 20	0.150	0.285	0.072	0.480
FFU 21	0.150	0.314	0.079	0.527
FFU 22	0.150	0.294	0.074	0.494
FFU 23	0.150	0.285	0.072	0.480
FFU 24	0.150	0.262	0.066	0.440
FFU 25	0.150	0.262	0.066	0.440
FFU 26	0.156	0.299	0.078	0.500
FFU 27	0.156	0.351	0.092	0.590
FFU 28	0.156	0.321	0.084	0.539
FFU 29	0.156	0.276	0.072	0.462
FFU 30	0.156	0.277	0.073	0.468
FFU 31	0.156	0.297	0.078	0.500
FFU 32	0.156	0.314	0.082	0.526
FFU 33	0.145	0.440	0.107	0.738

Unit	Airflow/ (m³/s)	Fan total Power rise/ kPa	Power electric/ kW	SFP/ (kW/(m³/s))
FFU 34	0.145	0.440	0.107	0.738
FFU 35	0.304	0.236	0.120	0.395
FFU 36	0.155	0.500	0.130	0.839
FFU 37	0.155	0.490	0.127	0.820
FFU 38	0.110	0.452	0.083	0.755
FFU 39	0.110	0.458	0.084	0.764
System	5.970	-	3.184	0.534

5.5.2 Annual energy usage

Table 29 presents the annual air-conditioning power during cooling hours for the decentralized system.

Table 30 presents the annual air-conditioning power during heating hours for the decentralized system. Values for the annual energy usage representing the sum in between the annual conditioning power during cooling and heating hours, and the annual fan electric power of the decentralized system are available in Table 31.

Regarding the annual fan electric power, as previously mentioned, it is calculated based on the SFP_{System} parameter. Alternatively, this logic is validated by calculating the annual fan electric power of all individual fans, where the result checks with the SFP_{System} method.

In terms of the centralized system, as the methodology prescribes, the air conditioning power is not divided in between cooling and heating hours but rather provided continuously for the annual duration of 8760 hours. Therefore,

Table 32 presents the annual energy use of the centralized system.

Table 29. Air conditioning power, cooling hours - decentralized design

Process (Performed in)	Usage/ kWh
Cooling (AHU, 1.1)	35 484
Heating (AHU, 1.1)	21 419
Cooling (internal cooling unit, 1.3)	30 708

Table 30. Air conditioning power, heating hours - decentralized design

Process (Performed in)	Usage/ kWh
Cooling (AHU, 1.1)	0
Heating (AHU, 1.1)	34 085
Cooling (internal cooling unit, 1.3)	68 557

Table 31. Annual energy usage - decentralized design

Category	Usage/ kWh
Cooling hours	87 611
Heating hours	102 642
Annual fan electric power	27 926
Total	218 179

Table 32. Annual energy usage - centralized design

Process (Performed in)	Usage/ kWh
Cooling (AHU)	904 329
Heating (AHU)	615 740
Annual fan electric power	86 813
Total	1 606 882

5.6 Life cycle cost

The first three scenarios present a world in which energy remains at the same price or becomes more expensive at different rates. Due to the large difference in annual energy usage between the two designs, a clear gap emerges by the end of the 20-year analysis period. On average, the centralized system is six to seven times more expensive than the decentralized system. It is observed that although the initial investment for the centralized system's components is roughly 21% lower than that of the decentralized system, the order changes when the first-year energy running cost is considered. The centralized design is inherently more expensive from the outset, given that the entire fiscal year is considered.

Scenario 4 presents a world in which energy becomes less expensive over time. Although the first year's running costs make the first design more expensive, the gap between the two designs narrows as energy prices decline, unlike in the other three scenarios.

Results for the four scenarios are presented in the four figures below.

The initial costs of the two designs, excluding the first year running costs, are shown in Table 33.

Table 33. Initial investment cost

Design	Initial investment/ EUR
Decentralized HVAC System	243 928
Centralized HVAC System	194 031

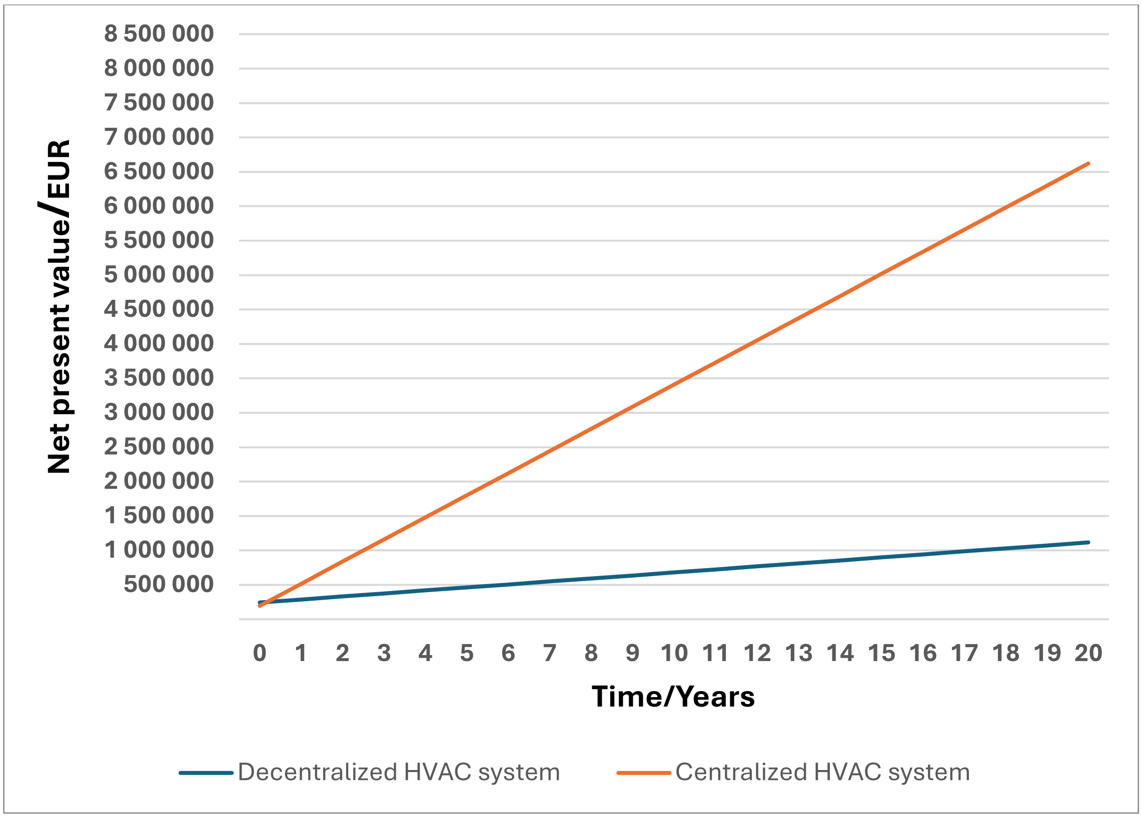

Fig. 21. Life cycle cost comparison between the decentralized and centralized design – Scenario 1: Real energy prices stagnate over time.

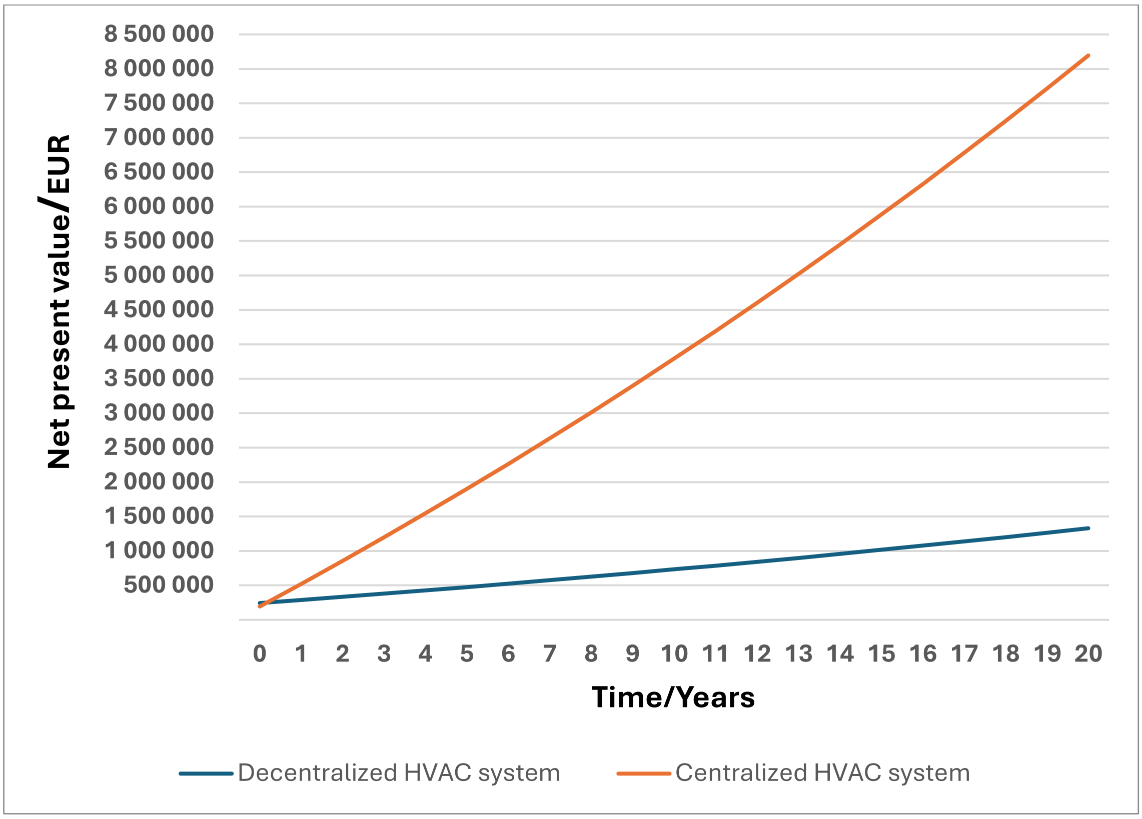

Fig. 22. Life cycle cost comparison between the decentralized and centralized design – Scenario 2: Real energy prices increase over time at a faster pace than Scenario 3.

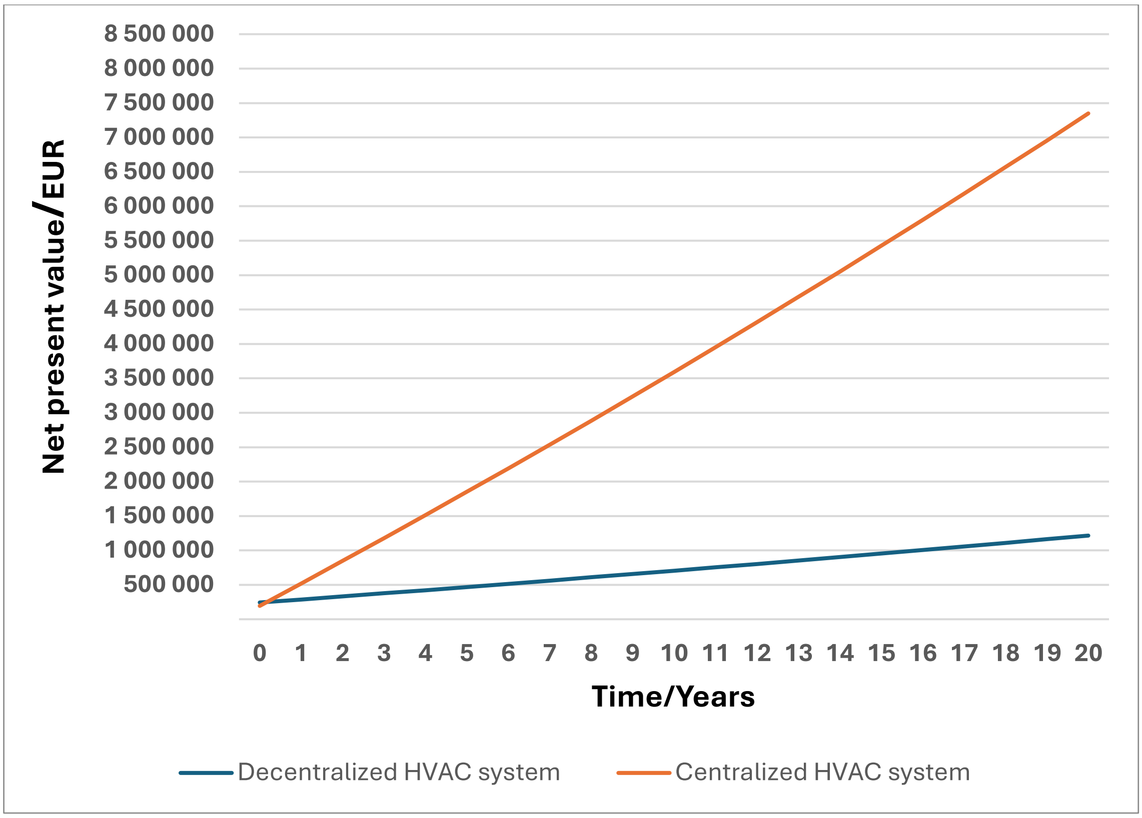

Fig. 23.Life cycle cost comparison between the decentralized and centralized design – Scenario 3: Real energy prices increase over time at a slower pace than Scenario 2.

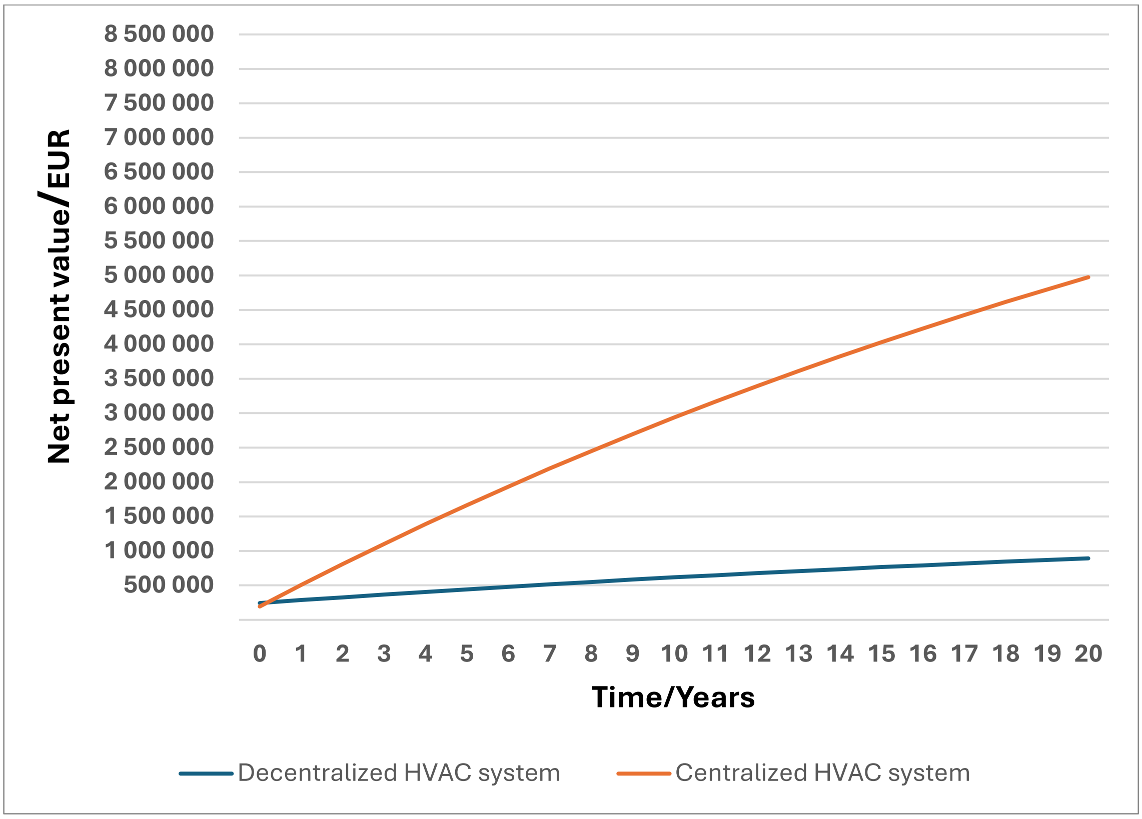

Fig. 24. Life cycle cost comparison between the decentralized and centralized design – Scenario 4: Real energy prices decrease over time.

6 Discussion

As the name of this study implies, the primary aim was to compare, economically and technically, the existing decentralized HVAC system, using FFUs as the primary source of airflow in the cleanroom facility, with a newly designed centralized system that combines the entire air-conditioning process into a single, larger AHU. While the overall comparison basis is achieved, there are some limitations of the study that cannot be simply overlooked that hinder the potential of the study, such as the reverse-engineered energy use of the existing, decentralized system, and the fact that, compared to the decentralized system, where individual rooms, such as personnel airlocks and changing rooms, are conditioned to different, higher, temperatures than cleanrooms, lowering the energy use, the centralised system treats all the rooms as equals when it comes to air conditioning, and is unable to provide different temperatures to different rooms.

6.1 Computational fluid dynamics

When comparing the accumulated CFD results with the data received from the company that conducted the validation, the pressure cascade is nearly identical, with only a small margin. This result indicates that the CFD is set up correctly and that the data can be trusted.

Cleanroom 1 is nearly at the design temperature limit, with only a 0.7°C margin before overheating. This is because CR1 houses a large packaging machine that generates 10kW of heat in a relatively small space, raising the temperature. The fact that the temperature is at that level can probably be attributed to the system's insufficient cooling capacity, because ACH is already higher than the design values, and the age of air variable is on the lower side as well, indicating adequate airflow. On the other hand, due to the lack of heat gain in CR2, the temperature stays exactly at a design value of 19°C.

Furthermore, the age of air is acceptable in both cleanrooms, highlighting, as stated in the previous paragraph, that airflow in the different spaces is adequate to exchange the air within a reasonable time. Though if we incorporate the results of the air behavior study on CR1, which exchanged some of the supply diffusers on the ceiling to exhaust diffusers, where the idea was to straighten the airflow around the machine, resulting in lower age of air time and higher *UDAF*, we see that the change is, again, marginal, only decreasing the age of air by roughly six seconds.

UDAF is, at best, average in both cleanrooms. This indicates that the airflow direction is not optimized for the given spaces. This can be attributed to the fact that in CR1, a large packaging machine stands in the middle of the room, reaching almost to the ceiling, disturbing the downwards flowing airflow and forcing it to flow around the obstacle, disturbing the air coming from the supply diffusers that are not directly above the machine as well. Furthermore, the fact that the exhaust diffusers are located on the walls, forcing the air to flow horizontally as it is extracted from the cleanrooms, contributes to the average results. It could be argued that if the main goal of the HVAC system is to promote strictly vertical, unidirectional flow, the exhaust diffusers should be located under the raised floor rather than on the walls.

6.2 System energy and overall performance

The overall energy use of the decentralized system is significantly lower than that of the centralized system in all aspects event though they are both designed with similar design specifications, except for the fact that the decentralized system is able to provide per-room-based air conditioning, compared to the centralized system, which can only air condition to a specific temperature for all rooms in the project.

The SFP for the centralized system is more than three times that of the other system. This can be attributed to the decentralized system's significantly shorter ducts and fewer fittings, due to per-room air conditioning. This means the air does not need to flow all the way back to the central AHU and then back into specific rooms after mixing with the incoming exterior air, as in a centralized system. Furthermore, it can be argued that the SFP value of the new centralized system would be lower if a bigger AHU size is chosen during the design. This alone, however, would not be enough to overcome the static pressure differences relative to decentralized systems with significantly shorter duct runs. All of this results in significantly higher annual energy use for the fans in the centralized system.

Moreover, for the actual air conditioning, comprising heating and cooling coils, energy use, it seems as though splitting the conditioning capacity into smaller units among the rooms is a better choice for the system design strategy. This statement can be attributed to the centralized system's heating and cooling energy use, in which heating is split between two heating coils and one cooling coil, all situated in a single large AHU. Though this can be concluded from the results, it's important to keep in mind that the centralized system has to condition the air to slightly different conditions than the decentralized system, which has per-room air-conditioning capabilities. What's more, the received original project did not include any Mollier diagrams for the air-conditioning process or any air state values; most of the results had to be reverse-engineered, further increasing the risk of inaccurate and imperfect data.

Furthermore, the design, at the moment, features pressure cascades and ACH values that are, in some cases, significantly larger compared to the originally designed requirements, such as, for example, CR1 being pressurized to 46.8 Pa while only 30 Pa above atmospheric pressure is required. Modifying the ACH and leakage ports to meet the original design conditions would most likely result in significantly lower overall energy use for the system, saving both money and energy. On the other hand, since CR1 is at its temperature limits, the cooling system would need to be reworked and fitted with higher capacity to handle the same heat loads with lower ACH values inside the cleanroom.

6.3 Economic viability and LCC

"Prediction is very difficult, especially about the future." (Niels Bohr, n.d.)

Debating economic logic is beyond the purpose of this study. Therefore, four different scenarios representing stagnating, increasing, and decreasing energy prices were presented.

Initial cost calculations report an investment difference of roughly 50 000 EUR, in favor of the centralized system. Although the centralized system is 50 000 EUR cheaper than the decentralized system, from a life-cycle cost perspective, it is the clear underperformer within those boundaries.

In scenario 1, where real energy prices are stagnant over time, a difference of roughly 5 500 000 EUR is observed in favor of the decentralized system, or 110 times the additional initial investment required for the decentralized system. The total running cost of the centralized system at the end of the 20-year period is roughly 6 times that of the decentralized system.

Both Scenario 2 and Scenario 3 represent increasing real energy prices over time. The most favorable outcome among the two scenarios for the centralized system is Scenario 3, where the running cost of the centralized system requires roughly an additional 6 100 000 EUR in capital, or 122 times the extra amount that would have to be invested initially for the decentralized system. The total running cost of the centralized system at the end of the 20-year period is roughly 6.5 times that of the decentralized system.

Out of the four scenarios, scenario 4, where real energy prices are decreasing over time, is the most favorable for the centralized system, although still requiring roughly an additional 4 080 000 EUR in capital for its life cycle cost or 81.6 times the extra amount which would have to be invested initially for the decentralized system. The total running cost of the centralized system at the end of the 20-year period is roughly 5.5 times that of the decentralized system.

Supposing a prospective client would not possess the additional 50 000 EUR needed for the initial investment in the decentralized system, and the amount would have to be borrowed from a potential lender under a fixed interest rate of 8%, and a repayment period of 20 years. Depending on the fees, the total repayment to the bank over 20 years would amount to roughly 100 000 EUR ("Bussines Loan Calculator," n.d.), of which 50 000 EUR represents interest.

The 8% fixed interest rate considered represents a much grimmer scenario than the current 4.1% interest rate in Slovakia (Trading Economics, n.d.). The monthly repayment would account for roughly 416 EUR.

In the 20th year of scenario 4, when the real energy price would reach its lowest point due to constant decreases over the years, the difference in running costs between the two systems would be roughly 153 600 EUR in favor of the decentralized system, or a monthly difference of 12 800 EUR. Roughly 31 times the monthly repayment to the potential lender of the extra capital needed for the difference in the initial investment of the decentralized system.

6.4 Industry recommendation

The results suggest that designing a strictly centralized system, as in this study, is not beneficial beyond initial costs and should probably be avoided. In scenarios similar to this one, it's more beneficial to either design a completely decentralized system or a hybrid system that can provide different temperatures to different rooms while keeping the ductwork short, thereby reducing frictional losses.

6.5 Prospective future work

One possibility to improve the reliability of this study is to use a new, or design from the ground up, decentralized system in which all the necessary information is available to conduct a proper system analysis and subsequent comparison with the centralized system.

Moreover, since the study suggests that the air conditioning energy use is significantly lower while being configured as a per-room-based system, it would be beneficial to study a hybrid system, where a large AHU would take care of airflow, mixing, and filtering, while smaller cooling and heating units adjacent to the cleanrooms would take care of temperature and humidity.

Another possibility is to include environmental calculations, such as life-cycle assessments for both systems, when assessing the feasibility of different solutions, as only the economic aspect has been considered in this study.

The analysis method presented in this study could be extended to multiple case studies across different sectors of the manufacturing industry where cleanrooms are applicable to facilitate more general conclusions and observations.

7 Conclusion

7.1 Primary verdict

When comparing strictly energy and economy, it is found that the decentralized system, in this scenario, while having higher initial costs for the components, quickly surpasses the centralized system in future economic viability and, thus, for that matter, in energy efficiency due to significantly lower ductwork resistance and lower air conditioning annual energy use.

A strictly centralized system, in the given configuration, cannot provide different air states to rooms with different requirements, such as dressing rooms and cleanrooms in this study, resulting in over-conditioning, higher energy use, and reduced economic viability. This conclusion suggests that a one-size-fits-all AHU for this specific application, with varying air-state requirements across rooms, is technically and economically suboptimal.

7.2 Project data validation

CFD proved to be an essential tool for validating project requirements. This is highlighted by the fact that the validation data provided with the project closely align with the CFD software results for temperature and pressure differences relative to the atmosphere. Thus, concluding that validation can be done using computational tools only, rather than relying only on physical data from real-world measurements.

7.3 The “Cleanroom 1” case study

The fact that cleanroom 1 comes very close to overheating while featuring a much higher ACH than the original design requirements suggests that ACH in such a high-heat-load environment isn’t the whole story a designer needs to consider. Internal heat gains from machinery, people, and other heat-producing elements must be the starting point for determining cooling capacity, to avoid operating systems at the very edge of their capabilities while ensuring adequate indoor conditions suitable for the given tasks in the cleanrooms.

7.4 Economic viability

This study conducted a life-cycle cost analysis comparing decentralized and centralized HVAC solutions across four real discount rate scenarios.

Quantities for the decentralized system were extracted from the existing drawings, while quantities for the centralized system were extracted from the 3D Revit model. A list of equipment prices was determined for both systems based on data obtained or assumed with the partner company. Based on this data, it was determined that the initial investment for the decentralized system is 21% higher than that of the centralized system.

Running cost was determined based on current energy prices in Slovakia and energy usage calculations. Energy usage was determined for both systems based on the annual conditioning power, using the enthalpies prescribed by the Mollier charts and the weather file, and the annual fan electric power was calculated using the specific fan power determined from pressure loss calculations. It was determined that the annual energy usage of the centralized system is roughly 7.3 times that of the decentralized system, significantly impacting the life-cycle cost comparison, as a much higher energy bill must be accounted for.

At the end of the 20-year life-cycle cost calculation, the decentralized system outperforms the centralized system by a factor of 5.5 to 6.5. Under the given circumstances and within the set life-cycle cost boundaries, the centralized system is not a viable solution compared to the decentralized system on anything other than the initial cost.

References

Ansys, Inc., 2026. Ansys Workbench.

Ansys, Inc., 2024. Global Mesh Size, Ansys ICEM CFD Help Manual.

Ansys, Inc., 2023. Boundary Layer Options [WWW Document]. DS Mechanical. URL https://help.spaceclaim.com/dsm/6.0/en/Discovery/user_manual/meshing/mesh/r_mesh_boundary_layer_options.html (accessed 3.20.26).

Ansys, Inc., 2020. Introduction to Icepak in AEDT-Module 3 – Lecture 1: Meshing.

Ansys Workbench, n.d.

Arup Bhattacharya, Mohammad Saleh Nikoopayan Tak, Shervin Shoai-Naini, Fred Betz, Ehsan Mousavi, n.d. A Systematic Literature Review of Cleanroom Ventilation and Air Distribution Systems. Aerosol Air Qual. Res. 23. https://doi.org/10.4209/aaqr.220407

ASHRAE, 2025. 2025 ASHRAE Handbook—Fundamentals, SI (International System). ed. ASHRAE, Peachtree Corners, GA.

ASHRAE, 2019. History of Cleanrooms.

ASHRAE, n.d. ASHRAE Weather Data Center.

Autodesk Revit, n.d.

Beising Rüdiger, 2007. Climate change and power industry - State of the scientific research. VGB PowerTech.

Berry Pam M., Brown Sally, Chen Minpeng, Kontogianni Areti, Rowlands Olwen, Simpson Gillian, Skourtos Michalis, 2015. Cross-sectoral interactions of adaptation and mitigation measures. Climatic Change. https://doi.org/10.1007/s10584-014-1214-0

Bussines Loan Calculator, n.d.

Camfil, 2024a. CleanSeal Side C [WWW Document]. Camfil Products. URL https://www.camfil.com/en/products/housings--frames-,-a-,-louvres/terminal-housing/cleanseal/cleanseal-side-c-_-56881 (accessed 3.20.26).

Camfil, 2024b. CleanSeal Top C [WWW Document]. Camfil Products. URL https://www.camfil.com/sv-se/produkter/filterskap-ramar-intagsgaller/terminal-housing/cleanseal/cleanseal-top-c-_-22326?srsltid=AfmBOooid_f1XTcTFeylQfr961E4PbttdixC-1JyMZjWCltRLMVkg_Li (accessed 3.20.26).

Camfil, 2024c. CleanSeal V3 Family Brochure.

Camfil, n.d. Sound Level & dp - Graph Finder for CleanSeal Front Plates with Megalam MD/MX/MG14.

Chen Yiling, Li Nan, Zhao Yu, Zhao Wei, n.d. Study on Energy Consumption Influencing Factors of HVAC Systems for Cleanrooms in Semiconductor Fabs. Lecture Notes in Civil Engineering. https://doi.org/10.1007/978-981-99-4049-3_66

Christoph Nikendei, Till J. Bugaj, Frederik Nikendei, Susanne J. Kühl, Michael Kühl, 2020. Climate change: Causes, consequences, solutions and public health care implications. Zeitschrift fur Evidenz, Fortbildung und Qualitat im Gesundheitswesen. https://doi.org/10.1016/j.zefq.2020.07.008

Cleanroom Technology Market (2025 - 2030), n.d.

Cleanroom.net, 2024. What is Unidirectional Airflow? [WWW Document]. Cleanroom.net. URL https://cleanroom.net/faqs/what-is-unidirectional-airflow/ (accessed 3.20.26).

CoreGain LTD, n.d. LED Lights.

Darcy, H., 1856. Les fontaines publiques de la ville de Dijon. Victor Dalmont, Paris.

Density of air, 2026. . Wikipedia.

Devender Dahiya, Boeing Laishram, 2024. Life cycle energy analysis of buildings: A systematic review. Building and Environment 252. https://doi.org/10.1016/j.buildenv.2024.111160%2520Get%2520rights%2520and%2520content

EUROPEAN COMMISSION, 2022. The Rules Governing Medicinal Products in the European Union.

Fedotov A., 2014. Saving energy in cleanrooms 22, 14–18.

Grasshopper, n.d.

Gravitational acceleration, 2026. . Wikipedia.
HoodFilters.com, 2019. Are Round Grease Ducts Better Than Rectangular Grease Ducts? Foodservice Blog. URL https://blog.hoodfilters.com/2019/04/05/ductmate-f2-hi-temp-round-grease-duct-access-door-review/ (accessed 10.4.26).
IDA ICE, n.d.
Indra Permana, Fujen Wang, Alya Penta Agharid, 2025. Performance improvement through CFD and field measurement in a unidirectional airflow cleanroom for wafer manufacture. Journal of Building Engineering 100. https://doi.org/10.1016/j.jobe.2024.111715
International Energy Agency, 2025. World Energy Outlook.
International Organization for Standardization, 2022. ISO 14644-4:2022.
International Organization for Standardization, 2015. ISO 14644-1:2015.
Jhy-Ming Tsao, Shih-Cheng Hu, 2007. A comparative study on energy consumption for HVAC systems of high-tech FABs. Applied Thermal Engineering 27, 2758–2766. https://doi.org/10.1016/j.applthermaleng.2007.03.016
Justin Z. Lian, 2024. Quantifying the present and future environmental sustainability of cleanrooms. Cell Reports Sustainability 1.
KHANKARI KISHOR, 2019. Dynamics of Unidirectional Airflow. ASHRAE Journal 61, 20–39.
Kumaresan B., Vijayaraghavan N., 2015. A study on the sectors that increase the percentage of carbon dioxide which causes global warming using fuzzy cognitive maps. International Journal of Applied Engineering Research.
Ladybug tools, n.d.
MagiCAD for Revit, n.d.
Marcel G.L.C. Loomans, Molenaar P.C.A., Kort H.S.M., Joosten P.H.J., 2019. Energy demand reduction in pharmaceutical cleanrooms through optimization of ventilation. Energy and Buildings 202.
Martinich Jeremy, Crimmins Allison, 2019. Climate damages and adaptation potential across diverse sectors of the United States. Nature Climate Change. https://doi.org/10.1038/s41558-019-0444-6
Matej Mikulic, 2025. Global pharmaceutical industry - statistics & facts. statista.
Merzkirch Alexander, Maas Stefan, Scholzen Frank, Waldmann Daniele, 2016. Field tests of centralized and decentralized ventilation units in residential buildings - Specific fan power, heat recovery efficiency, shortcuts and volume flow unbalances. Energy and Buildings 116, 376–383. https://doi.org/10.1016/j.enbuild.2015.12.008
Ministry of Foreign Affairs and European Affairs of the Slovak Republic, n.d. Public holidays.
Mollier sketcher, n.d.
Murphy’s law, n.d. URL https://en.wikipedia.org/wiki/Murphy%27s_law
Niels Bohr, n.d. Niels Bohr, Quotes. URL https://www.goodreads.com/quotes/23796-prediction-is-very-difficult-especially-about-the-future
Niraj P. Koirala, 2025. Geopolitical risks and energy market dynamics. Energy Economics 150.
OneBuilding.org, 2024. Climate.OneBuilding.org [WWW Document]. Climate.OneBuilding.org. URL https://climate.onebuilding.org/#gsc.tab=0 (accessed 3.20.26).
Permana Indra, Agharid Alya Penta, Singh Nitesh, Wang Fujen, 2024. Full-scale evaluation of FFU configurations in an optical cleanroom injection molding for improving thermal performance and contaminant removal. Case Studies in Thermal Engineering. https://doi.org/10.1016/j.csite.2024.105076
Pinar Mert Cuce, Erdem Cuce, 2026. Role of HVAC in building energy consumption: a critical review. Journal of Thermal Analysis and Calorimetry 151, 3059–3080. https://doi.org/10.1007/s10973-026-15322-9
Qian Ye, 2011. An essay on global carbon budget approaches-Are we ready to deal with global climate changes now? Frontiers of Earth Science. https://doi.org/10.1007/s11707-011-0184-z
R. J. Knudsen, S. M. N. Knudsen, 2021. Laminar airflow decreases microbial air contamination compared with turbulent ventilated operating theatres during live total joint arthroplasty: a nationwide survey. Journal of Hospital Infection 113, 65–70. https://doi.org/10.1016/j.jhin.2021.04.019
Reynolds number, n.d.

Semiconductor Industry Association, 2025. Global Semiconductor Sales Increase 4.7% Month-to-Month in October. Semiconductor Industry Association.

Skeie Ragnhild Bieltvedt, Fuglestvedt Jan, Berntsen Terje, Lund Marianne Tronstad, Myhre Gunnar, Rypdal Kristin, 2009. Global temperature change from the transport sectors: Historical development and future scenarios. Atmospheric Environment. https://doi.org/10.1016/j.atmosenv.2009.05.025

Slovak Office of Standards, Metrology and Testing, n.d. Slovak Office of Standards, Metrology and Testing. URL https://www.normoff.gov.sk/

Slovakia electricity prices, 2025. URL https://www.globalpetrolprices.com/Slovakia/electricity_prices/

Solemma LLC, 2024. ClimateStudio Documentation [WWW Document]. URL https://climatestudiodocs.com/ (accessed 2.15.25).

S&P Global, 2026. S&P Global Unveils Top 10 Sustainability Trends to Watch in 2026. S&P Global.

Statista Research Department, n.d. Average inflation rate in Slovakia from 1994 to 2030.

Sun Wei, Mitchell John, Flyzik Keith, 2010. Development of cleanroom required airflow rate model based on establishment of theoretical basis and lab validation, in: ASHRAE Transactions. American Society of Heating Refrigerating and Air-Conditioning Engineers.

SystemAirCAD, n.d.

Thamarai P., Deivayanai V.C., Saravanan A., Vickram A.S., Yaashikaa P.R., 2024. Carbon mitigation in agriculture: Pioneering technologies for a sustainable food system. Trends in Food Science and Technology. https://doi.org/10.1016/j.tifs.2024.104477

Trading Economics, n.d. Slovakia Bank Lending Rate.

United Nations, 2015. PARIS AGREEMENT.

Vijayan Dhanasingh Sivalinga, Devarajan Parthiban, Mohanavel Vinayagam, Sankaran Naveen, Kannan Sathish, Ahsan Md. Shamim, 2025. A Review of Sustainable Implications of Energy-Efficient Buildings in the Environment. Advances in Civil Engineering. https://doi.org/10.1155/adce/9584777

Xinran Zeng, Chunhui Li, 2025. Energy Efficiency Optimization of Air Conditioning Systems Towards Low-Carbon Cleanrooms: Review and Future Perspectives. https://doi.org/10.3390/en18133538

Yang Bi, Nan Hu, Parastoo Sadeghian, 2025. Numerical study on the application of low-turbulence air curtain surrounding laminar airflow distribution in operating rooms. Indoor/Outdoor Airflow and Air Quality 18, 601–617. https://doi.org/10.1007/s12273-024-1229-7

Yu-Ra Son, Jeong-Hoon Yang, 2020. Fundamental Study on Prediction of Static Pressure Loss in Horizontal Aluminum Flexible Ducts. Korean Institute of Architectural Sustainable Environment and Building Systems 14, 195–207. https://doi.org/10.22696/jkiaebs.20200018

Zhiyao Ma, Bowen Guan, Xiaohua Liu, Tao Zhang, 2020. Performance analysis and improvement of air filtration and ventilation process in semiconductor clean air-conditioning system. Energy and Buildings 228. https://doi.org/10.1016/j.enbuild.2020.110489

Zhiyao Ma, Xiaohua Liu, Tao Zhang, 2021. Measurement and optimization on the energy consumption of fans in semiconductor cleanrooms. Building and Environment. https://doi.org/10.1016/j.buildenv.2021.107842

Zhonglin Xu, 2013. Fundamentals of Air Cleaning Technology and Its Application in Cleanrooms, 1st ed. Springer Berlin. https://doi.org/10.1007/978-3-642-39374-7

Zonghua Huang, Cheng Zeng, Zhichu Wang, Jun Lu, Qian Xiang, Xingcheng Huo, Tingdong Tan, Yan Li, Wenmao Feng, Guitao Zhang, n.d. Optimizing Vertical Unidirectional Airflow in Cleanrooms: An Integrated Approach to Floor Perforation, Plenum, and Fan Filter Unit Configurations. Atmosphere. https://doi.org/10.3390/atmos16060632

Appendix A

AHU schematics

This schematic depicts the design of an AHU used in the centralized system. The legend is placed below the AHU so the reader understands what each section of the AHU does. Along with legends, the power ratings and pressure drops of all components can be seen either below or above the relevant AHU sections.

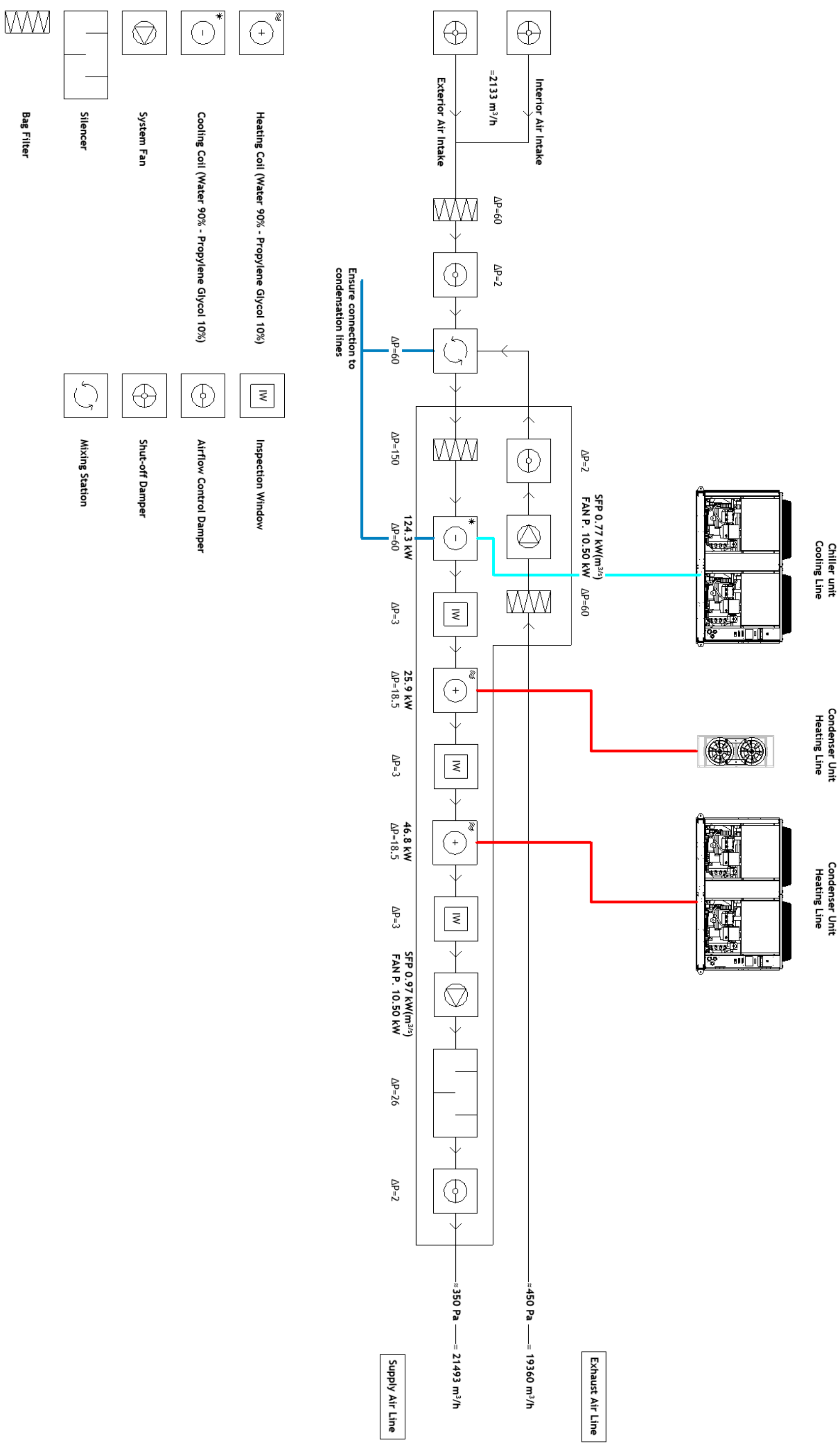

Appendix B

Summer Mollier diagram along with data from Mollier Sketcher – Centralized Design

This is a printed version of the Mollier diagram used to dimension the AHU, along with data for each point for the summer season. Each point can be traced to a data document that contains all the necessary information about the air state.

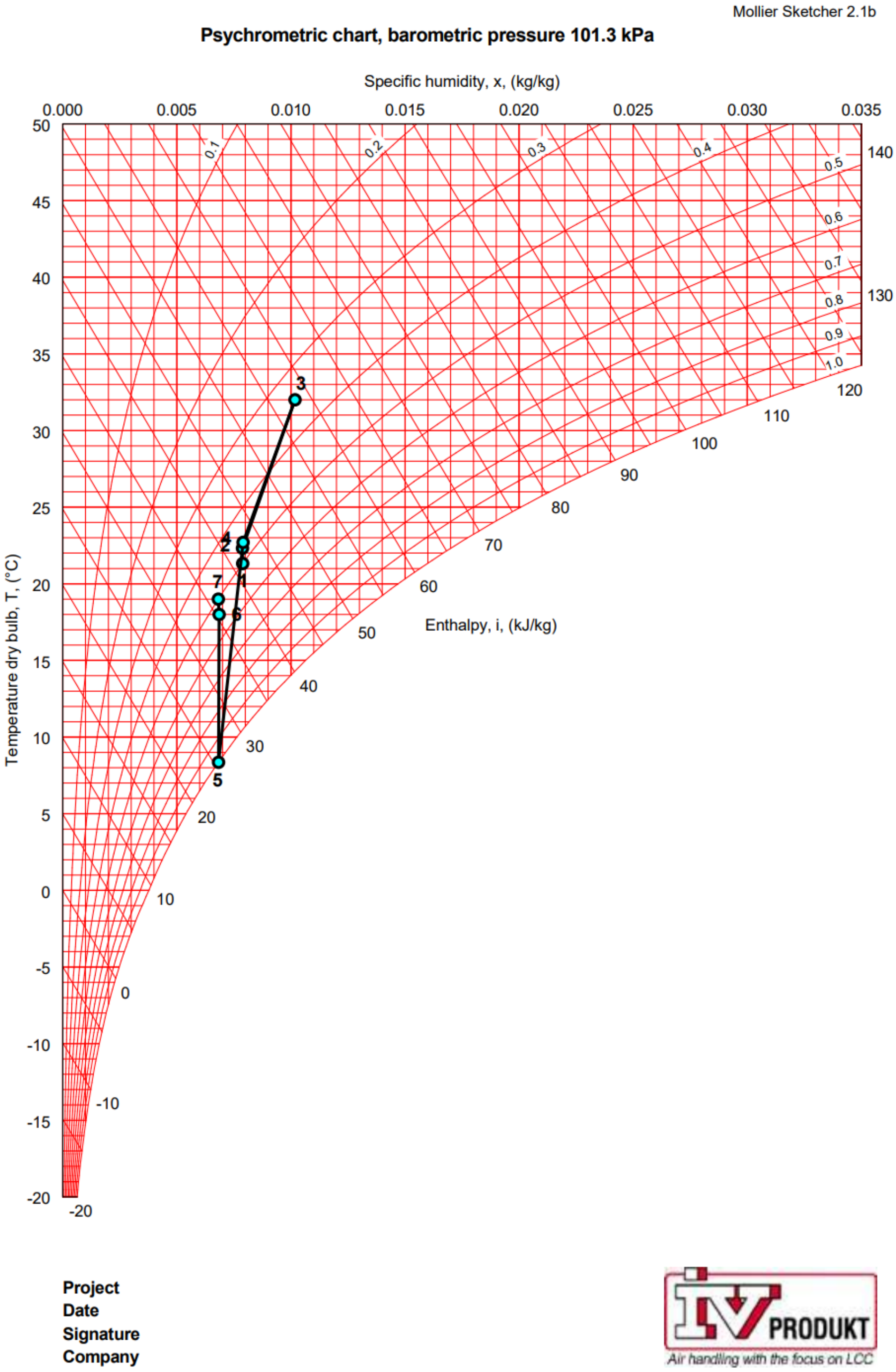

Project data

Project
Date
Signature
Company

Flow data

Air flow	5.97 m³/s
Density	1.20 kg/m³
Atm. pressure	1013 mbar

Process

Nbr	Name	Temp (°C)	Relative humidity (%)	Specific humidity (g/kg)	Enthalpy (kJ/kg)	Supplied power (kW)	Sensible power (kW)	Water (l/min)
1	Out CR	21.317	50	7.88	41.4			
2	After Fan	22.317	47	7.88	42.5	7.2	7.3	0.0
3	Out Summer	32	34.3	10.18	58.2	112.8	71.7	1.0
4	After mixing	22.7	46.1	7.91	42.9168	-109.5	-68.9	-1.0
5	After Cooling	8.35	100	6.82	25.6	-124.3	-104.9	-0.5
6	After Heating	18	53.5	6.85	35.5	70.9	70.3	0.0
7	Desired Temperature	19	50	6.82	36.4	6.6	7.3	0.0

Appendix C

Winter Mollier diagram along with data from Mollier Sketcher – Centralized Design

This is a printed version of the Mollier diagram used to dimension the AHU, along with data for each point for the winter season. Each point can be traced to a data document that contains all the necessary information about the air state.

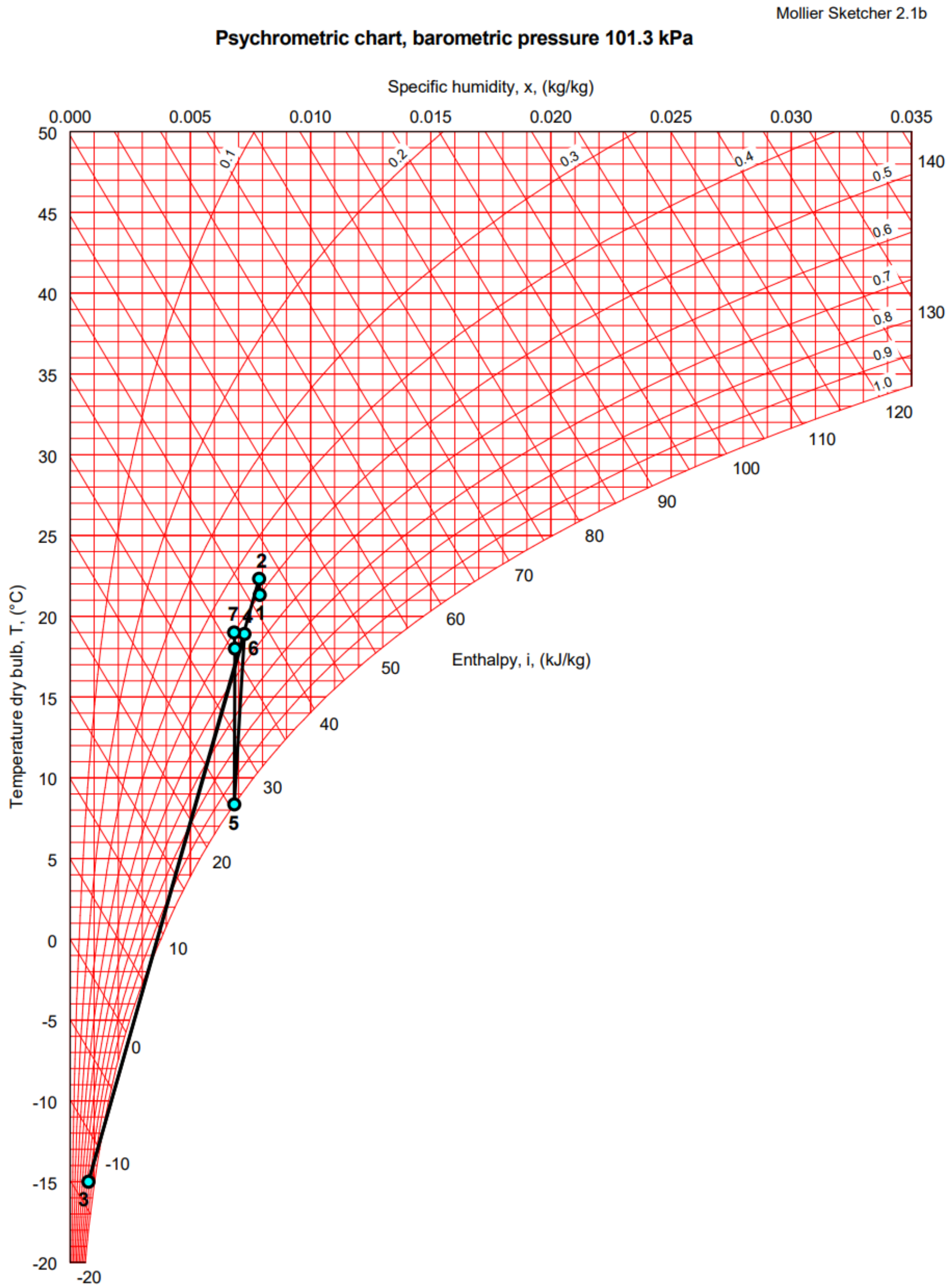

Project
Date
Signature
Company

PRODUKT
Air handling with the focus on LCC

Project data

Project

Date

Signature

Company

Flow data

Air flow	5.97 m³/s
Density	1.20 kg/m³
Atm. pressure	1013 mbar

Process

Nbr	Name	Temp (°C)	Relative humidity (%)	Specific humidity (g/kg)	Enthalpy (kJ/kg)	Supplied power (kW)	Sensible power (kW)	Water (l/min)
1	Out CR	21.317	50	7.88	41.4			
2	After Fan	22.317	46.88	7.86	42.4	6.9	7.3	0.0
3	Out Winter	-15	74.7	0.76	-13.2	-398.4	-271.1	-3.1
4	After Mixing	18.9	53.5	7.25	37.38	362.4	246.0	2.8
5	After Cooling	8.35	100	6.82	25.6	-84.7	-77.0	-0.2
6	After Heating	18	53.5	6.85	35.5	70.9	70.3	0.0
7	Desired Temperature	19	50	6.82	36.4	6.6	7.3	0.0

Appendix D

Winter Mollier diagram along with data from Mollier Sketcher – Decentralized Design

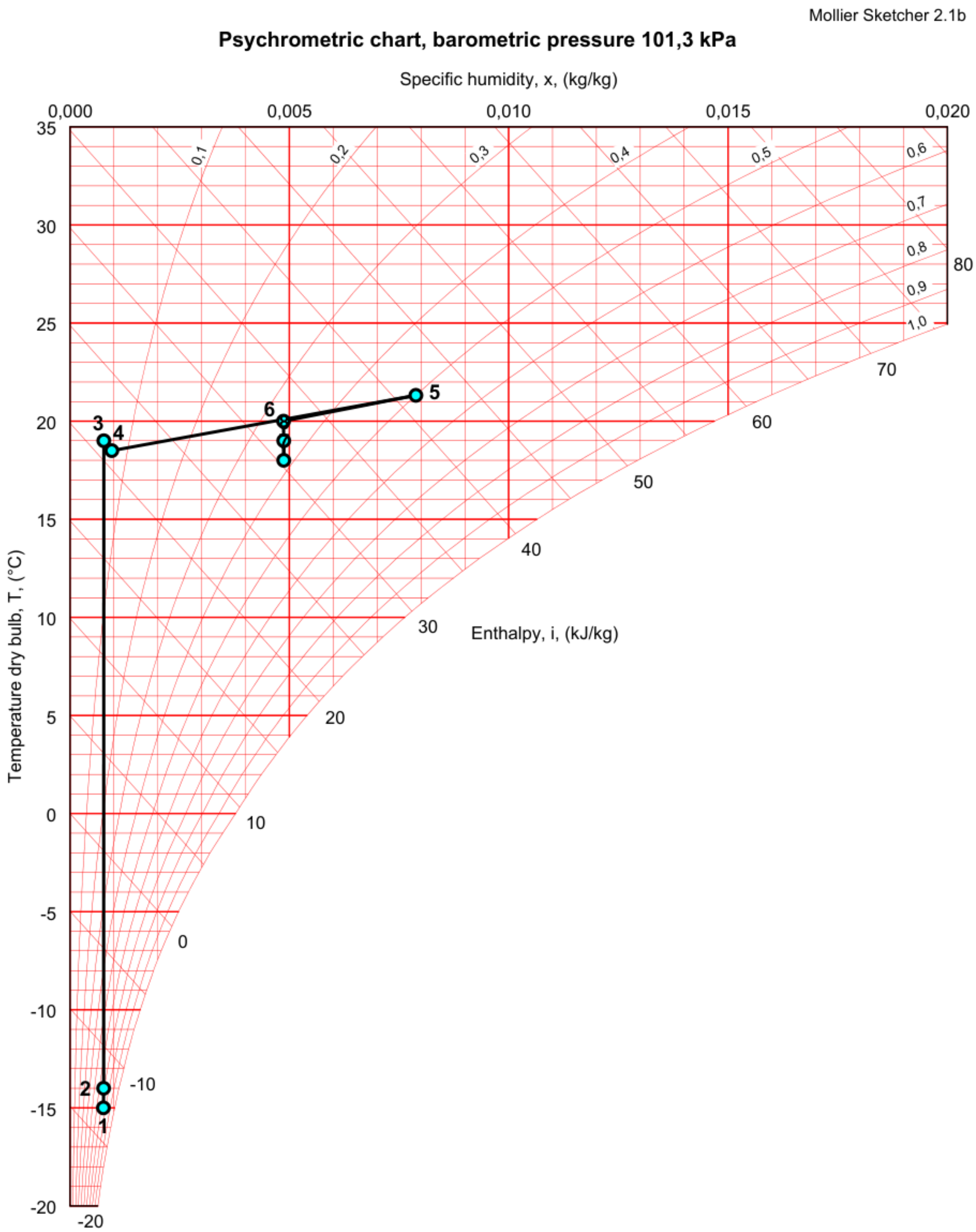

Project Degree project, Current AHU, Winter
Date 16.03.2026
Signature VMA
Company

Air handling with the focus on LCC

Project data

Project	Degree project, Current AHU, Winter
Date	16.03.2026
Signature	VMA
Company	

Flow data

Air flow	0,59 m³/s
Density	1,20 kg/m³
Atm. pressure	1013 mbar

Process

Nbr	Name	Temp (°C)	Relative humidity (%)	Specific humidity (g/kg)	Enthalpy (kJ/kg)	Supplied power (kW)	Sensible power (kW)	Water (l/min)
1	out	-15	74,7	0,76	-13,2			
2	After fan	-14	68,6	0,76	-12,2	0,7	0,7	0,0
3	after heating	19	5,7	0,77	21,0	23,5	23,5	0,0
4	desired	18,5	7,2	0,95	21	0,0	-0,4	0,0
5	Out CR	21,317	50	7,88	41,4	14,5	2,2	0,3
6	After Mixing	20	33,6	4,87	32,447	-6,4	-1,0	-0,1
7	After Cooling	18	38,1	4,87	30,4	-1,4	-1,4	0,0
8	Desired	19	35,8	4,87	31,4	0,7	0,7	0,0

Appendix E

Summer Mollier diagram along with data from Mollier Sketcher – Decentralized Design

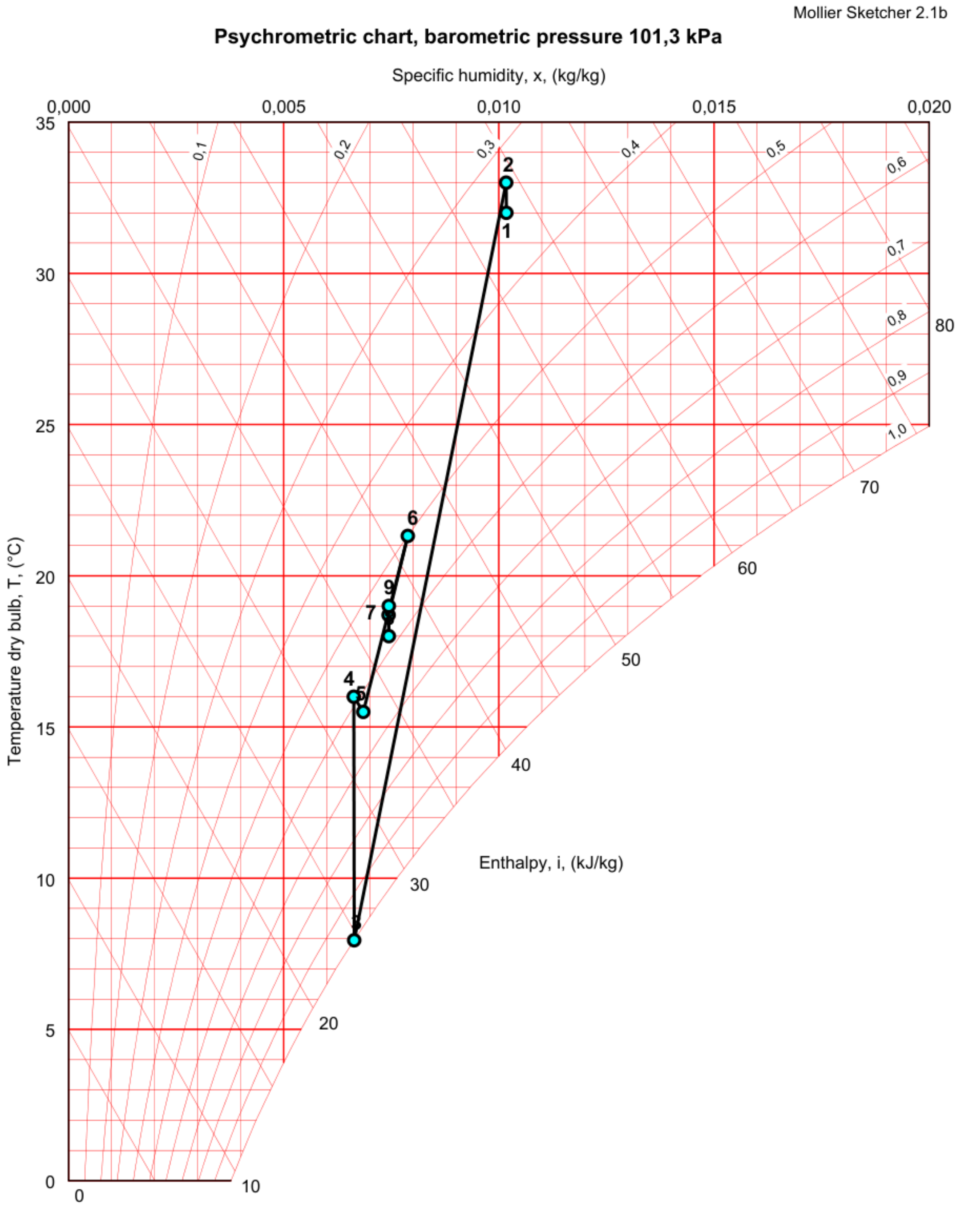

Project Degree project, Current AHU, Summer
Date 16.03.2026
Signature VMA
Company

Air handling with the focus on LCC

Project data

Project	Degree project, Current AHU, Summer
Date	16.03.2026
Signature	VMA
Company	

Flow data

Air flow	0,59 m³/s
Density	1,20 kg/m³
Atm. pressure	1013 mbar

Process

Nbr	Name	Temp (°C)	Relative humidity (%)	Specific humidity (g/kg)	Enthalpy (kJ/kg)	Supplied power (kW)	Sensible power (kW)	Water (l/min)
1	out	32	34,3	10,17	58,2			
2	After Fan	33	32,4	10,17	59,2	0,7	0,7	0,0
3	after cooling	7,95	100	6,64	24,7	-24,4	-18,2	-0,2
4	After Heating	16	58,8	6,63	32,9	5,8	5,8	0,0
5	Desired AHU	15,5	62,7	6,85	32,9	0,0	-0,4	0,0
6	out CR	21,317	50	7,88	41,4	6,1	4,2	0,0
7	after mixing	18,7	55,5	7,44	37,65	-2,7	-1,9	0,0
8	after cooling	18	58,0	7,44	36,9	-0,5	-0,5	0,0
9	Desired	19	54,5	7,44	38,0	0,7	0,7	0,0

Appendix F

Air conditioning power script – extracted from Grasshopper

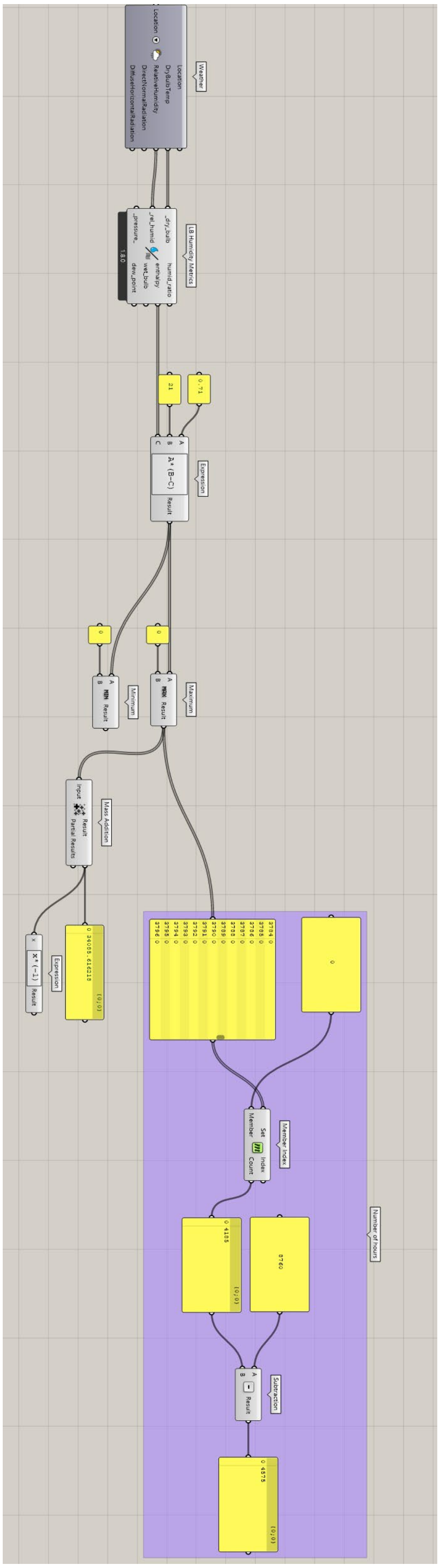

Appendix G

Existing decentralized system – Ventilation schematics, plans

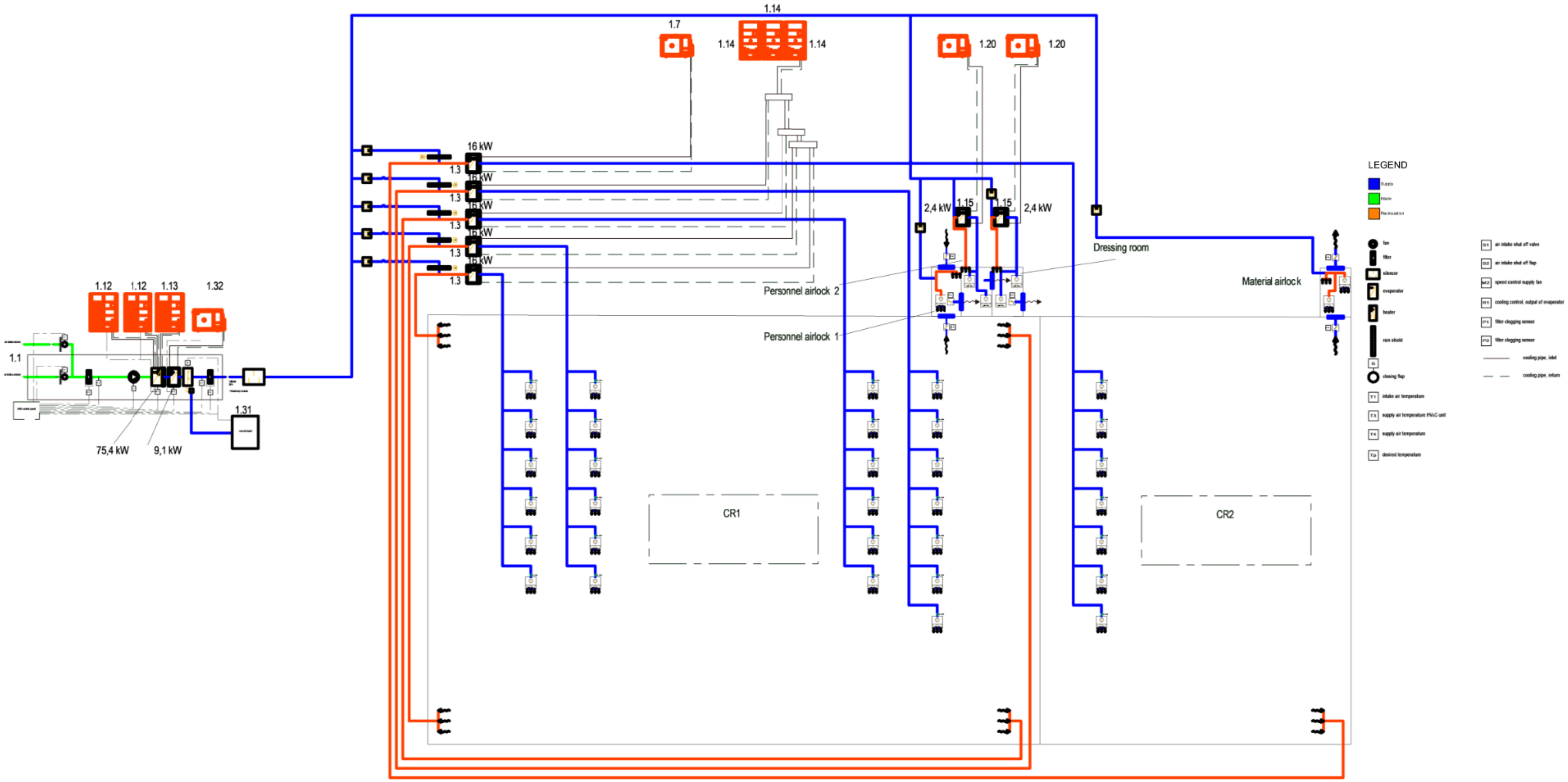

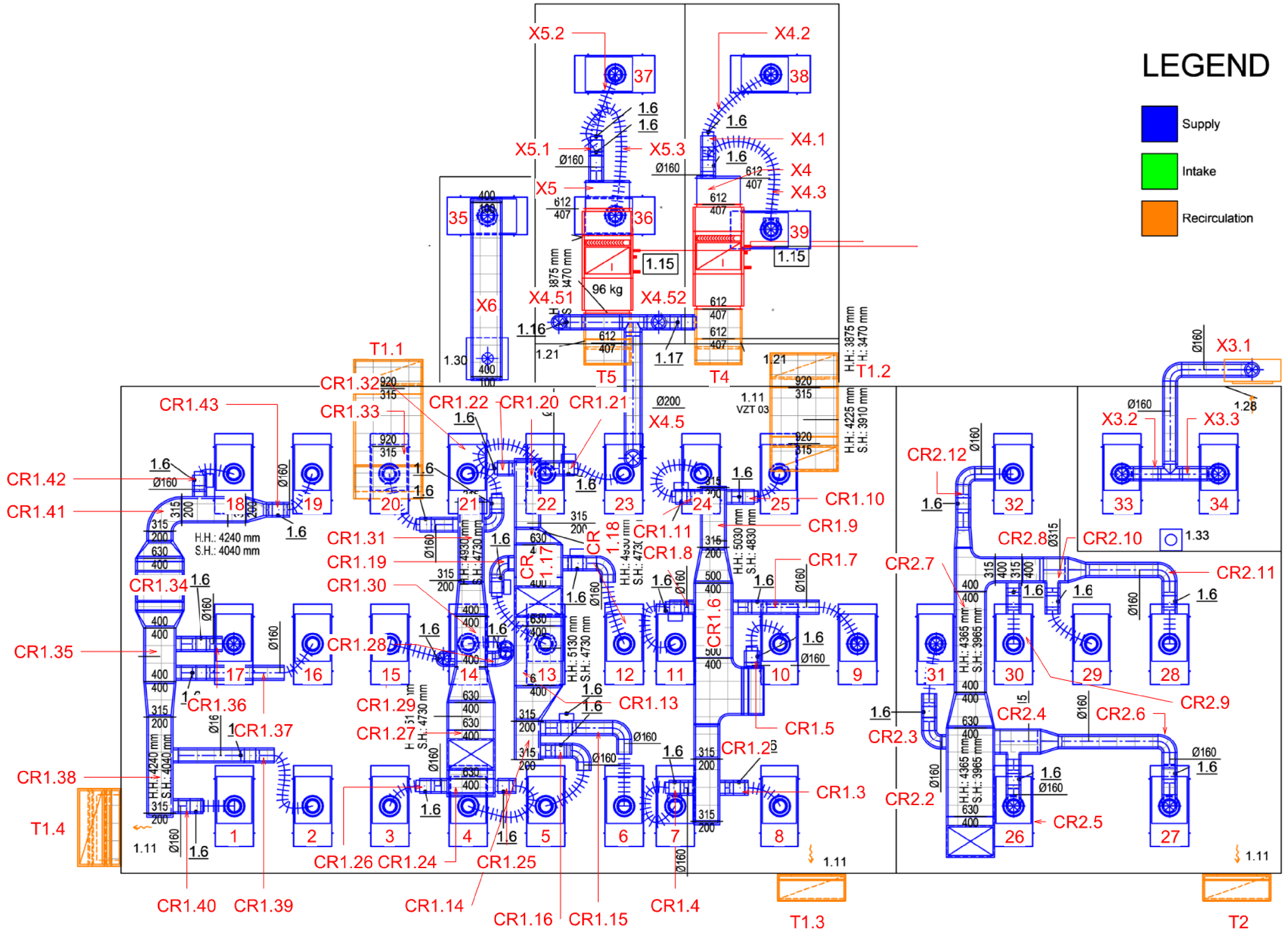
LEGEND
Supply
Intake
Recirculation
T1.1
T1.2
T1.3
T1.4
T2
T4
T5
X3.1
X3.2
X3.3
X4
X4.1
X4.2
X4.3
X4.5
X4.51
X4.52
X5
X5.1
X5.2
X5.3
X6
CR1.3
CR1.4
CR1.5
CR1.6
CR1.7
CR1.8
CR1.9
CR1.10
CR1.11
CR1.13
CR1.14
CR1.15
CR1.16
CR1.19
CR1.20
CR1.21
CR1.22
CR1.24
CR1.25
CR1.26
CR1.27
CR1.28
CR1.29
CR1.30
CR1.31
CR1.32
CR1.33
CR1.34
CR1.35
CR1.36
CR1.37
CR1.38
CR1.39
CR1.40
CR1.41
CR1.42
CR1.43
CR2.2
CR2.3
CR2.4
CR2.5
CR2.6
CR2.7
CR2.8
CR2.9
CR2.10
CR2.11
CR2.12
H.H.: 4240 mm
S.H.: 4040 mm
H.H.: 3875 mm
H.H.: 3470 mm
H.H.: 4225 mm
S.H.: 3910 mm
H.H.: 5130 mm
S.H.: 4730 mm
H.H.: 5030 mm
S.H.: 4830 mm
H.H.: 4365 mm
S.H.: 3965 mm
1.11
VZT 03
1.15
1.16
1.17
1.21
1.28
1.30
1.33
96 kg
Ø160
Ø200

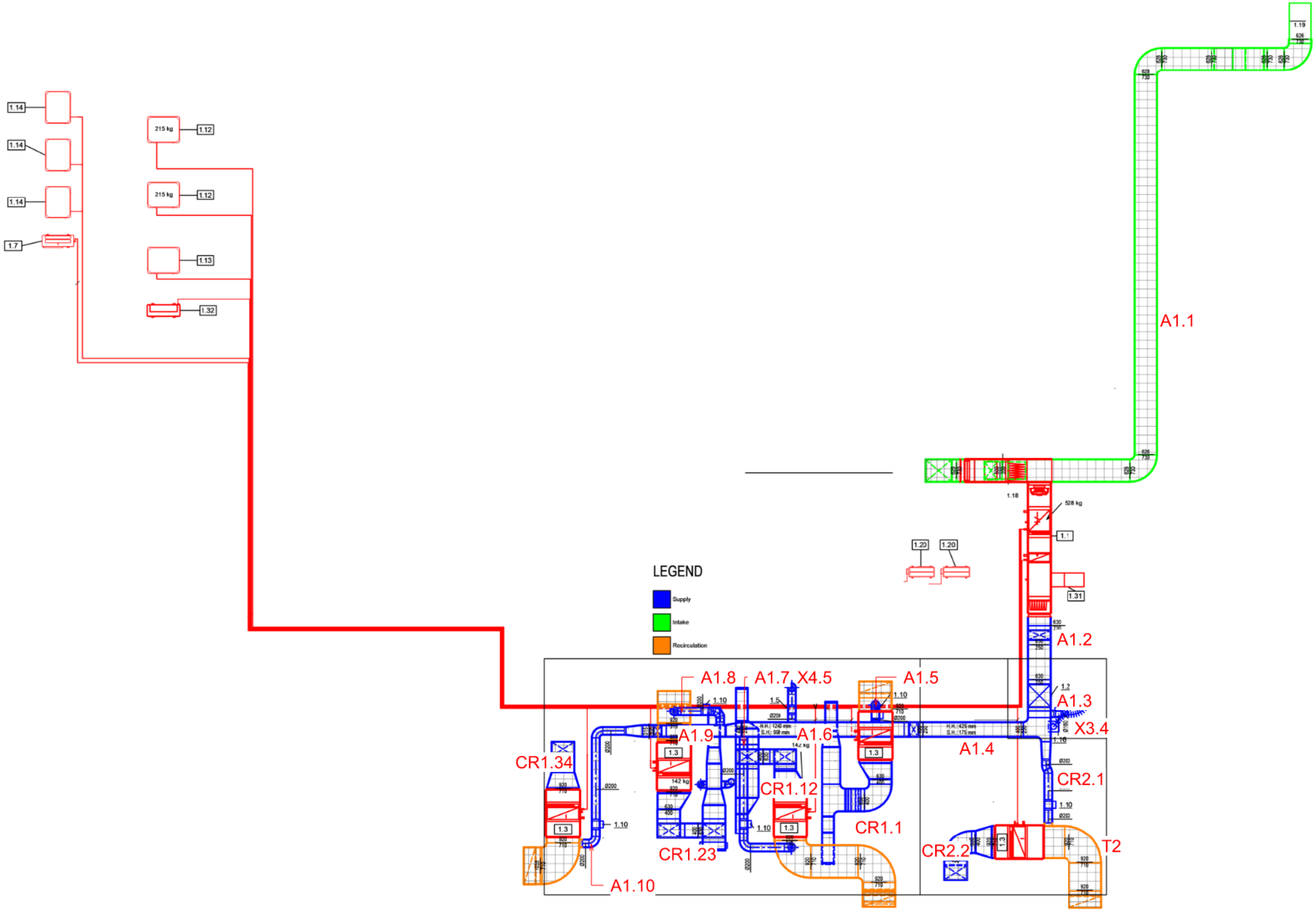
LEGEND
Supply
Intake
Recirculation
1.14
1.14
1.14
1.7
215 kg
1.12
215 kg
1.12
1.13
1.32
1.19
A1.1
1.18
528 kg
1.20
1.20
1.31
A1.2
A1.8
A1.7
X4.5
A1.5
A1.3
X3.4
A1.9
A1.6
A1.4
CR1.34
CR2.1
CR1.12
CR1.1
CR1.23
CR2.2
T2
A1.10

Appendix H

Existing decentralized system – Pressure loss calculations

Room Number	Branch sections	Airflow	Duct size (round)	Loss (Pa/m)	Duct Length (m)	Pressure drop duct (Pa)	Junctions (m)	Pressure drop junctions (Pa)	Additions (Damper, flex duct, wall/ceiling suction, diffuser etc) (Pa)	Total drops branch (Pa)	FFU + Damper (Pa)	H14 Filter	Total FFU	FFU ID
Above ceiling, from AHU	A1.1	597	763	0.15	22	3.3	5 X Elbow	7.5	50	60.8	0	0	0	
	A1.2	597	448	0.35	3	1.05	Diameter reducer, double elbow	7.7	0	8.75	0	0	0	
	A1.3	597	763	0.15	1.6	0.24	Double elbow	3	0	3.24	0	0	0	
	A1.4	458	357	0.6	4.6	2.76	Tee, Double elbow	21	0	23.76	0	0	0	
	A1.5	105	200	0.7	0.8	0.56	Double elbow, diameter reducer	15.4	20	35.96	0	0	0	
	A1.6	270	357	0.25	4	1	Diameter reducer	0.5	0	1.5	0	0	0	
	A1.7	90	200	0.55	4.5	2.475	Double elbow, diameter reducer	12.1	20	34.575	0	0	0	
	A1.8	90	200	0.55	1.5	0.825	Double elbow, diameter reducer	12.1	20	32.925	0	0	0	
	A1.9	90	284	0.1	3	0.3	Diameter reducer, double elbow	2.2	0	2.5	0	0	0	
	A1.10	90	200	0.55	3.7	2.035	Double elbow	11	20	33.035	0	0	0	
Above ceiling, in between	X4.5	52	200	0.2	2.4	0.48	Double elbow, tee	7	0	7.48	0	0	0	
	X4.51	30	160	0.15	1	0.15	Double elbow	3	0	3.15	0	0	0	
	X4.52	22	160	0.15	0.4	0.06	Double elbow	3	0	3.06	0	0	0	
Personnel airlock 1	X6	304	226	2.8	2.6	7.28	Elbow, Diameter red.	33.6	30	70.88	100	65	165	35
Personnel airlock 2	X5	310	564	0.1	0.4	0.04	Diameter reducer	0.2	0	0.24	0	0	0	
	X5.1	310	160	15	0.5	7.5	Elbow	150	0	157.5	0	0	0	
	X5.2	155	160 (flex)	20	0.8	16	-	0	0	16	100	65	165	37
	X5.3	155	160 (flex)	20	1.3	26	-	0	0	26	100	65	165	36
Dressing room	X4	220	564	0.1	0.4	0.04	Diameter reducer	0.2	0	0.24	0	0	0	
	X4.1	220	160	7	0.5	3.5	Elbow	70	0	73.5	0	0	0	
	X4.2	110	160 (flex)	20	1	20	-	0	0	20	100	65	165	38
	X4.3	110	160 (flex)	20	1.3	26	-	0	0	26	100	65	165	39
Material airlock	X3.1	290	160	12	2.2	26.4	Double elbow, tee	420	30	476.4	0	0	0	
	X3.2	145	160	3.5	0.5	1.75	Elbow	35	0	36.75	100	65	165	33
	X3.3	145	160	3.5	0.5	1.75	Elbow	35	0	36.75	100	65	165	34
	X3.4	30	160	0.25	0.4	0.1	-	0	50	50.1	0	0	0	
CR2	CR2.1	109	200	0.7	1.45	1.015	Double elbow, diameter reducer	15.4	20	36.415	0	0	0	
	CR2.2	1090	567	0.4	1.8	0.72	Double elbow, diameter reducer	8.8	0	9.52	0	0	0	
	CR2.3	156	160	4	0.6	2.4	Elbow	40	0	42.4	100	65	165	31
	CR2.4	312	315	0.55	0.7	0.385	-	0	0	0.385	0	0	0	
	CR2.5	156	160	4	1	4	Elbow	40	0	44	100	65	165	26
	CR2.6	156	160	4	2	8	Double elbow, diameter reducer	88	0	96	100	65	165	27
	CR2.7	624	452	0.35	1.4	0.49	Diameter reducer, Tee	5.95	0	6.44	0	0	0	
	CR2.8	156	315	0.15	0.8	0.12	-	0	0	0.12	0	0	0	
	CR2.9	156	160	4	0.2	0.8	Diameter reducer	8	10	18.8	100	65	165	30
	CR2.10	156	160	4	0.4	1.6	Diameter reducer	8	10	19.6	100	65	165	29
	CR2.11	156	160	4	1.4	5.6	Elbow, diameter reducer	48	10	63.6	100	65	165	28
	CR2.12	156	160	4	0.9	3.6	Diameter reducer, elbow	48	5	56.6	100	65	165	32
CR1	CR1.1	1050	567	0.3	0.5	0.15	Diameter reducer, elbow, tee	8.1	0	8.25	0	0	0	
	CR1.2	300	284	0.7	1.4	0.98	-	0	0	0.98	0	0	0	
	CR1.3	150	160	4	0.4	1.6	Diameter reducer	8	5	14.6	100	65	165	8
	CR1.4	150	160	4	0.4	1.6	Diameter reducer	8	10	19.6	100	65	165	7
	CR1.5	150	160	4	0.1	0.4	Diameter reducer	8	10	18.4	100	65	165	10
	CR1.6	600	505	0.2	1.1	0.22	-	0	0	0.22	0	0	0	
	CR1.7	150	160	4	1.2	4.8	Diameter reducer	8	10	22.8	100	65	165	9
	CR1.8	150	160	4	0.4	1.6	Diameter reducer	8	10	19.6	100	65	165	11
	CR1.9	300	284	0.7	0.8	0.56	Diameter reducer	1.4	0	1.96	0	0	0	

CR1.10	150	160	4	0.4	1.6	Diameter reducer	8	10	19.6	100	65	165	25
CR1.11	150	160	4	0.3	1.2	Diameter reducer	8	10	19.2	100	65	165	24
CR1.12	900	567	0.25	1	0.25	Triple elbow, diameter reducer	8	0	8.25	0	0	0	
CR1.13	300	567	0.1	1	0.1	Elbow	1	0	1.1	0	0	0	
CR1.14	300	284	0.7	0.55	0.385	Diameter reducer	1.4	0	1.785	0	0	0	
CR1.15	150	160	4	1.2	4.8	Elbow, diameter reducer	48	10	62.8	100	65	165	6
CR1.16	150	160	4	0.4	1.6	Elbow, diameter reducer	48	10	59.6	100	65	165	5
CR1.17	600	567	0.15	0.5	0.075	Elbow	1.5	0	1.575	0	0	0	
CR1.18	150	160	4	0.6	2.4	Elbow, diameter reducer	48	20	70.4	100	65	165	12
CR1.19	150	160	4	0.3	1.2	Elbow, diameter reducer	48	20	69.2	100	65	165	13
CR1.20	300	284	0.7	0.9	0.63	Diameter reducer	1.4	0	2.03	0	0	0	
CR1.21	150	160	4	5	20	Diameter reducer	8	10	38	100	65	165	22
CR1.22	150	160	4	0.1	0.4	Diameter reducer	8	20	28.4	100	65	165	23
CR1.23	900	567	0.25	1.4	0.35	Triple elbow	7.5	0	7.85	0	0	0	
CR1.24	300	567	0.1	0.4	0.04	Elbow	1	0	1.04	0	0	0	
CR1.25	150	160	4	0.1	0.4	Diameter reducer	8	20	28.4	100	65	165	4
CR1.26	150	160	4	0.2	0.8	Diameter reducer	8	5	13.8	100	65	165	3
CR1.27	600	567	0.15	0.4	0.06	Elbow, diameter reducer	1.8	0	1.86	0	0	0	
CR1.28	150	160	4	0.3	1.2	Diameter reducer,elbow	48	20	69.2	100	65	165	14
CR1.29	150	160	4	0.5	2	diameter reducer, elbow	48	20	70	100	65	165	15
CR1.30	300	452	0.15	0.7	0.105	Diameter reducer	0.3	0	0.405	0	0	0	
CR1.31	300	284	0.7	1.1	0.77	-	0	0	0.77	0	0	0	
CR1.32	150	160	4	0.1	0.4	Elbow, diameter reducer	48	10	58.4	100	65	165	21
CR1.33	150	160	4	0.3	1.2	Diameter reducer	8	20	29.2	100	65	165	20
CR1.34	900	567	0.25	1	0.25	Elbow, diameter reducer	3	0	3.25	0	0	0	
CR1.35	600	452	0.4	0.7	0.28	Diameter reducer	0.8	0	1.08	0	0	0	
CR1.36	150	160	4	0.4	1.6	Diameter reducer	8	5	14.6	100	65	165	17
CR1.37	150	160	4	1.3	5.2	Diameter reducer	8	20	33.2	100	65	165	16
CR1.38	300	284	0.7	1.3	0.91	Diameter reducer	1.4	0	2.31	0	0	0	
CR1.39	150	160	4	1.1	4.4	Diameter reducer	8	20	32.4	100	65	165	2
CR1.40	150	160	4	0.2	0.8	Diameter reducer	8	5	13.8	100	65	165	1
CR1.41	300	284	0.7	0.9	0.63	Elbow, diameter reducer	8.4	0	9.03	0	0	0	
CR1.42	150	160	4	0.2	0.8	Diameter reducer	8	10	18.8	100	65	165	18
CR1.43	150	160	4	0.2	0.8	Diameter reducer	8	20	28.8	100	65	165	19

Recirculation Towers	Duct size (round)	Airflow	Pa/m	Duct Length (m)	Total duct (Pa)	Junctions	Pressure drop junctions (Pa)	Additions (Damper, flex duct, wall/ceiling suction) (Pa)	H14 Filter, 4 each (Pa)	Total Tower (Pa)	
T1.1	608	810	0.15	6	0.9	Double elbow	3	120	260	383	T1.1
T1.2	608	945	0.2	6	1.2	Double elbow	4	120	260	384	T1.2
T1.3	608	810	0.15	6	0.9	Triple elbow	4.5	120	260	384.5	T1.3
T1.4	608	810	0.15	4.5	0.675	Triple elbow	4.5	120	260	384.5	T1.4
T2	608	981	0.25	4.1	1.025	Elbow	2.5	120	260	382.5	T2
	608	1090	0.3	1.4	0.42	Elbow	3				
T4	564	198	0.1	3.7	0.37	Elbow	1	60	260	321	T4
T5	564	279	0.1	3.7	0.37	Elbow	1	60	260	321	T5

Machines	Elements	Drop (Pa)	Total Machine (Pa)	Amount
1.3	Damper	40	140	5
	Cooling Coil	100		
1.15	Damper	40	140	2
	Cooling Coil	100		
1.1	AHU	350	350	1

ID	Airflow (L/s)	Airflow (m^3/s)	Path	Pressure loss (Pa)	Pressure loss (kPa)
FFU 1	150	0.15	T1.4 ,1.3 ,CR1.34, CR1.35, CR1.38 , CR1.40	268.7666667	0.269
FFU 2	150	0.15	T1.4 ,1.3 ,CR1.34, CR1.35, CR1.38 , CR1.39	287.3666667	0.288
FFU 3	150	0.15	T1.1,1.3,CR1.23 ,CR1.24,CR1.26	268.6283333	0.269
FFU 4	150	0.15	T1.1,1.3,CR1.23 ,CR1.24,CR1.25	283.2283333	0.284
FFU 5	150	0.15	T1.3, 1.3, CR1.12, CR1.13, CR1.14, CR1.16	315.4175	0.316
FFU 6	150	0.15	T1.3, 1.3, CR1.12, CR1.13, CR1.14, CR1.15	318.6175	0.319
FFU 7	150	0.15	T1.2, 1.3, CR1.1, CR1.2, CR1.4	261.2685714	0.262
FFU 8	150	0.15	T1.2, 1.3, CR1.1, CR1.2, CR1.3	256.2685714	0.257
FFU 9	150	0.15	T1.2, 1.3, CR1.1, CR1.6, CR1.7	264.0335714	0.265
FFU 10	150	0.15	T1.2, 1.3, CR1.1, CR1.5	259.5785714	0.26
FFU 11	150	0.15	T1.2, 1.3, CR1.1, CR1.6, CR1.8	260.8335714	0.261
FFU 12	150	0.15	T1.3, 1.3, CR1.12, CR1.17, CR1.18	325.16875	0.326
FFU 13	150	0.15	T1.3, 1.3, CR1.12, CR1.17, CR1.19	323.96875	0.324
FFU 14	150	0.15	T1.1,1.3,CR1.23,CR1.27,CR1.28	323.9733333	0.324
FFU 15	150	0.15	T1.1,1.3,CR1.23,CR1.27,CR1.29	324.7733333	0.325
FFU 16	150	0.15	T1.4 ,1.3 ,CR1.34 ,CR1.35 ,CR1.37	287.0116667	0.288
FFU 17	150	0.15	T1.4 ,1.3 ,CR1.34 ,CR1.35, CR1.36	268.4116667	0.269
FFU 18	150	0.15	T1.4,1.3,CR1.34 ,CR1.41 ,CR1.42	276.8566667	0.277
FFU 19	150	0.15	T1.4,1.3,CR1.34 ,CR1.41 ,CR1.43	286.8566667	0.287
FFU 20	150	0.15	T1.1,1.3,CR1.23,CR1.27, CR1.30, CR1.31, CR1.33	284.5608333	0.285
FFU 21	150	0.15	T1.1,1.3,CR1.23,CR1.27, CR1.30, CR1.31, CR1.32	313.7608333	0.314
FFU 22	150	0.15	T1.3, 1.3, CR1.12, CR1.17,CR1.20, CR1.21	293.78375	0.294
FFU 23	150	0.15	T1.3, 1.3, CR1.12, CR1.17,CR1.20, CR1.22	284.18375	0.285
FFU 24	150	0.15	T1.2, 1.3, CR1.1, CR1.6, CR1.9, CR1.11	261.4135714	0.262
FFU 25	150	0.15	T1.2, 1.3, CR1.1, CR1.6, CR1.9, CR1.10	261.8135714	0.262
FFU 26	156	0.156	T2, 1.3, CR2.2, CR2.4, CR2.5	298.5525	0.299
FFU 27	156	0.156	T2, 1.3, CR2.2, CR2.4, CR2.6	350.5525	0.351
FFU 28	156	0.156	T2, 1.3, CR2.2, CR2.7, CR2.8, CR2.11	320.2266667	0.321
FFU 29	156	0.156	T2, 1.3, CR2.2, CR2.7, CR2.8, CR2.9	275.4266667	0.276
FFU 30	156	0.156	T2, 1.3, CR2.2, CR2.7, CR2.8, CR2.10	276.2266667	0.277
FFU 31	156	0.156	T2, 1.3, CR2.2, CR2.3	296.76	0.297
FFU 32	156	0.156	T2, 1.3, CR2.2, CR2.7, CR2.12	313.1066667	0.314
FFU 33	145	0.145	X3.1, X3.2	439.95	0.44
FFU 34	145	0.145	X3.1, X3.3	439.95	0.44
FFU 35	304	0.304	X6	235.88	0.236
FFU 36	155	0.155	T5, 1.3, X5, X5.1, X5.3	499.99	0.5
FFU 37	155	0.155	T5, 1.3, X5, X5.1, X5.2	489.99	0.49
FFU 38	110	0.11	T4, 1.3, X4, X4.1, X4.2	451.99	0.452
FFU 39	110	0.11	T4, 1.3, X4, X4.1, X4.3	457.99	0.458
AHU	597	0.597	A1.2 + A1.3 + A1.4 + A1.6 + A1.9 + A1.10	72.785	0.073

LUND UNIVERSITY

Divisions of Energy and Building Design, Building Physics and Building Services

Department of Building and Environmental Technology